Application of Microfluidics in the Field of Diabetes and Islets

BY
Mohammad Nourmohammadzadeh
B.S., Shiraz University, 2008
M.S., Shahid Bahonar University of Kerman, 2011

THESIS

Submitted as partial fulfillment of the requirements
for the degree of Doctor of Philosophy in Bioengineering
in the Graduate College of the
University of Illinois at Chicago, 2015

Chicago, Illinois

Defense Committee:
Dr. José Oberholzer, Chair and Advisor
Dr. Yong Wang, Surgery
Dr. David Eddington
Dr. Michael Stroscio
Dr. Solomon Afelik, Surgery

Acknowledgements

I would like to thank my advisors Dr. Oberholzer and Dr. Wang for their encouragement, guidance, and support throughout my Ph.D. research and thesis. I am very grateful to my thesis committee members, Dr. Eddington, Dr. Stroscio, and Dr. Afelik for their insights and perspective throughout the completion of my doctoral education at UIC. I also would like to thank Dr. Eddington for allowing me to use his laboratory equipment to complete parts of my research. I would like to give a special thank you to the UIC islet isolation team for their assistance and technical support during my research.

I'd like to thank my fellow graduate students, research technicians, collaborators, and the multitude of undergraduates who contributed to this research. I am very grateful to all of you.

I would especially like to thank my amazing family for the support, love, and constant encouragement I have gotten over the years. In particular, I would like to thank my parents and my brothers. I undoubtedly could not have done this without you. Your remarkable source of energy kept me motivated and smiling throughout this process.

Finally, I would like to dedicate this thesis to my brother, Dr. Morteza Nourmohammadzadeh. You have set an example of excellence as a brother, mentor, friend, and role model. It was you who originally generated my love for science, engineering, and medicine with visits to your hospital and lessons on mathematics and physics. Although it has been years since our last science discussion, I still take your valuable lessons with me, every day.

TABLE OF CONTENTS

List of Tables

List of Figures

Abstract

Type I Diabetes Mellitus (TIDM) is an autoimmune disease, which involves the destruction of beta-cells leading to insulin deficiency and an increase in blood glucose levels. Microencapsulation of human islets is a promising therapy for treatment of TIDM without the need for immunosuppressants. However, one disadvantage associated with microencapsulation is the possible induction of islet hypoxia due to the prevention of revascularization and an increase in the oxygen diffusion distance. In order to investigate the effects of hypoxia on encapsulated islets, a microfluidic array was developed and integrated with oxygenation control to provide and mimic various hypoxic conditions. We were able to demonstrate that hypoxia impairs the function of microencapsulated islets at the single islet level, showing a heterogeneous pattern reflected in intracellular calcium signaling, mitochondrial energetic, and redox activity. Our approach demonstrated an improvement over conventional hypoxia chambers. This work demonstrates the feasibility of array-based cellular analysis and opens up new modality to conduct informative analysis and cell-based screening for microencapsulated pancreatic islets.

One of the major challenges of current in vivo tools to study islets and diabetes is the limited number of islets that can be assessed in a single device. Another challenge is the inability to satisfactorily assess the heterogeneous property of individual islets, especially when testing a large quantity of islets simultaneously. Examination of heterogeneous properties at the individual islet level often provides more detailed physiological or pathophysiological information than averaging-based population methodologies. For example, it will enable better understanding of human islet functionality from a reasonable sample size and will provide a better predictive value for islet transplant outcomes if many individual islets can be individually assessed instead of averaging a bulk response. In this report, the aim is to develop a novel microfluidic islet array, based on the hydrodynamic trapping principle, for investigating the complexity of physiological or pathophysiological behavior of individual pancreatic islets in a larger islet population. Furthermore, we aim to explore the feasibility of array-based

cellular analysis to provide more informative data on pancreatic islets and to act as a platform to evaluate antidiabetic drugs.

Our Lab collaboration with MIT determined that fibrosis of materials is largely dependent on the size and shape. It has been proven that islets prepared in 1.5-mm alginate capsules were able to restore blood-glucose control for up to 180 days, a period more than five times longer than for conventionally sized 0.5-mm alginate encapsuleted islet. These new findings propose that the in vivo biocompatibility of biomedical devices can be significantly enhanced simply by tuning their spherical dimensions. In third project, a new platform has been designed, verified and successfully tested that can be successfully applied to investigate and study the properties of 1.5 mm macrocapsules and also to evaluate the functionality of islets inside these microcapsules. The device is capable of immobilizing macrocapsules for short-term and long-term dynamic and static stimulation and live cell imaging. Using this new platform, we are continuing the study on macrocapsules to investigate how the size/volume of the immune-isolation material affects islet functionality.

Lastly, in order to achieve insulin independence, a minimum of 5000 IEq/ kilogram patient body weight is needed per islet cell transplantation. Currently, islet quantification prior to transplantation is conducted manually, which can result in increased variability in total counts as well as being time-consuming. To overcome this challenge a microfluidic based islet quantification platform integrated with a smartphone has been proposed for accurate, cost-effective and rapid islet cell counting and quantification.

In these four projects, we were able to demonstrate an array of applications for microfluidic technology in the study of both naked and encapsulated islet cells that can help to better understand diabetes.

Chapter I. Introduction

The Pancreas and Islet of Langerhans

The human pancreas is a gland with dual exocrine–endocrine function and consists of four different components; the exocrine tissue (98%), the ducts, the endocrine cells (1-2%), and the connective tissue[1]. Exocrine cells release digestive enzymes for nutrient digestion. On the other hand, endocrine cells maintain glucose balance by secreting several hormones. The specific cells found within the pancreas are known as the islets of Langerhans and are localized within the endocrine tissue. The islets of Langerhans or islets are composed of five different cell types. α-cells are responsible for glucagon secretion that can cause the liver to convert stored glycogen into glucose during periods of hypoglycemia (figure 1). The α-cells make up 3~10% of the islet cell mass. β- cells are responsible for insulin production, which is essential for the breakdown of glucose[2]. β- cells make up 65~85% of the islet cell mass. Insulin secretion is primarily controlled by the glucose-stimulated pathway. Delta-cells produce somatostatin that can inhibit insulin and glucagon secretion by the excretion of certain hormones[3]. Pancreatic polypeptide (PP) cells release PP hormones, and the fifth type of cell found in islets is the epsilon cells[4]. There are approximately one million islets distributed throughout an average human pancreas. Single islets are comprised of between 1,000-2,000 individual cells. An adult human islet ranges in size from 50 to 400 μm in diameter and is surrounded by a thin collagen layer. In addition a highly dense network of capillaries and glial sheets separate the exocrine tissue from the endocrine cells[5]. The dense capillary structure found within the islet vasculature provides oxygen and glucose to the cells as well as aids in the circulation of hormones within the islets. Glucose is the primary component that controls the release of insulin within the β- cell cycle. When glucose enters the β- cell via the GLUT2 transporters, the glucose is converted into a metabolized glucose state via an enzymatic reaction from the enzyme glucokinase. When the glucose is broken down a sufficient amount of ATP is generated. Increased production of ATP

leads to the closure of K^+/ATP channels. In turn, the closed K^+/ATP channels leads to an increase in the K^+ ions within the β- cell which eventually leads to the depolarization of the cell membrane. This depolarization causes the Ca^{+2}/voltage gated ion channels to open, causing an influx of Ca^{+2} ions within the cytoplasm of the β- cell. The influx of Ca^{+2} ions results in the exocytosis of insulin granules. The release of insulin occurs in a two-phase biphasic manner. The first phase releases insulin that has been initially stored within the insulin granules; the release of insulin from this phase occurs much quicker compared to the second phase of insulin release. In the second phase, insulin release is much more prolonged as glucose must first be metabolized. ATP is produced and released and the membrane depolarized to allow an influx of Ca^{+2} ions[6], which in turn allows for insulin secretion.

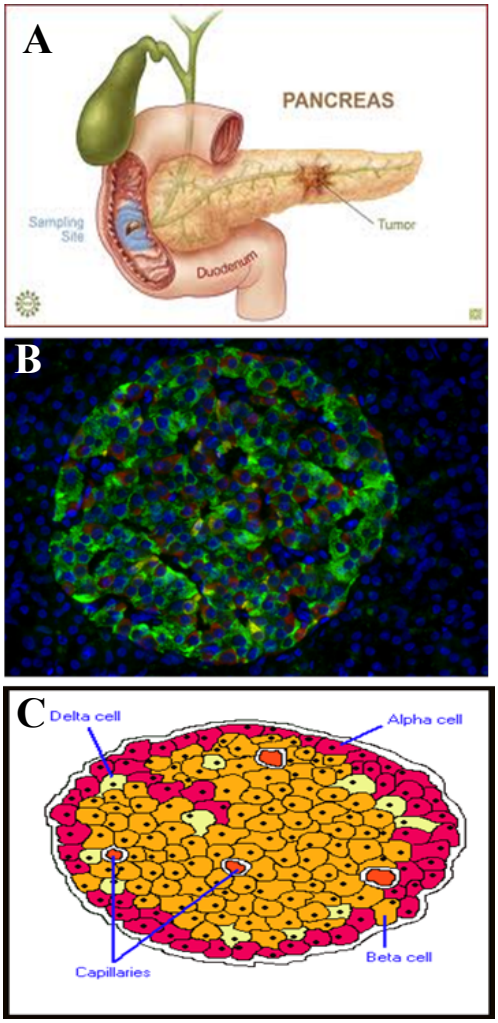

Figure1. A. The pancreas is positioned in the back of the abdomen. The organ produces digestive enzymes and various hormones, which are delivered to the small intestine (duodenum) and bloodstream respectively. The most important hormone in glucose regulation produced by the pancreas is insulin. Insulin is produced by specialized cells in the islets of the pancreas, known as beta cells. **B.** Mouse pancreatic islet is a spherical group of hormone-producing cells. Insulin is highlighted in green, glucagon in red, and the nuclei in blue. **C.** Schematic of an islet. https://en.wikipedia.org

Diabetes and classification

Diabetes is a group of metabolic diseases described by hyperglycemia resulting from deficiencies in insulin secretion, insulin function, or both. The chronic hyperglycemia of diabetes is associated with dysfunction, long-term damage, and failure of organs, particularly eyes, nerves, kidneys, and blood vessels[7]. There are two major types of diabetes and several factors exist that affect the development of these diseases.

Type I

Type I diabetes accounts for almost 5–10% of all types of diabetes in the general population. It was known as juvenile-onset diabetes or insulin dependent diabetes. This type of diabetes (figure 2) is caused by autoimmune destruction of the β -cells in the islets[7]. The rate of β -cell destruction varies from person to person diagnosed with this type of diabetes. In children the rate of β- cell damage happens at a much faster rate in comparison to adults[7]. Ketoacidosois is the main indicator of the development of diabetes within children and adults[7]. Other individuals have modest fasting hyperglycemia that can alter to adjust to hyperglycemia and/or ketoacidosis induced by an infection or other stresses[7]. In adulthood, many variables affect β-cell function sufficiency to prevent ketoacidosis for several years[7]. Especially, these individuals ultimately become insulin-dependent to prolong their life expectancy, however, are at a higher risk to be identified with ketoacidosis as time progresses[7]. At the latter stage of this disorder, there exists little or no insulin secretion at all, as established by undetectable or low plasma C-peptide levels. Immune-mediated diabetes can happen at any age, even in the later stages of juvenile[7]. Autoimmune destruction of β -cells can be connected to environmental factors and also genetics in the family history, many of which are still unknown[7]. Though patients identified with this type of diabetes are less expected to be obese, the presence of obesity is not incompatible with the diagnosis[7]. Moreover, patients diagnosed with this type I diabetes are at a higher risk of being diagnosed with other types of autoimmune disorders[7]. Individuals with type I diabetes often

suffer from episodic ketoacidosis and exhibit varying degrees of insulin deficiency between episodes. A need for insulin replacement therapy in patients diagnosed with this disease may come and go, and vary from individual to individual based on the severity of the disease[7].

Type II diabetes

Type II diabetes accounts for 90–95% of the diabetes population. Type II diabetes has been before indicated to as adult-onset or non-insulin dependent. Type II diabetes (figure2) is categorized by people who have insulin resistance and usually have relative insulin deficiency[7]. For some individuals with type II diabetes, insulin injections are not necessary. There exist many different aspects that affect the onset of this type of diabetes[7]. Though the specific reasons are not known, autoimmune destruction of β- cells is not a direct reason. The majority of individuals with Type II diabetes are considered obese. Obesity is identified to have the capability to cause insulin resistance. Ketoacidosis is rarely identified in this type of diabetes[7]. Type II diabetes is hard to diagnose and can go undetected for years as hyperglycemia progresses over time and gradually and at earlier stages is often not severe enough for the patient to notice any of the classic symptoms of diabetes. Insulin resistance may be resolved in patients who lose weight or may be improved with medication and treatment. However, it is hard and difficult to get normal insulin release over-time for these patients [7]. There exist many reasons that contribute to a higher risk of developing type II diabetes, such as obesity, age and lack of activity[7].

Currently, one of the promising therapies that exists for Type I diabetic patients is clinical islet transplantation[7]. Clinical islet transplantation is a fast, non-invasive procedure that involves a small incision in the patient's abdomen. Often the patient can go home the same day or following day of the procedure[7].

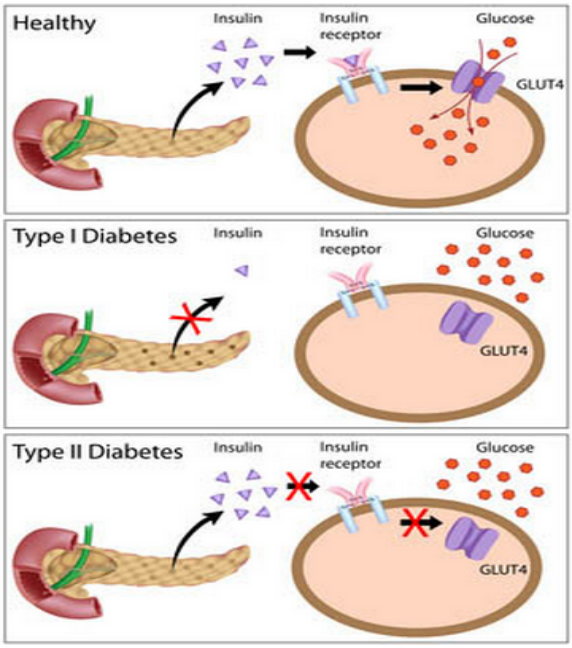

Figure 2. Diabetes and glucose - insulin action and diabetes type I and II.
http://www.noahhealth.org/what-is-diabetes

Clinical Islet Transplantation

The idea of transplanting pancreas extracts in patients was first stated in 1894[8]. The scientist Williams used pieces of a sheep's pancreas oral treatment and therapy[8,9]. Sheep xenografts without immunosuppressive drug were used and the outcomes were a complete failure[8]. In 1972, Ballinger and Lacy described that islet isografts into rats diabetic could result in normal glucose levels[8,10]. Furthermore, these outcomes led investigators to further examine these results and by the 1980s successful transplantation of islet autografts was reported[11,12,13]. In the autograft method, a patient identified with pancreatitis undergoes complete organ islolation and pancreatectomy in order to comfort the pain initiated by the pancreatitis. Then the pancreas will be digested with collagenase, and purified for transplant. Islets then infused into the patient's portal vien[8]. By 1992, researchers[14] described that 265,000 individual islets is sufficient to accomplish insulin independence within a diabetic patient[8].

By 1980s, the first allogeneic islet transplantation was successfully conducted[15]. However, globally, the overall rates of insulin independence after transplantation were described to be less than 10%[8,16]. By 2000, diabetes researchers reported to achieve 100 % success in 7 patients[8,17,18]. The improved rate of success caused from new methods and modified approaches used when compared with the conventional methods of immunosuppressive treatments[8]. Islet cells transplantation is a promising cure for type I diabetes patients, but there exist some limitations to this treatment. One of these factors is that a high number of high quality purified islets must be yielded from each isolation in order to be transplanted into the matching recipient[8].

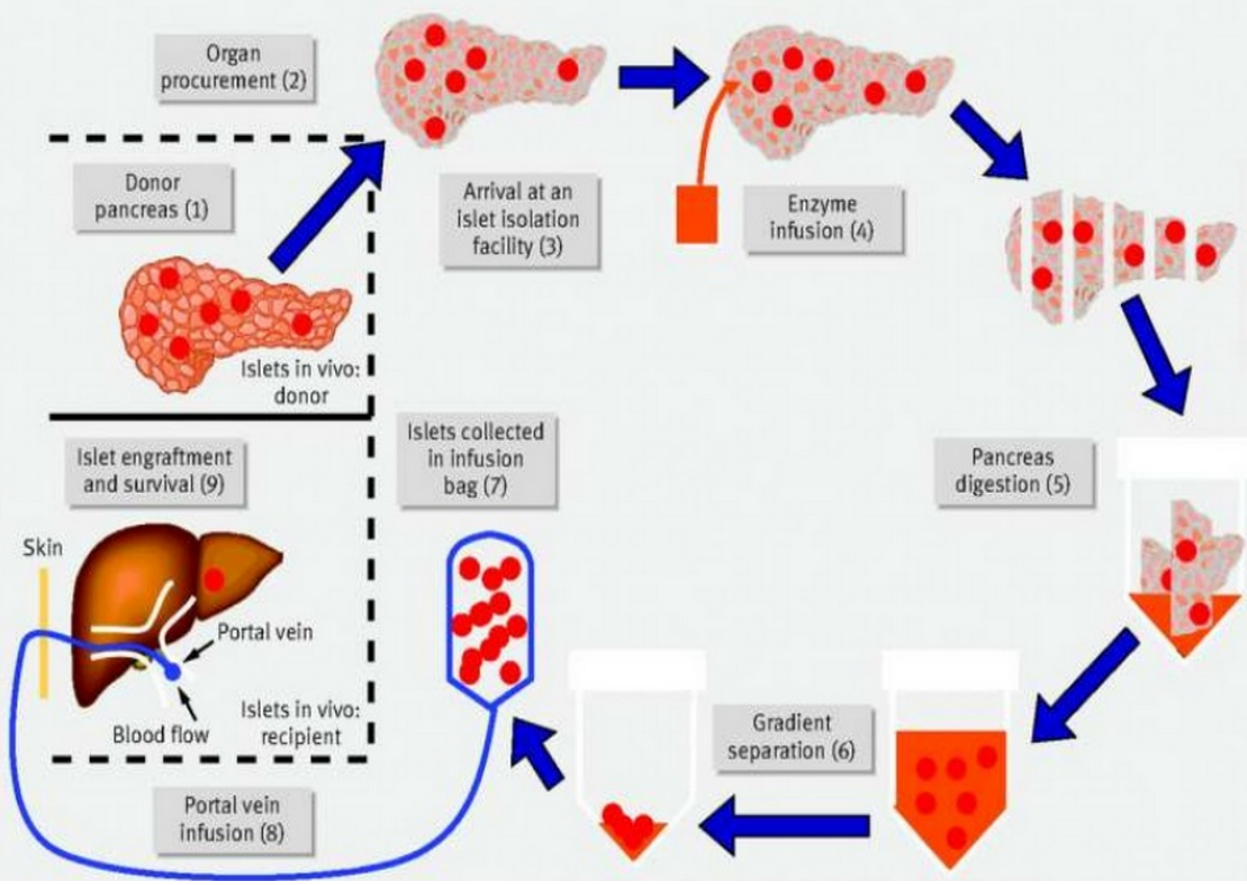

Figure 3. Pancreatic islet isolation and transplantation from the donor to the recipient. Adapted from http://www.slideshare.net/.

The procedure of islet isolation is a complex process involving the following steps as illustrated in figure 3. Enzyme is perfused into the pancreas to digest the surrounding collagen and to free the individual islets via the enzymatic process, then mechanical digestion of the pancreas is conducted using a so called Ricordi chamber, purification procedure is done using a density based method to separate purified islets from the exocrine tissue. The last step of human islet isolation is to culture islets[8].

A main limitation to the process of clinical islet transplantation is the loss of islets during culture before transplantation[8,12].

After transplantation, the immunosuppressive drugs provides a protection from the recipient immune system and stops the destruction of the islets.

Another reason of islet cell loss is the fact that islets do not have a fully vascularized network to provide the appropriate nutrients to survive[8]. The formation of vasculature network takes longer to develop within a human body than within a rodent system. Also, there are low oxygen level in the liver and the low levels of oxygen induces hypoxia, which is a major contributor to islet loss as previously described[8].

The instant blood-mediated inflammatory reaction further promotes formation of platelets. The platelets then induce the formation of fibrin. The fibrin influences macrophages, and this promotes an instant inflammatory reaction, which is another main contributor to islet loss[12]. Many researchers are investigating potential alternatives to overcome all these drawbacks with clinical islet transplantations. One method is to protect the islets from a immune reaction via the process of islet microencapsulation.

This in turn would eliminate the need for immunosuppressive drugs[8]. This will be discussed further in following sections.

As described before, Islet transplantation is a promising therapy for type I diabetes. However, in order to be successful in all patients that receive this therapy, it is crucial to evaluate islet function and quality prior to transplantation. Current standard assays for the evaluation of human islet cell functionality do not provide adequate examination and quantification of the cells. Therefore, an easy, fast, and predictable procedure to evaluate human islets to increase successful outcomes for human islet cell transplantations would be greatly useful. A microfluidic platform that enables fast and effective islet functionality evaluation prior to transplantation is discussed in detail in project 2. The microfluidic chip proposed here can provide a fast and effective evaluation of the functionality of islet cells prior to transplantation.

Islet microencapsulation

The protection of islets by a semi-permeable membranes from the recipient immune system has been examined since the 1970s. However, until now research results in both academic and industrial institutions has led in variable achievement in rodent models. However, results in non-human models and initial clinical trials have not established very successful in proving non-immunoreactive encapsulation results in vivo[19,20]. The principle behind the cell encapsulation procedure is the envelopment of the islets in a semi-permeable membrane (figure 4). The porous membrane should let the passage of oxygen, glucose , insulin and nutrients, while simultaneously preventing the passage of immune cells and antibodies[19].

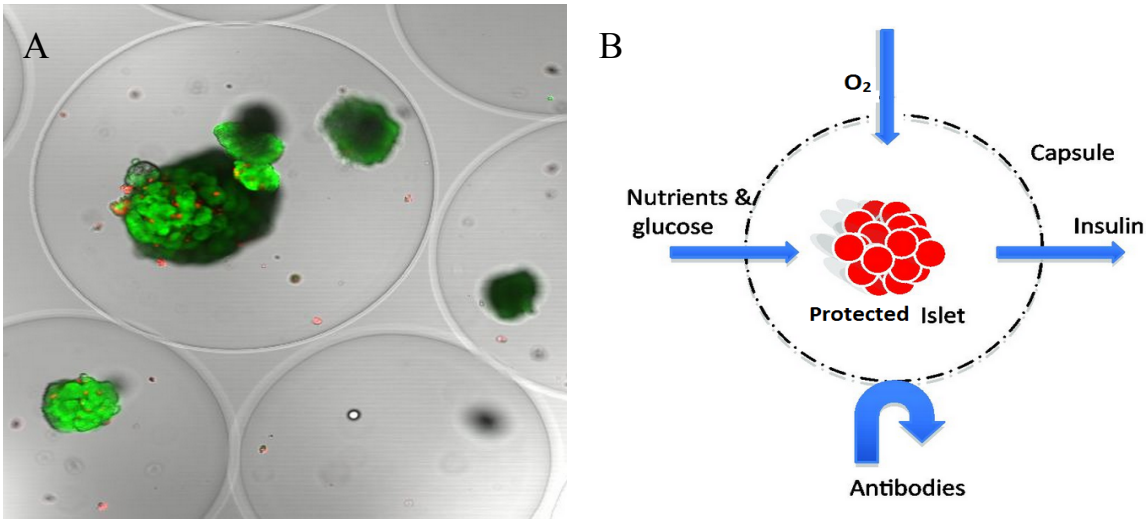

Figure 4. A. Magnified image of encapsulated rat islets. Viable cells stain green ____. Non-viable cells stain red **B.** Schematic representation of microcapsules, which act as barriers to protect the islet. The ultimate goal of immunoisolation is to encapsulate islets using a highly biocompatible biomaterial that allows for the passage of minuscule essential molecules such as oxygen and insulin, while preventing the entry of larger molecules and unwanted immune cells.

Methods of Encapsulation

There are three major encapsulation methods examined for islet transplantation. These methods of encapsulation are classified as intravascular macrocapsules, extravascular macrocapsules, or microcapsules (figure 5)[21,22,23, 24]. Microencapsulation (figure 5) is the process of encapsulation of cells, including individual islets or clusters of islets inside microcapsules[25]. There are many methods in order to manufacture microcapsules including double emulsion, and electrified coaxial liquid jets[26,27]. Microcapsules have the capability to deliver nutrient and oxygen transport as a result of the large surface area–to-volume ratio. A main obstacle to microencapsulation is the challenge of removing capsules post-transplantation. The fabrication of biocompatible capsules has been a huge challenge for investigators and researchers in the scientific field. Also, microencapsulated islet graft failure is unavoidable and certain factors have to be examined and understood in order to provide the minimal amount of failure including the factors that influence a graft to fail as will be discussed in the next section.

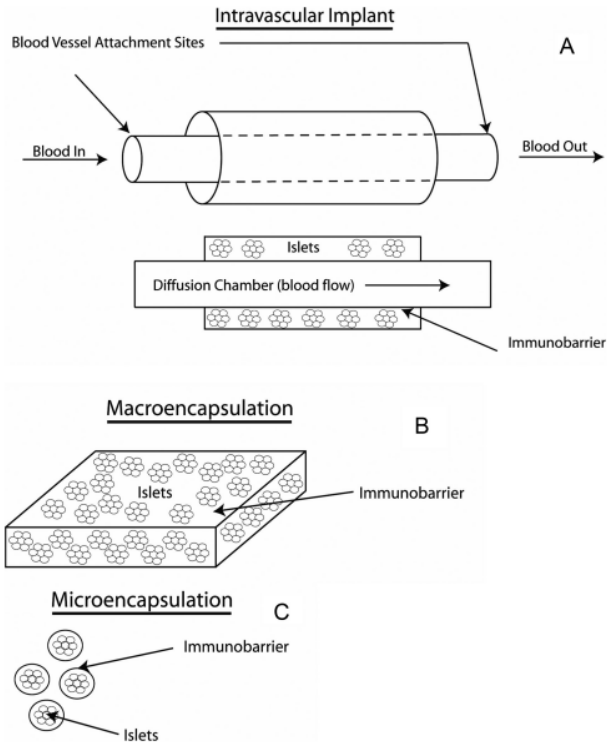

Figure 5. Three methods of encapsulating islet cells. Adopted from reference 57.

Causes of in vivo microencapsulated islet graft failure

Better understanding of the reasons of in vivo micro-encapsulated islet cell graft failure is necessary. A clear fact is that microencapsulated auto-graft and allo-graft survival rates are comparable, suggesting graft failure is not due to allograft recognition[28]. It has been demonstrated that prior to graft failure, there is an increase in central necrosis, a decrease in islet function, and overgrowth of the micro-encapsulated islet cell graft[29,30]. Consequently, there are three main reasons that lead to micro-encapsulated islet cells transplant failure that can be related to these issues. The first reason might be the bio-compatibility of the capsules. The materials used to fabricate micro-capsules are not biocompatible which results in overgrowth. The second reason can be linked to the immune-protective properties of the micro-capsules. Immuno-protection is not effective because capsules may allow small immune factors to pass resulting in apoptosis and eventually islet graft failure. The third reason is the gap between the encapsulated islets and the blood supply. An increase in diffusion distance can cause insufficient oxygen supply to islets, and irreversible hypoxia. The hypoxia ultimately leads to islet cell necrosis[30]. The hypoxia might play a vital role in the increase of replication within the islets and is discussed in further detail in the next section.

Hypoxia

An important issue that influences encapsulated islet cells graft failure is hypoxia (figure 6). Islets are made of a network of capillaries. These capillaries deliver the essential nutrients and oxygen essential for islet survival. During the procedure of islet isolation these capillaries are damaged. Micro-capsules further hinder revascularization of islet cells[29]. Encapsulated islets suffer from permanent hypoxic stress, because the appropriate supply of oxygen is incomplete[29]. Furthermore, insulin secretion is impaired by increased diffusion distance[30-32]. As a result, successful reversal of diabetes in rodents requires a higher islet cell mass[30,33]. Despite

being exposed to hypoxia, encapsulated islet cells are able to maintain normoglycemia up to few months. Therefore, it suggest that hypoxia is either restricted in severity or limited to only a fraction of the islet cells.

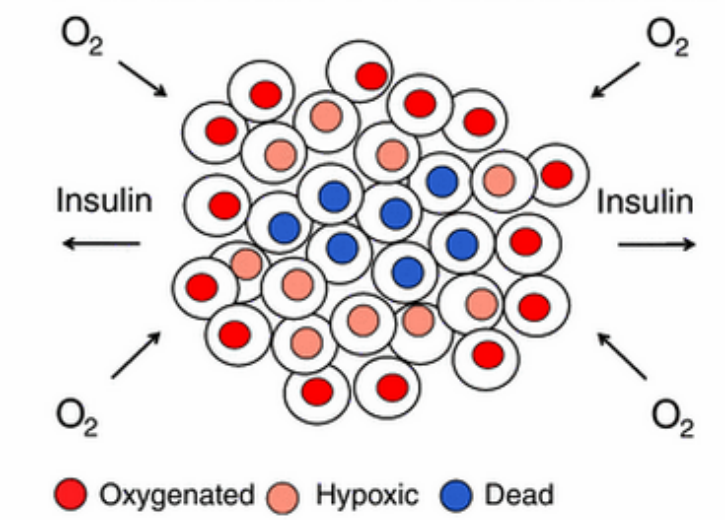

Figure 6. Importance of oxygen availability for the survival of encapsulated islets.(Adopted from ref 19)

A potential solution to reduce hypoxia negative outcome is to improve and modify the resistance of the overall islet cells[34,35]. Also an alternative implantation site can be a well-vascularized implantation site and such investigation are ongoing. As many factors are being investigated in order to reduce microencapsulated graft failure, researchers are interested in analyzing cellular interactions in the single cell level. Novel and innovative methods need to be further developed and introduced within the scientific field in order to analyze cells at the single cell level. In order to further understand the mechanism of hypoxia it is necessary to study encapsulated islets in vitro in real time. This allows for better understanding of the mechanisms involved in hypoxia and aid in developing effective solutions. In project 1 and 3, two microfluidic platforms are presented which allow for in vitro analysis of encapsulated islets subjected to hypoxia. These devices can be effective in vitro tools to analyze encapsulated islets under various conditions.

Dynamic Single Cell Analysis

Researchers in chemical biology, biomedical science have a great interest in how cells behave[36] (figure 7). Key processes like stem cell differentiation and proliferation are linked to the cellular micro-environment[37,38]. Some biological signals initiate from cell-contact mechanisms, including cell–cell interaction and cell–extracellular matrix(ECM) contacts. Also physical signals, including mechanical, electrical, and thermal factors have a huge impact [39-48]. Unfortunately, cells under identical conditions show a heterogeneous response and behaviors[49-53]. Cross talk between signaling pathways, the small number of molecules involved in signaling and localization of reactions lead to stochastic behavior in these systems[49,54,55]. As a result of heterogeneity in a population, interest has been mostly on the analysis of many individual cells to define the distribution in responses[56-58]. Currently, research has being focused on providing uniform and in-vitro situation for cells that allows other parameters to be evaluated in a dynamic and high-throughput method[36]. One of the major advantages of using novel microfluidics is that these platforms deliver examination of single cells with increased precision in comparison to studying cells as a group population. This concept can be applied for islets as well. All microfluidic

platforms presented here allow us to study islets and capsules individually which leads to a better understanding of islet physiology and behavior. Often times, bulk experimental procedures can be misleading in the overall results and analysis as will be discussed in the following chapter.

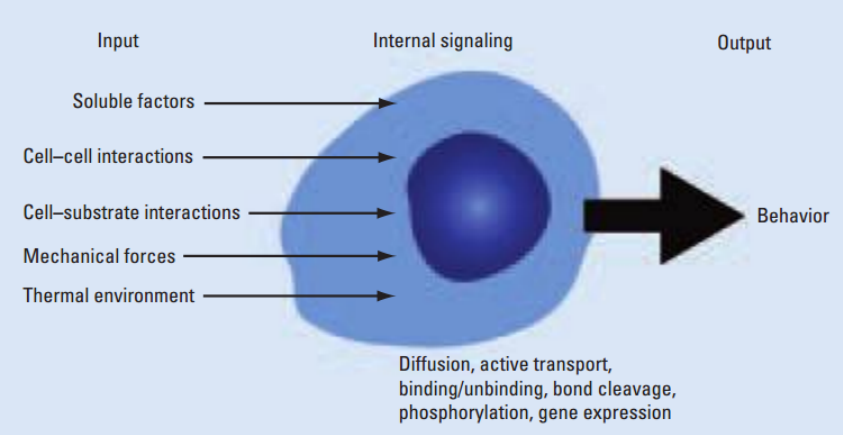

Figure 7. Input–output response for the cellular machine. (adopted from reference 36)

Misleading Bulk Experiments

Bulk approaches are selected because they are simple methods for studying intracellular mechanisms[36, 37]. However, there are some issues associated with this approach. For example, sometimes when same designed tests are conducted many times, bulk-methods do not deliver the accurate and reliable of the behavior in cells[36,54](figure 8). The concept of using microfluidics to analyze cells and islets at the individual level has made it possible to overcome these issues as microfluidic devices can be designed and fabricated to trap single cells and islets that remain stationary thus allowing for proper analysis to take place. These key features provided by lab-on-a-chip methodologies will be discussed in the project 2.

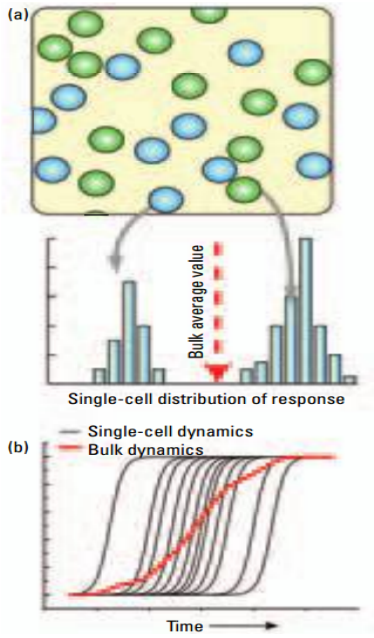

Figure 8. False outcomes can be achieved when the bulk-blended of cell population is studied. Adopted from reference 36.

Microfluidic Techniques

Cell and Particle Trapping in Microfluidic Systems

The capability to duplicate ideal situations for well defined micro-environments and controlled temporal/chemical/thermal variations is important for cell–cell interactions high-resolution and cell behavior studies[36,37,57,58,59]. A crucial point to the fast lab-on-a-chip advance in cell-biology is that microfluidics delivers a tool that can offer precise definition of a confined microenvironment with high temporal and spatial resolution in a multiplex setup[60-63]. An specific area for this equipment is pharmaceutical studies linked to drug screening output[57,64,65,66]. In order to completely apply the advantages of microfluidic integrated cell assays, methods for long-term cell immobilization at defined locations are vital.

An straightforward approach for trapping particles in a parallel fashion is to apply micro-well arrays (figure 9). Although simple, micro-well approach fails to effectively immobilize particles and the precise manipulation of a given particle's position is not possible. Therefore, other methods must be studied, developed and applied to better immobilize particles that enable researches to control particle positions inside microfluidic chips.

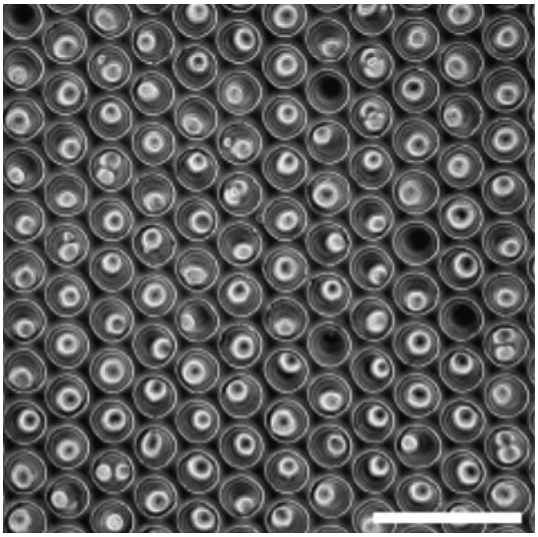

Figure 9. Microwell array for single cell trapping. Adopted from reference 67.

Hydrodynamic Cell Trapping

The most common method for particle/cell trapping within microfluidic platforms is through the creation of side channels localized within a main transport channel. A verity of different trapping mechanism are shown in figures 10 to 13 [57,68,69,70,71-76].

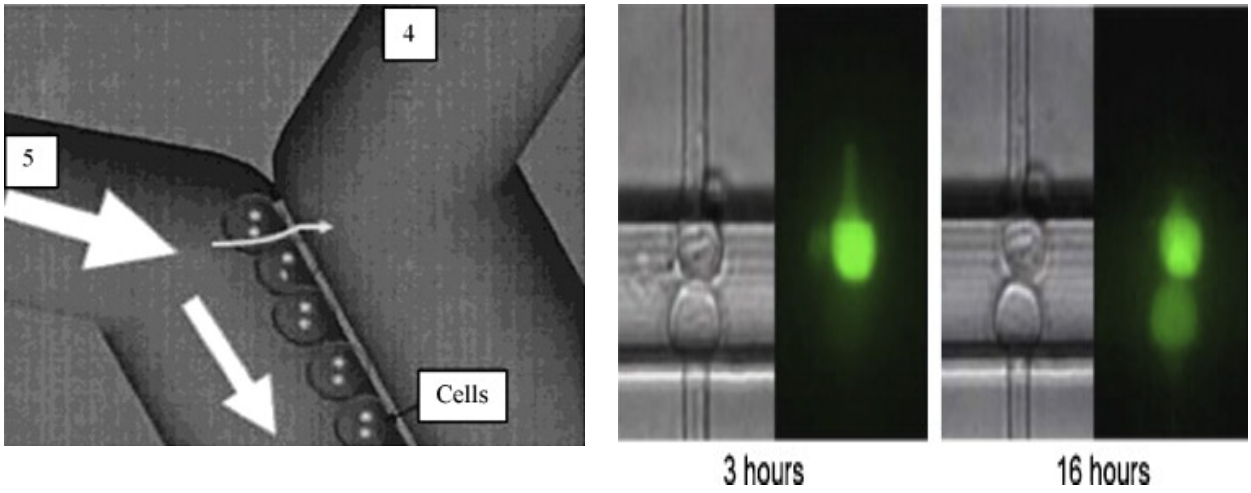

Figure 10. cell trapping mechanism adopted with permission from reference 68.

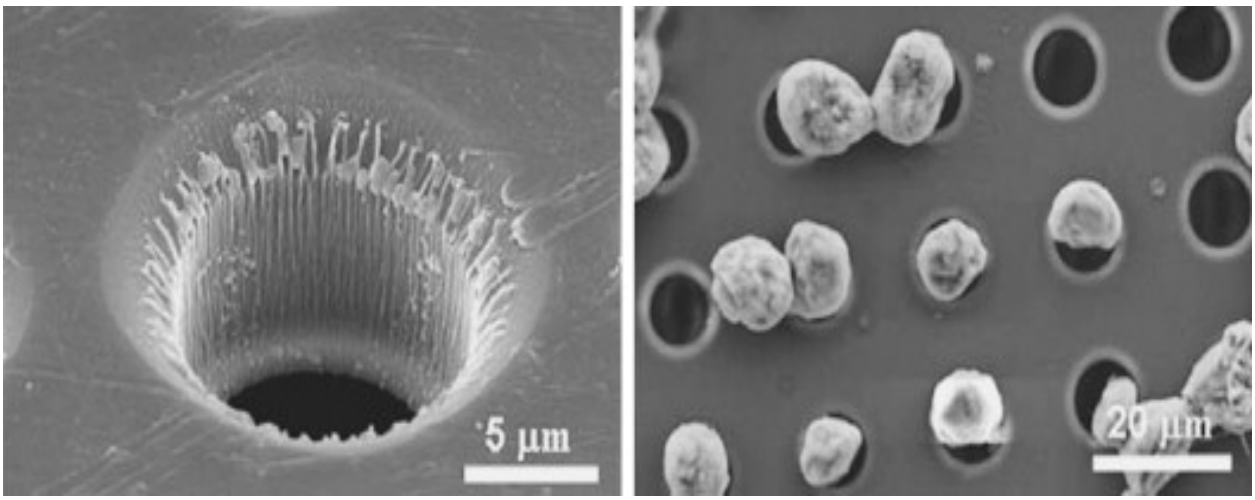

Figure 11. cell trapping mechanism adopted with permission from reference 68.

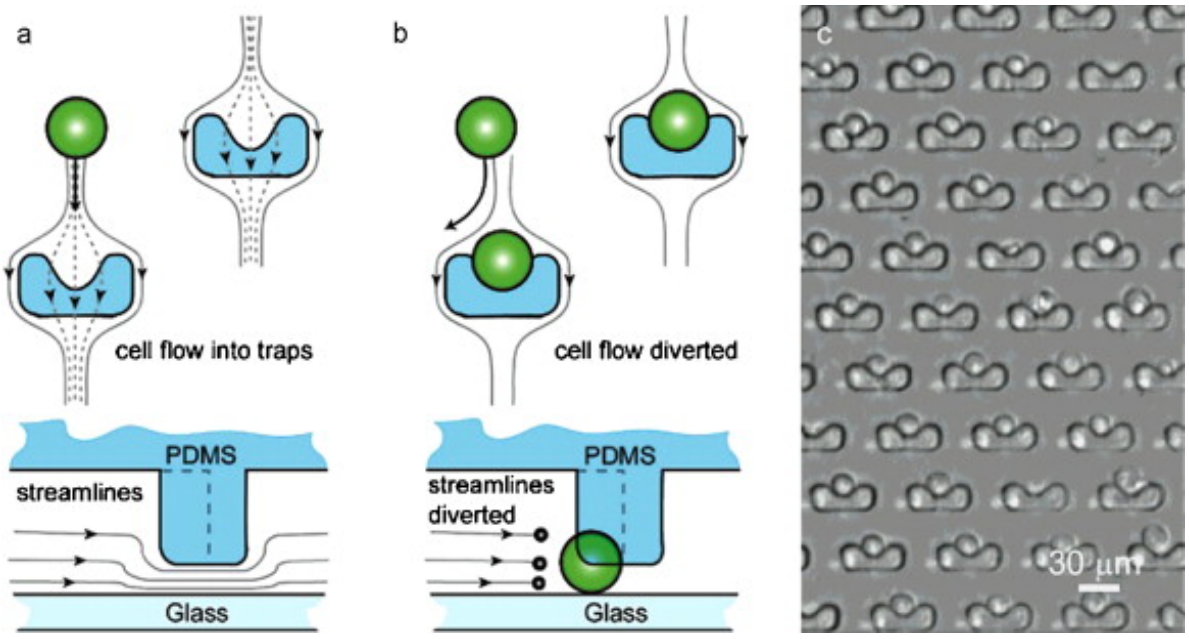

Figure 12. cell trapping mechanism adopted with permission from reference 68.

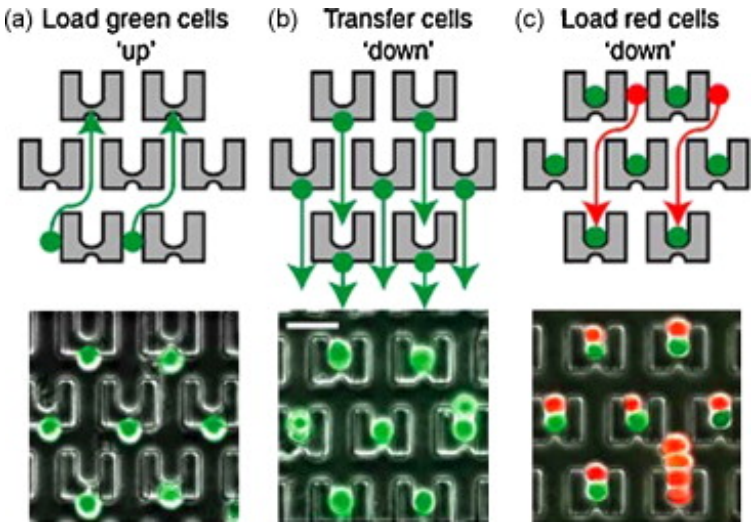

Figure 13 cell trapping mechanism adopted with permission from reference 68.

An innovative technique for particle trapping proposed by Tan and Takeuchi[72]. They designed a chip with an group of hydrodynamic based trapping locations in conjunction with a cup-shaped channel. The trapping locations are positioned via cross channels that connect two main path and have a lower flow resistance than the loop path until a cell is immobilized, leading to a systematic trapping of all particles[72] (figure 14). This trapping system was later tested for cells trapped in alginate beads, showing its application to be used for particle monitoring[73,74].

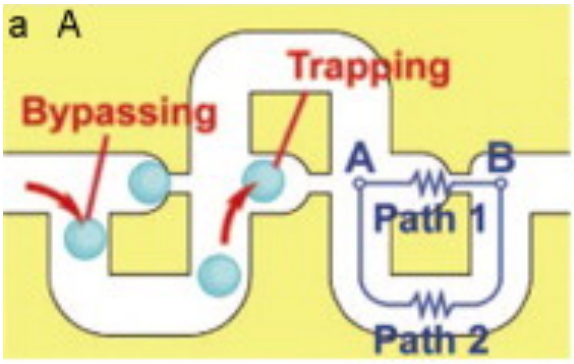

Figure 14. Schematic of loop channel and cross-flow trapping mechanism. Adopted from reference 72.

Specific Aims

Specific Aim 1: To investigate the effect of hypoxia on physiology of microencapsulated pancreatic islets using a microfluidic array with integrated oxygenation control for real-time live-cell imaging.

Specific Aim 2: To design, fabricate and characterize a microfluidic array for real-time and high content live-cell imaging of human pancreatic islets.

Specific Aim 3: To design, fabricate and validate a microfluidic platform for dynamic stimulation and real time imaging of macro-capsules in order to investigate islet function in macrocapsules.

Specific Aim 4: To design and build a cost-effective and rapid cell-phone based islet counting platform.

Chapter II. Materials and Methods

Human Islet Isolations

Human islets were extracted based on the following protocol. Human pancreata were obtained from organ procurement organizations following formal research consent and transported to the cell isolation facility at the University of Illinois at Chicago (UIC). No donor randomizations were applied. The isolation, purification, and culture procedures were performed as previously described[74,78]. Briefly, the pancreata were trimmed and distended with collagenase and then digested using a modified Ricordi semi-automatic method. Post-digestion, islets were purified using the UIC-UB gradient[78] in a Cobe 2991 cell separator (Cobe 2991, Cobe, CO) and subsequently placed in Final Wash culture solution (Mediatech, VA) in incubator supplemented with ITS (Invitrogen, CA), Sodium bicarbonate (Sigma, MO), Hepes, Human Albumin (Grifols, CA) and Ciprofloxacin (Hospira INC., USA).

Rat Islet Isolation

In brief, 15mL Collagenase type XI at a concentration of 2.2 mg/mL (Sigma, MO) was injected via the common bile duct into the pancreas and digested in a 37ºC water bath for 15 min[74,79]. The digested tissue was then purified by density based gradients (Mediatech Inc. Herndon, VA) through centrifugation for 15 minutes at 640 g. The purified islets were placed in RPMI solution containing 10 percent fetal calf serum (FBS), and 1% penicillin-streptomycin (Invitrogen, NJ) with glutamine, for 24 hrs at 37ºC. All procedures conducted in accordance with guidlines approved by the UIC Office of Animal-Care and Institutional Biosafety Committee[79].

Mice Islet Isolation

0.375 mg per mL Collagenase enzyme (Roche, Applied Science, IN) was dissolved in HBSS (Mediatech Inc. VA), and injected via the bile duct for pancreatic distention[74,79]. After excision, the pancreata were digested in 15 mL conical tubes at 37°C for 11 min, gently shaken, and washed in HBSS solution. Density based gradient (Mediatech Inc., VA) was used for islet

purification[74,79]. Islets were then placed in RPMI solution 1640 containing 10 percent FBS at 37°C.

Hypoxia Treatment

Human islet hypoxia was achieved by pelleting. In brief, 2,000 IEq of human islets placed into a 1.5 mL tube with 1 mL culture media and then pelleted by brief centrifugation of the cells for 5 s at a speed of 1,000 rpm. All islets were maintained in a pellet for a period of 30 min at 37°C. Post-pelleting, the islets were transferred to a six-well plate with 2.5 mL of additional culture media and immediately cultured with fluorescent dyes for viability.

Encapsulation in Ca^{2+}/Ba^{2+} Alginate Microbeads

Briefly, 1 mL of 2.0% (w/v) alginate (NovaMatrix, Sandvika, Norway: 63–67% G, MW 200 – 240 kDa) in 0.3 M mannitol (pH 7.2-7.4) was loaded into a 5 mL syringe[74]. Isolated islets were then added to the syringe constituting a final suspension of 1.8% (w/v) alginate and islet solution. This suspension was dripped using a syringe pump and an electrostatic microbead generator (7 kV, flow: 10 ml/hr per 0.35 mm needle) over a period of 5 min, resulting in alginate microbeads of 400 – 550 μm in diameter in a gelling solution (50 mM CaCl2 and 1 mM BaCl2, pH 7.2-7.4). The microbeads were stirred in the gelling bath for another 5 min to ensure that the gel was saturated[74]. The alginate microbeads were then washed and cultured in RPMI containing 10% FBS and 1% penicillin/streptomycin (Invitrogen, NJ) for 24 hrs culture at 37ºC and 5% CO_2.

Design Idea and Trapping Principle of the Microfluidic Array

This microfluidic array is a three-layer, poly-dimethylsiloxane (PDMS) device. The cell array is designed based on the hydrodynamic trapping principle (figure15), which was first described by Tan and Takeuchi[72] with some dimensional modifications in consideration of capsule size range (400-550 μm). The top layer consists of four areas: 1.) an inlet channel for islet cell loading and fluid delivery (2 mm in diameter); 2.) a serpentine channel (width = 575 mm and height =600 mm) to facilitate cell loading by dampening pressure and arranging particles prior to the trapping of microencapsulated islets; 3.) a capsule-trapping array composed of square-wave shaped

loop channels superimposed onto a straight channel. An array of U-cup shape kinetic pockets along the straight channel is designed to trap the microcapsules. The U-cup diameter of the pocket is 550 μm and has a depth of 450 μm. There is an exit flow at the apex of the U-cup with a reduction in width (175 μm). When flow carries a particle to the junction between the U-cup and loop channel, the flow encounters less resistance in the straight channel through the unoccupied cup. As a particle is trapped in this cup, the resistance is increased in the straight channel and the flow is redirected into the loop channel. This flow then carries subsequent particles towards the next trap, iterating the trapping downstream throughout the device. 4.) finally, there is an outlet for collecting flow waste. The middle layer of this device is a 100 μm gas-permeable PDMS membrane layer for oxygen control. The bottom layer is a gas channel for delivery of various oxygen concentrations (2 mm inlet diameter and 300 μm in height).

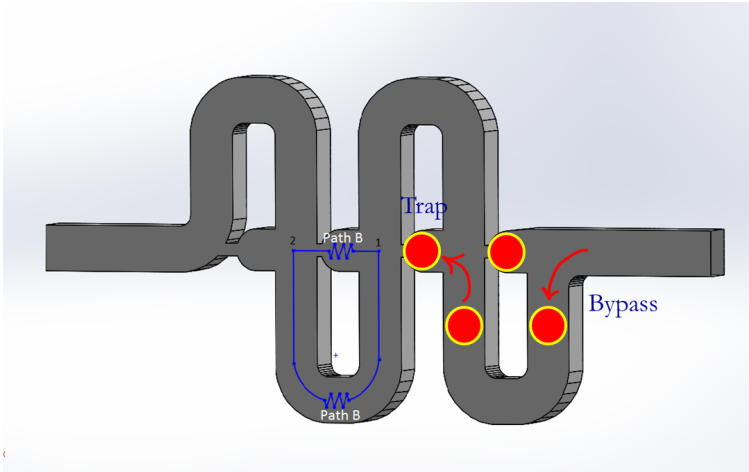

Figure 15. Schematic representation of trapping mechanism for trapping microcapsules.

Calculation of Pressure Drop for Designing Microchannel Geometry

In order to optimize the trapping efficacy for microcapsules, flow resistance of the straight and looped channels were calculated using the Dary-Weisbach equation[72], which was modified by Poiseuille's Law for a rectangular channel. After simplification, the following expression was used for resistance:

$$\Delta P = \frac{C(\alpha)}{32} * \frac{\mu L Q P^2}{A^3} \qquad \text{Equation 1}$$

were α is the aspect ratio, L is the length.

With no particles trapped, the straight channel and the loop channel share the same pressure input. If the resistance for the straight channel is less than that of the loop channel, then the volumetric flow will be greater, allowing a particle to be directed into the U-cup pocket.

$$\frac{Q_1}{Q_2} = \frac{C_2(\alpha_2)}{C_1(\alpha_1)} * \frac{L_2}{L_1} * \left(\frac{P_2}{P_1}\right)^2 * \left(\frac{A_1}{A_2}\right)^2 = \frac{C_2(\alpha_2)}{C_1(\alpha_1)} * \frac{L_2}{L_1} * \left(\frac{W_2 + H}{W_1 + H}\right)^2 * \left(\frac{W_1}{W_2}\right)^2 > 1 \qquad \text{Equation 2}$$

W_2 / W_1 are two important design parameters that determine the capture efficiency when the channel height is constant. For higher capture efficiency, it is desirable to maximize L_2 / L_1 and minimize W_2 / W_1; however, there are constraints in determining these dimensions. The width of path 1 (W_1) should be smaller than the diameter of the capsules in order to be an effective trap. On the other hand, the width of path 2 (W_2) and the channel height (H) should be larger than the capsule diameter to allow for continuous flow without clogging. Our geometry is designed to be efficient at trapping capsules with diameters of 400 μm to 550 μm. Based on the calculation, the device geometry was derived as shown in table 1 to trap encapsulated islets.

Table 1. Geometry of the microfluidic array for microencapsulated pancreatic islets.

	Width (μm)	Height (μm)	Length (μm)
Top Layer: Perfusion Channel Path 1	175	600	75
Top Layer: Perfusion Channel Path 2	575	600	5000
Middle Layer: Gas Membrane	N/A	100	N/A
Bottom Layer: Gas Channel	N/A	300	N/A

Computer Simulation

To better understand the flow behavior inside microfluidic chip and finalize the optimal design for microfluidic chip, a simulation modeling was carried out using COMSOL 4.4 (COMSOL Multiphysics, Sweden).

Device Fabrication

All microfluidic devices were made using photolithography. All steps are described in figure 16.

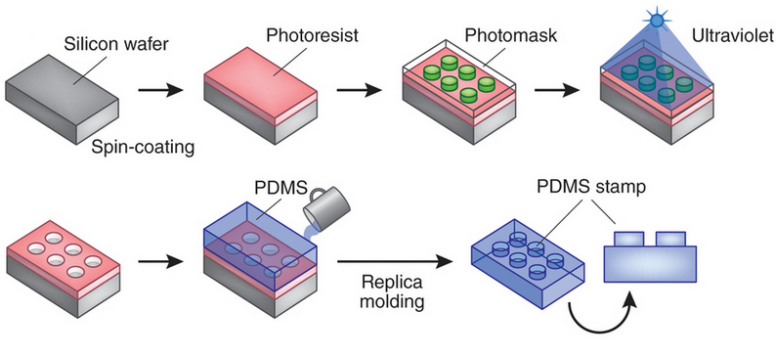

Figure 16. Photolithography steps Adopted from reference 70.

Device Fabrication Project 1

The components were first cleaned with scotch tape. Then, the liquid channel layer and the gas permeable component were bonded (figure 17) after surface exposure to oxygen plasma and annealed on a hotplate at 80ºC for 1 hr while pressed with a 1 kg weight. Next, a cork-borer (gauge 11) was used to puncture inlet and outlet holes for the liquid and gas channels. Finally, the gas channel layer exposed to oxygen plasma was bonded to the other side of the gas permeable PDMS and annealed on a hotplate at 80ºC for 1 hour while pressed with a 1 kg weight.

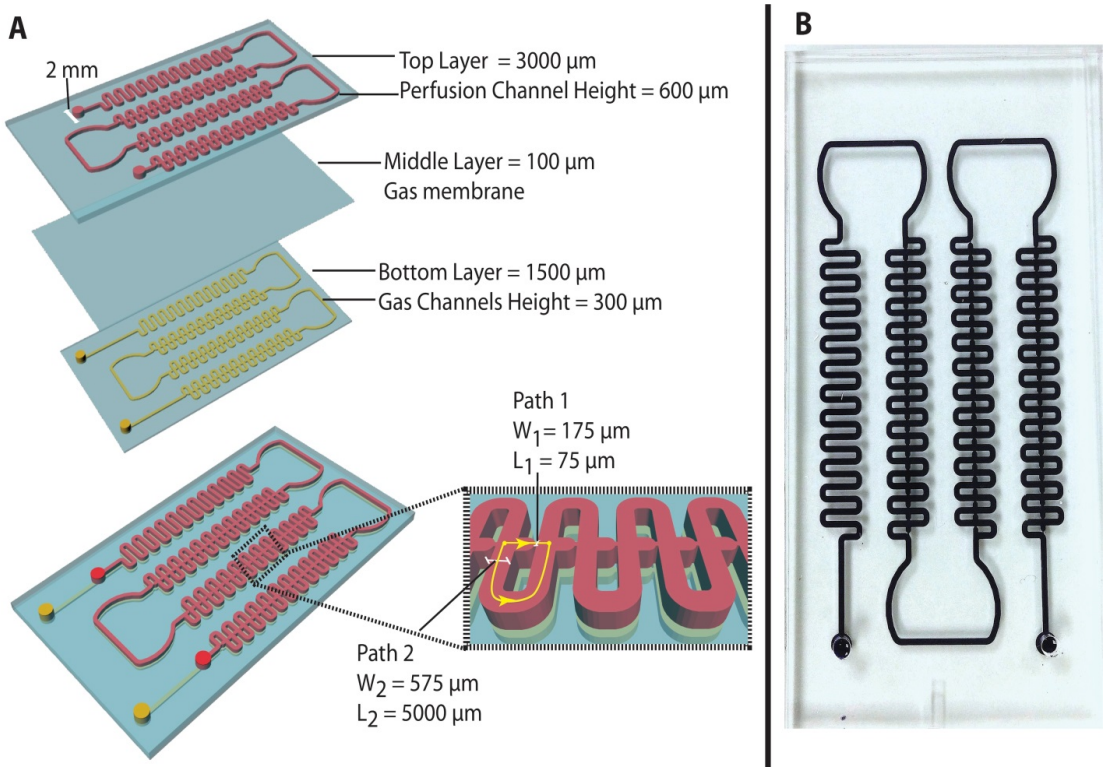

Figure 17. Schematics and photoimage of the three-layer microfluidic array: A. schematics of the microfluidic islet array and structure dimension and B. photoimage of the microfluidic array.

Device Fabrication Project 2

The array device (figure 18) was designed in AutoCAD and fabricated using photo-lithography.

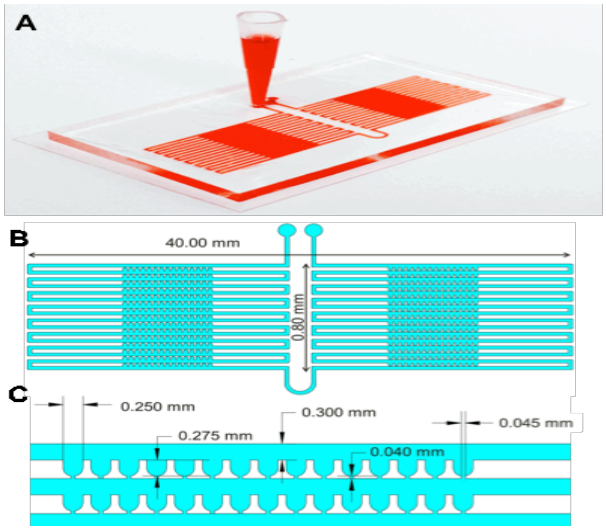

Figure 18. Microfluidic islet array. A. Photo image of the microfluidic islet array. B. Schematic of the microfluidic islet array. C. Geometrical dimension of the microfluidic islet array.

The PDMS mixture was cured for 2 hours at 80ºC. Next, a cork-borer (gauge 11) was used to puncture inlet and outlet holes for the inlet and outlet ports. After preparation of the PDMS component was finished, the device was assembled. The PDMS component was first cleaned with scotch tape. Then, PDMS component was bonded to thin coverslip (60 x 24 mm and 0.13 mm in thickness) after surface exposure to oxygen plasma and annealed on a hotplate at 80ºC for 1 hour while pressed with a 1 kg weight.

Device Fabrication Project 3

Three-layer devices (figure 19) were made by photo-lithography. The upper PDMS layer was fabricated with a 3D printed mold of 2mm thick (Makerbot 3D printer). The middle layer was prepared using 2mm punchers (Harris Uni-Core™). 20 holes were made in series with 1mm distance in between.

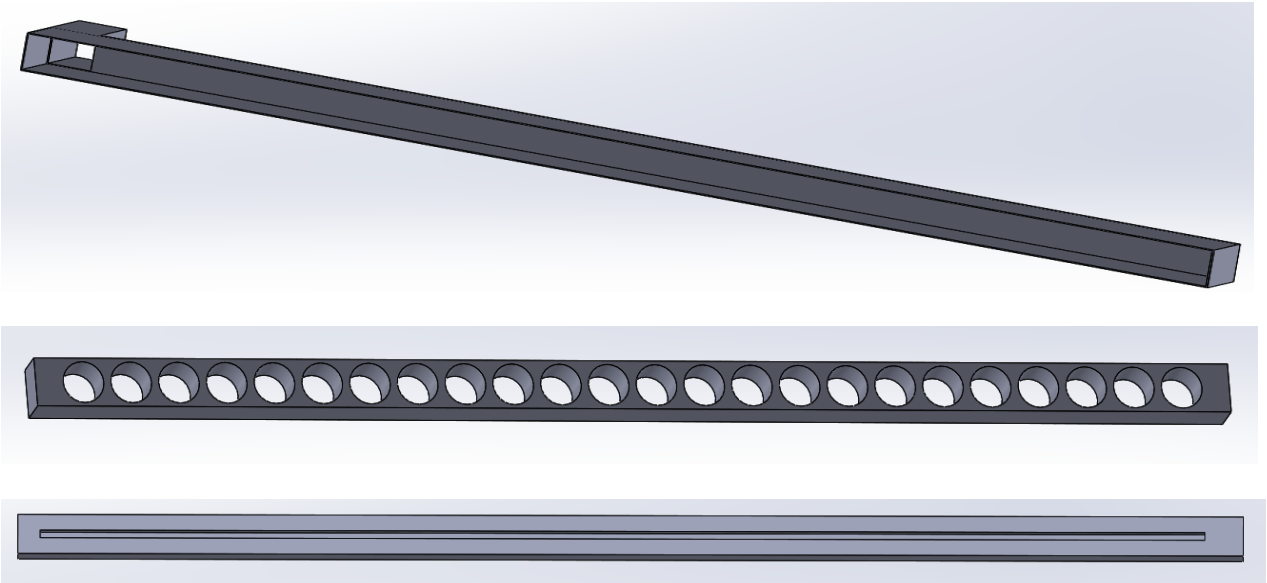

Figure 19. Three layers of the microfluidic device used for trapping macrocapsules.

Device Fabrication Project 4

3D Printed Device Fabrication and Microfluidic Chip

An iPhone frame and lens holder was designed using Autodesk. The part desined in CAD software and sent for fabrication to the Bioengineering Department at University of Illinois at Chicago. A Makerbot 3D printer was used and resin was used as the material. The microfluidic chip was designed in AutoCAD and fabricated using photolithography as described previously.

Fluorescence Imaging

In brief, islets were cultured with 5 μM Fura2 and 3μM Rho123 for 25 min in KRB2 solution. Details are explained in each section in results.

Confocal Imaging and Data Analysis

Islets were stained with CellTracker Green CMFDA for live cells (Invitrogen, USA), and propidium iodide (PI, Invitrogen, USA) for dead cells.

.

Microfluidic Assay

All MFD assays is explained in detailed in each project.

Statistical Analysis

Two-tailed unpaired t-tests were performed for pairs of data and two-way ANOVA were performed for multiple comparisons with the corresponding control group. P-values <0.05 were considered significant. Standard error bars were used in the appropriate figures. The programming software GraphPad Prism was used to make all statistical calculations.

Chapter III. Project 1 Results and Discussion

I have used some major parts of one of my published papers with the permission from the publication which is included in Appendix 4.

As described in introduction, islet transplantation is a promising therapy for patients with Type I diabetes mellitus (T1DM). Islet transplantation provides tight glycemic control without the need for exogenous insulin. However, islet transplantation requires immunosuppression that has unwanted side effects for both the patient and islet graft. The immunoisolation of islets in microcapsules has been heavily investigated to avoid immunosuppression. If successful, this strategy would have a significant impact on islet transplant outcomes. Despite initial promising results in both small animal and nonhuman primate transplant models, only short-term and partial graft function have been achieved in clinical trials[81,82]. Several factors have been proposed to be responsible for graft loss of microencapsulated islets: insufficient material biocompatibility, limited immunoprotective properties, inadequate permissibility of nutrient, hypoxia, and suboptimal insulin release[83,84]. While research has focused heavily on material biocompatibility and immune-protection, a comprehensive understanding of physiological or pathophysiological changes of microencapsulated islets is often constrained due to the availability of research tools. Functionality of microencapsulated islets is typically determined using glucose static incubation (GSI), where microencapsulated islets are challenged with glucose and the “bulk” insulin secreted is then quantified using enzyme-linked immunosorbent assay (ELISA). However, most of these assays are either static or examine a single parameter at a time and hence cannot be used to fully investigate the complexity of physiological and pathophysiological changes of encapsulated islets. In this project, we describe a microfluidic array based on the same principle, which allows for the entrapment and positioning of microencapsulated islets in an array. Furthermore, the device can be used to perform real-time fluorescence imaging of key insulin stimulation-secretion coupling factors at the single encapsulated islet. An oxygenation channel was then integrated to study the pathophysiological

changes under hypoxia, one factor proposed to contribute to the graft failure of microencapsulated islet. This work establishes a novel and reliable approach to perform high-content analysis of islet cells in the field of microencapsulation and islet transplantation.

Device Oxygenation Capability and Validation

An optical oxygen sensor was used to measure the oxygen level in the microfluidic array device. The oxygen probe uses photoluminescence-quenching of a ruthenium compound to detect oxygen molecules and has a reaction time of 15-20 s in gaseous phase and 30-45 s in aqueous media. Two-point sensor calibration was carried out according to the manufacturer's instructions, with 5% CO2/95% N2 and 21% O2/5% CO2 as references for 0% O2 and 21% O2, respectively. Oxygenation efficacy in the microfluidic channel was evaluated in both gaseous (diffused) and aqueous (dissolved) modes (figure 20 and figure 21).

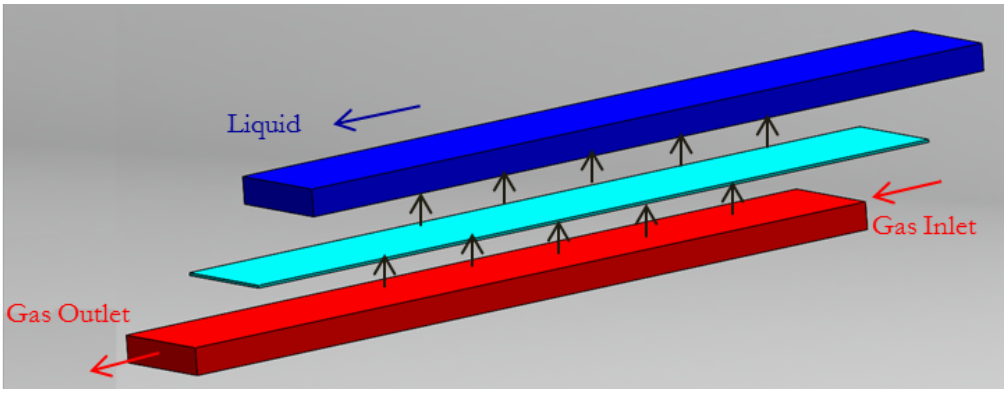

Figure 20. Schematic of gas diffusion mechanism in microfluidic device.

In both modes, the optical sensor was placed inside the microfluidic device with or without liquid and then various concentrations of oxygen in either a cyclic pattern of 5 and 21% O2 or a step-down pattern of 21-10-5-1% O2 were injected through the gas channel at a pressure of 2 psi.

In diffusive mode, as shown in figure 21A and 21B, the device was capable of creating and maintaining the targeted oxygen concentrations with high consistency. In cyclic oxygenation protocol (21-5-21%), the time needed to switch from 21% to 5% oxygen concentration was less than 40 s as was the reversion back to 21% from 5%. Equally important, both concentrations

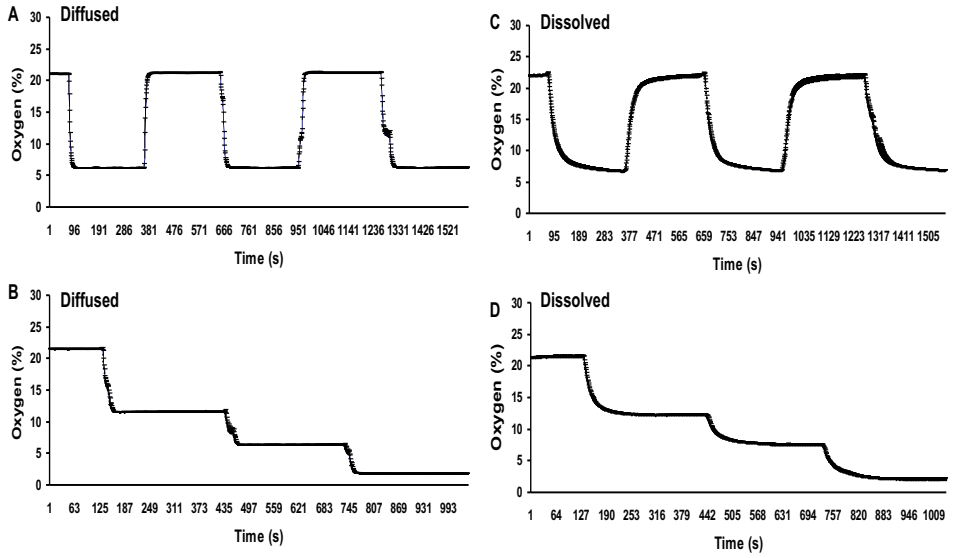

Figure 21. Characterization of device oxygenation in the microfluidic islet trapping array

were able to be well-maintained overtime (21.21% ± 0.05 and 6.22% ± 0.03). Similarly, the time needed to change from one oxygen concentration to another in step-down protocol was also less than 40 s and again was well-maintained overtime (21.33% ± 0.04, 11.53% ± 0.05, 6.33% ± 0.02, and 1.77% ± 0.02, respectively).

In dissolved mode shown in figure 21C and 21D, the time needed to switch from 21% (22.07% ± 0.13) to 5% (6.83% ± 0.08) was approximately 120 s, that was longer than in the diffusion mode, similar to the observation made in our previous published device 21. Similarly, the time needed to change from a particular oxygen concentration to another in the step-down protocol was less than 120 s and was stably maintained (20.87% ± 0.06, 11.63% ± 0.03, 6.45% ± 0.03, and 1.68% ± 0.03, respectively). It is worth noting that the oxygen sensor used in the oxygen evaluation has a measuring delay-time of 15-20 s in gas and 30-45 s in aqueous media. In reality, the oxygenation time is probably much faster than what was observed. Additionally, the exact concentrations of the oxygen tanks used in this study did not precisely correlate with the manufacturers labels and there was a 0.3-1.0% variation in the concentration.

Device Preparation and Cell Loading

The microfluidic array was first prepared by flowing 100% ethanol for 5 min through the device to prevent potential bubble formation and then rinsed with distilled water thoroughly. Before loading cells, the device was filled with Krebs-Ringer buffer (KRB) containing 2 mM glucose and then positioned on a glass heating stage at 37ºC. In order to allow high trapping efficacy and minimize shear force on microcapsulated islets, both islets and fluids containing insulin secretagogues were delivered into the device using a hydrostatic pressure-driven method. First, a 1 mL pipette tip was inserted into the inlet and filled with KRB2 up to 50 mm in height (50 mm higher than that of the outlet) while the outlet was clamped. The microencapsulated islets were hand picked under a dissecting microscope using a P20 pipette and transferred into the loading pipette. The outlet was then unclamped, which allowed the fluid and capsules in the inlet to flow

into the device by gravity. Using this method, one hundred capsules were arrayed in less than 30 s.

Evaluation of Flow Dynamics

COMSOL flow-velocity results within the microchannel and the region of the capsule immobilization site using a 2D simulation are shown in figure 22 with a close-up view of the velocity distribution and velocity streamlines around the trapping site (U-cup shape kinetic pockets). A laminar inflow boundary condition with a flow rate of 250 μL/min was applied to the device inlet and the boundary condition at the outlets was assigned with a pressure of 0 Pa. As observed from the simulation results, the highest flow velocity was located in the capsule immobilization site, while there was a decrease in flow-velocity from the trapping site to the loop channel. From the close-up view (figure 22), the velocity streamlines indicate that there is a partially diverted liquid into the immobilization site generated by a hydrodynamic force and would allow capsules to flow towards the immobilization sites. A particle occupying the U-cup pocket increases the flow resistance that allows flow to bypass the U-cup pocket and direct into the loop channels as shown in the 2D simulation of figure 22.

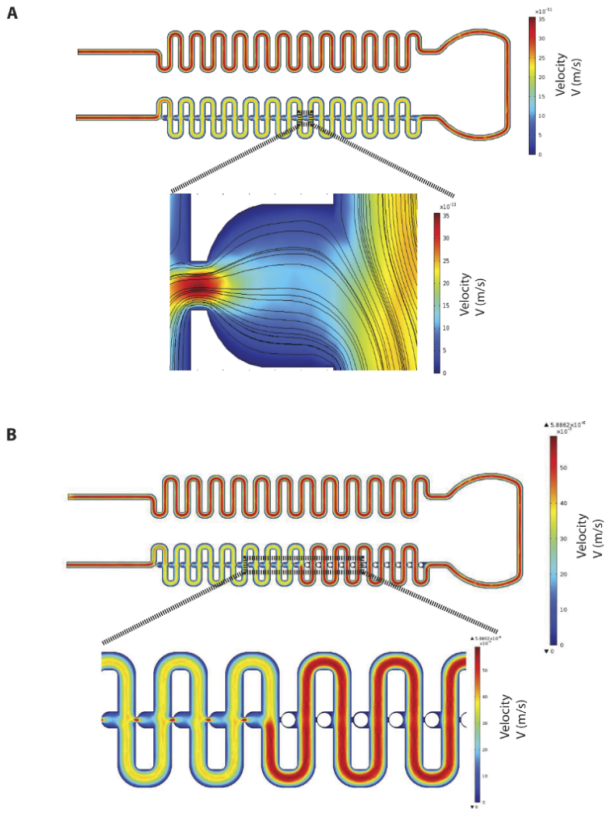

Figure 22. Characterization of microfluidic islet trapping array fluid dynamics: A. 2D CFD simulation of flow-velocity inside microchannel and region of capsule immobilization site and a close-up view of the velocity distribution and velocity streamlines around the trapping site and B. 2D CFD simulation of flow-velocity inside microchannel and capsule immobilization site when the immobilization site is occupied.

Loading and Trapping Efficacy of Microcapsulated Islets

Microfluidic arraying through differential fluidic resistance has been proven highly reliable and efficient in literature[79]. Additionally, this passive trapping mechanism is less sensitive to flow fluctuations caused by either spontaneous gas bubbles or switching of solutions. Our design for hydrodynamic confinement of microencapsulated islets was based on the same principle. As shown in figure 23, both artificially created air bubbles and empty alginate capsules (D = 500 μm) were successfully arrayed in the microfluidic array device with a high trapping efficiency (~ 99%). In figure 23C and 23D, it was shown that the microcapsulated human islets were also precisely positioned in the trap sites without any deformation of the capsules. Furthermore, the trapped microencapsulated islets could be easily retracted (released) for further analysis such as immunohistochemistry by flow inversion.

Comparable to previously reported hydrodynamic traps, the device design allows for a high trapping efficacy for microencapsulated islets with a specific size of 400-550 μm in diameter. Additionally, the device fabrication is straightforward in comparison to well-established methods. It has to be noted that the insertion of a serpentine channel, before the trapping area, greatly facilities the loading mechanism and increases the trapping efficacy as well as the hydrostatic-driven feed without the need of syringe pumps. Shear stress is considered a major concern when designing a hydrodynamic trap. Since shear stress scales linearly with the velocity, the hydrostatic-driven feed used for the capsule loading greatly reduces this shear stress as indicated with the normal morphology of the microcapsule.

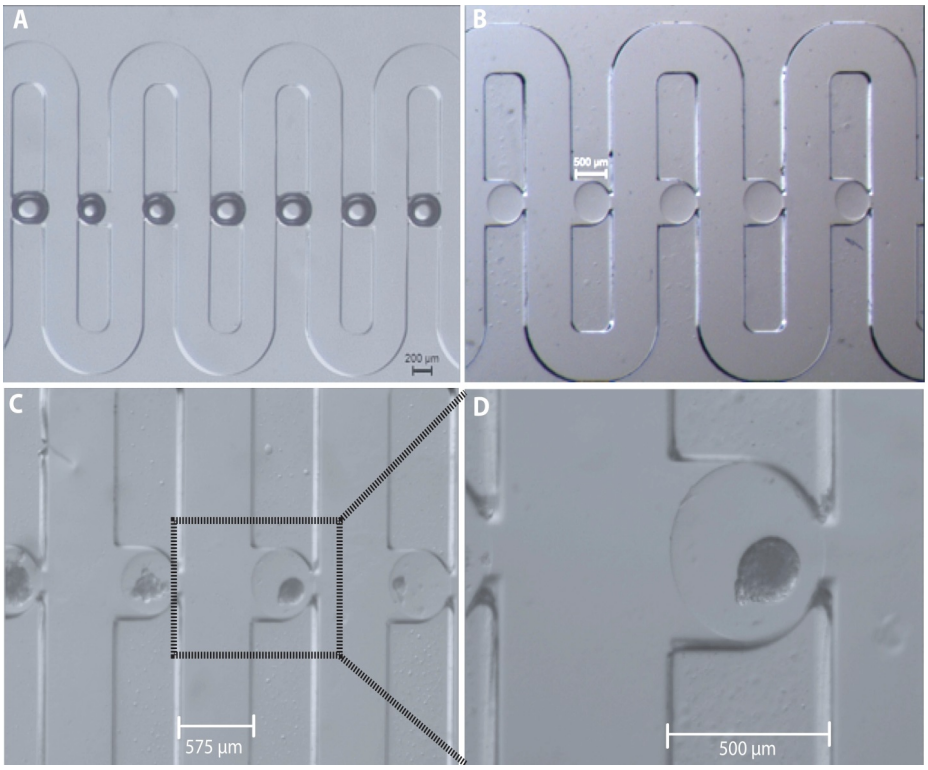

Figure 23. The trapping and immobilization capability of the microfluidic array: A. array of artificial air bubbles, B. array of empty microcapsules (500 µm size), C. array of microencapsulated human islets (500 µm), and D. close-view of single microencapsulated human islet.

The Responses of Microcapsulated Islets to Insulin Secretagogues under Normoxia Are Heterogeneous

The dynamic visualization of physiological and pathophysiological changes in individual encapsulated islets has clear advantages over existing “static and bulk” assays and can provide detailed spatiotemporal information of those changes in a quantified manner. The microencapsulation process is a very complex, multi-step process. Each manipulation step may be stressful and even detrimental to the viability of an islet. The current standard assay to determine the function and viability of a microcapsulated islet is glucose static incubation for bulk insulin secretion and inclusion/exclusion dyes for viability with limited limitations of the physiological changes of microencapsulated islets. Using this microfluidic-based islet-trapping array, we can observe individual islet responses to secretagogues, focusing on several key insulin stimulator-secretion coupling pathways.

Insulin secretion is controlled by β- cell electrical activity, metabolic events, and ion signaling, all of which display biphasic and pulsatile kinetic profiles in response to changes in blood glucose. The direct measurement of the stimulator-secretion coupling pathways has been traditionally applied for understanding islet physiology and function.

In response to 25 mM glucose and KCL challenges under normoxia, intracellular calcium changes of the microcapsulated human islets were shown to be heterogeneous, with a maximal mean of 5.91% ± 2.98 (max:13.2% and min:3.03%) (figure 24). In response to 30 mM KCl stimulation, intracellular calcium changes of microcapsulated rat islets also displayed a heterogeneous pattern with a maximal mean of 6.25% ± 1.68 (max: 9.14% and min: 4.14%) (figure 25). The changes in autofluorescence of NAD(P)H for the microencapsulated human islets in response to 25 mM glucose also showed a heterogeneous response with a maximal mean of 3.24% ± 2.10 (max: 6.91% and min: 0.62%) (figure 26).

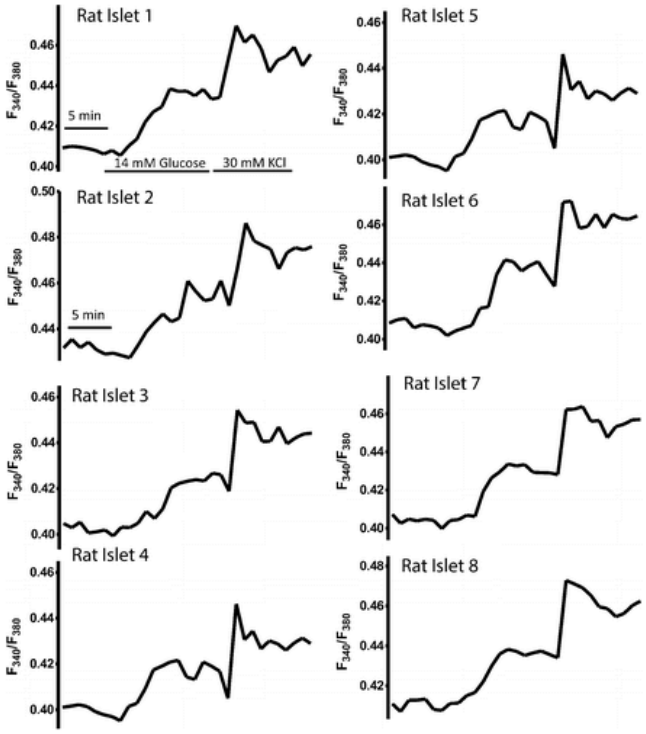

Figure 24. Microencapsulated rat islets show a heterogeneous $[Ca^{2+}]_i$ changes in response to glucose and KCl under 21% O2. Eight representative traces of $[Ca^{2+}]_i$ of microencapsulated rat islets in response to 14 mM glucose followed by 30 mM KCl under 21% O2 (n = 65 from three experiments).

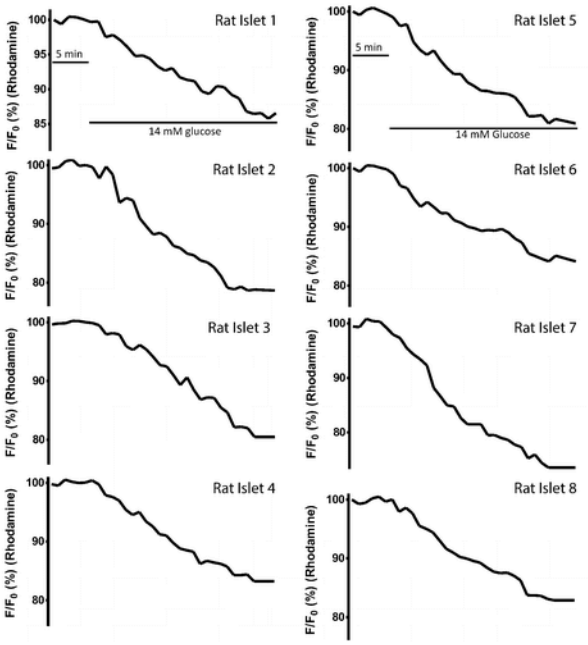

Figure 25. Microencapsulated rat islets show heterogeneous ψ_m changes in response to glucose and KCl under 21% O2. Eight representative traces of ψ_m changes of microcapsulated rat islets (n = 65 from three experiments).

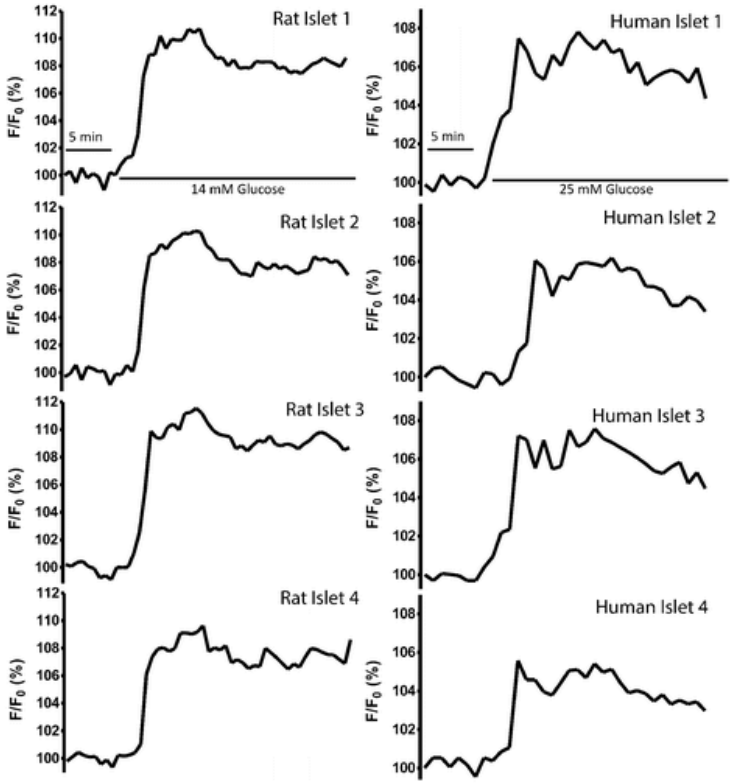

Figure 26. Microencapsulated rat and human islets show heterogeneous NAD(P)H changes of in response to glucose under 21% O2. (A) Four representative traces of NAD(P)H changes of microcapsulated rat islets in response to 14 mM glucose (n = 65 from three experiments). (B) Four representative traces of NAD(P)H changes of microcapsulated human islets in response to 25 mM glucose (n = 65 from three experiments).

In comparison to the static and "bulk" measurement, the microfluidic-based individual islet array integrated with live-cell imaging techniques can provide more detailed spatiotemporal information of an individual islet response to extracellular stimulators. In addition to serving as a tool to determine the functionality and viability of microencapsulated islets, the array may also be used in the future as a screening tool for therapeutics and biologics in order to improve the survival and function of microencapsulated islets.

Hypoxia Impaired the Function of Microcapsulated Islets

As explained before, Hypoxia is widely considered to be one of the primary factors associated with the functional loss of encapsulated islets and has also been linked to the immunoisolation failure of microencapsulation devices. Isolated islets are exposed to a hypoxic environment at many levels[85-91] : (i) isolated islets have a disrupted vascular network and are dependent on diffusion for their oxygen supply, (ii) the microcapsulation process further aggravates islet hypoxia by both preventing islet revascularization that normally occurs and increasing the oxygen diffusion distance due to capsule sizes that are often larger than 500 μm; (iii) the intraperitoneal space, a common transplant site for microencapsulated islets, has a low oxygen tension, where the O2 concentration is approximately 3.5-5% O2, which is significantly lower than the in situ pancreas[90]. In addition to loss of function, hypoxia may facilitate the attraction of macrophages and subsequently cause cell overgrowth on the microcapsule surface[86,91]. However, the in vitro study of the pathophysiological changes of microencapsulated islets is limited by the availability of suitable tools as described before.

Here, we investigated the impact of hypoxia on intracellular calcium signaling, mitochondrial potential changes, and NAD(P)H levels of microencapsulated islets.

Stimulation and oxygenation protocols used in hypoxia studies were listed as follow.

Table 2. Stimulation and oxygenation protocols as shown.

Step Number	Condition	[Glucose] (mM)	O2 (%)	Time (min)
1.	Control-LOW	2	21	10
2.	Control-High	25	21	15
3.	Return to baseline	2	21	15
4.	Hypoxia 1 pre-culturing	2	10	15
5.	Hypoxia 1 stimulus	25	10	15
6.	Return to baseline	2	21	15
7.	Hypoxia 2 pre-culturing	2	5	15
8.	Hypoxia 2 stimulus	25	5	15
9.	Return to baseline	2	21	15
10.	Hypoxia 3 pre-culturing	2	1	15
11.	Hypoxia 3 stimulus	25	1	15
12.	Return to baseline	2	21	15

As shown in figure 27A and 27B, the calcium influx changes of microencapsulated human islets in response to 25 mM glucose challenges were oxygen concentration-dependent and were inhibited by hypoxia. Under normoxia, the average intracellular calcium concentration increased by 10% ± 4.16 in response to 25 mM glucose stimulation, while hypoxic concentrations decreased intracellular calcium responses: 8.19% ± 2.5 in 10% O2, 3.57% ± 1.18% in 5% O2, and 1.70% ± 0.64 in 1% O2. ($p < 0.01$ when 21% vs. 5% and 1%, as well as $p < 0.01$ when 10% vs. 5% and 1%). Similarly, mitochondrial potential changes, often used as an indicator of cellular energetic status, were also inhibited in an oxygen concentration-dependent manner (21-10-5-1%): 17.23% ± 3.13, 8.83% ± 3.53, 6.40% ± 2.56, and 4.09% ± 1.37 ($p < 0.01$ when comparing 21% vs. 10, 5, and 1%; $p < 0.01$ when comparing 10% vs. 5% and 1%) as shown in figure 28A an 28B.

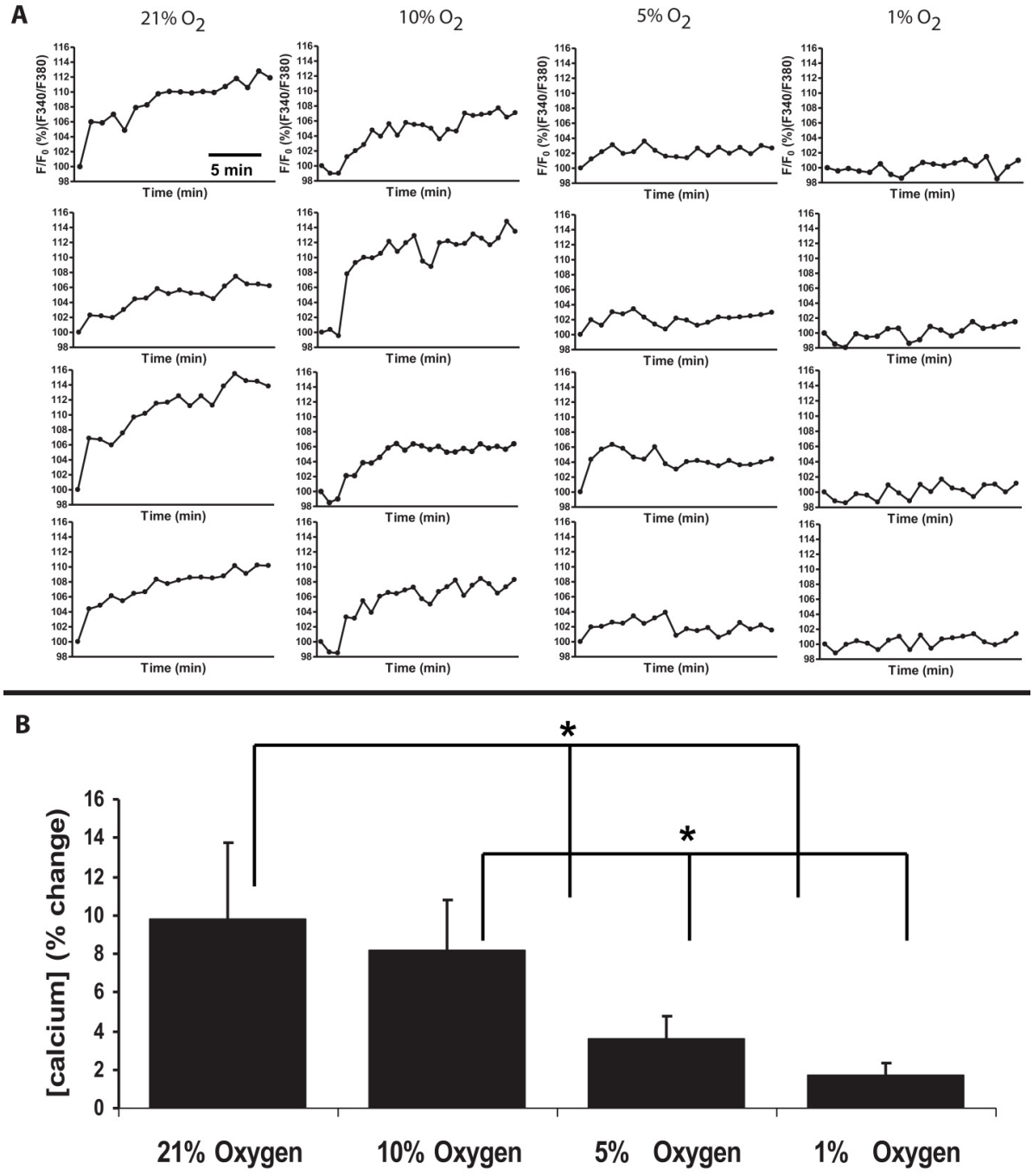

Figure 27. Hypoxia impaired $[Ca^{2+}]_i$ signaling of microencapsulated human islets. A. Representative traces of $[Ca^{2+}]_i$ of microencapsulated human islets in response to 25 mM glucose under hypoxic concentrations. B. Statistical analysis of $[Ca^{2+}]_i$ changes under hypoxic concentrations (n = 65 from three experiments. *$p < 0.001$).

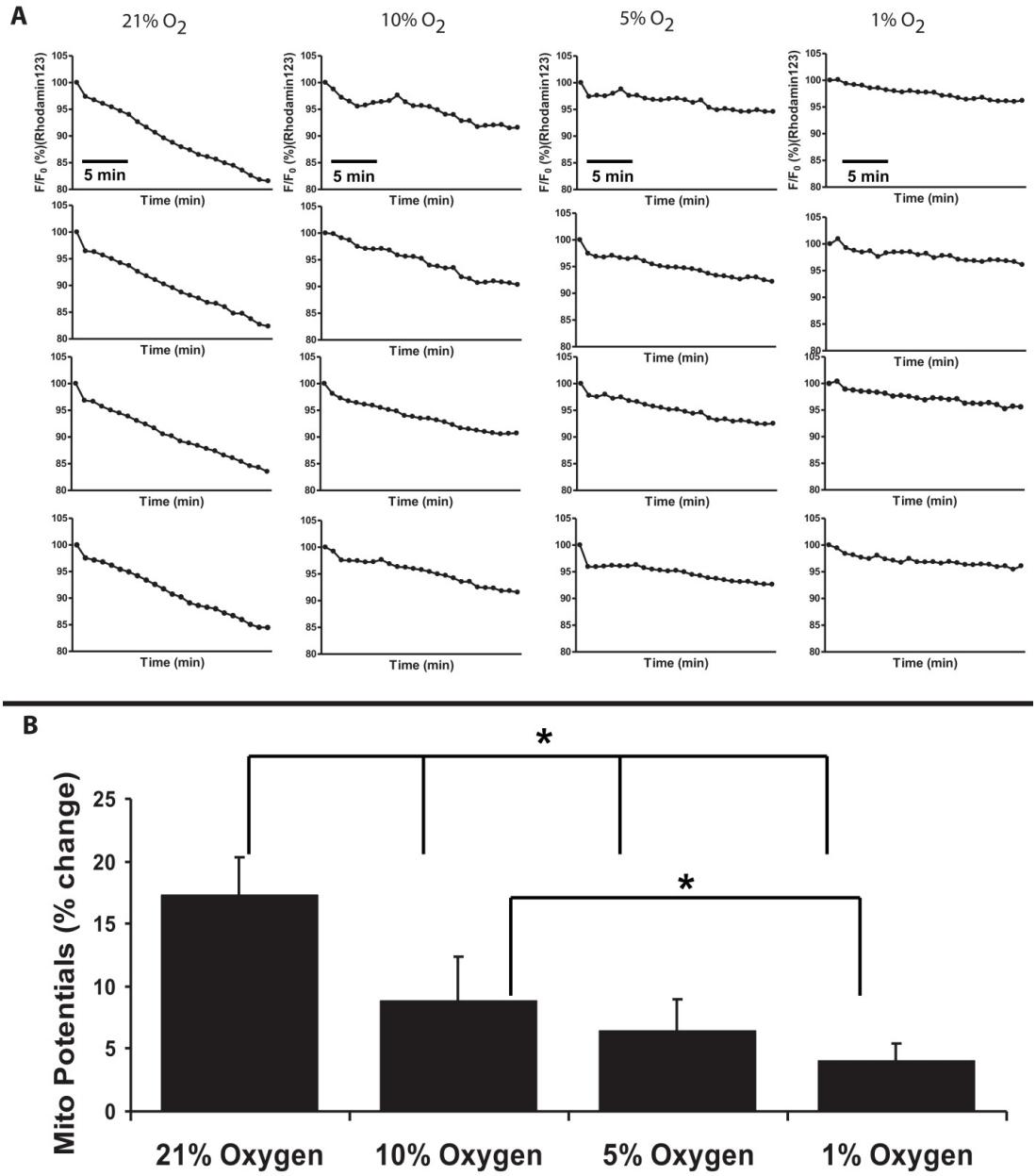

Figure 28. Hypoxia impaired ψ_m changes of microencapsulated human islets. A. Representative traces of ψ_m changes of microencapsulated human islets in response to 25 mM glucose under hypoxic concentrations. B. Statistical analysis of ψ_m changes under hypoxic concentrations; n = 65 from three experiments for each oxygen condition; *$p < 0.001$, **$p < 0.01$.

Glucose-stimulated insulin secretion is a complex metabolic process. NAD(P)H imaging by autofluorescence is a quantitative measure of the combined redox signal from NADH and NADPH (referred to as NAD(P)H). The glucose-induced β- cell redox potential can be used for the measurement of nutrient-stimulated NAD(P)H responses with excellent spatiotemporal resolution. In β- cells, NAD(P)H transfers its reducing power to the electron transport chain, resulting in ATP synthesis that further influence ATP-dependent insulin secretion. Therefore, a direct measurement of NAD(P)H in response to glucose will provide insight into glucose metabolism and mitochondrial functionality. Under normoxia, the mean NAD(P)H % change increase of the microencapsulated human islets in response to 25 mM glucose was 6.43% ± 4.05 (figure 29A and 29B). Under severe hypoxia (1% O2), the glucose-induced increase NAD(P)H level was significantly inhibited (1.87% ± 1.75; $p < 0.01$). Moderate hypoxia (10% and 5% O2) also depressed the nutrient-induced NAD(P)H levels (10% O2: 4.65% ± 2.17 and 5% O2: 4.79% ± 2.84), but the changes did not reach statistical significance when compared to 21% normoxia ($p > 0.05$).

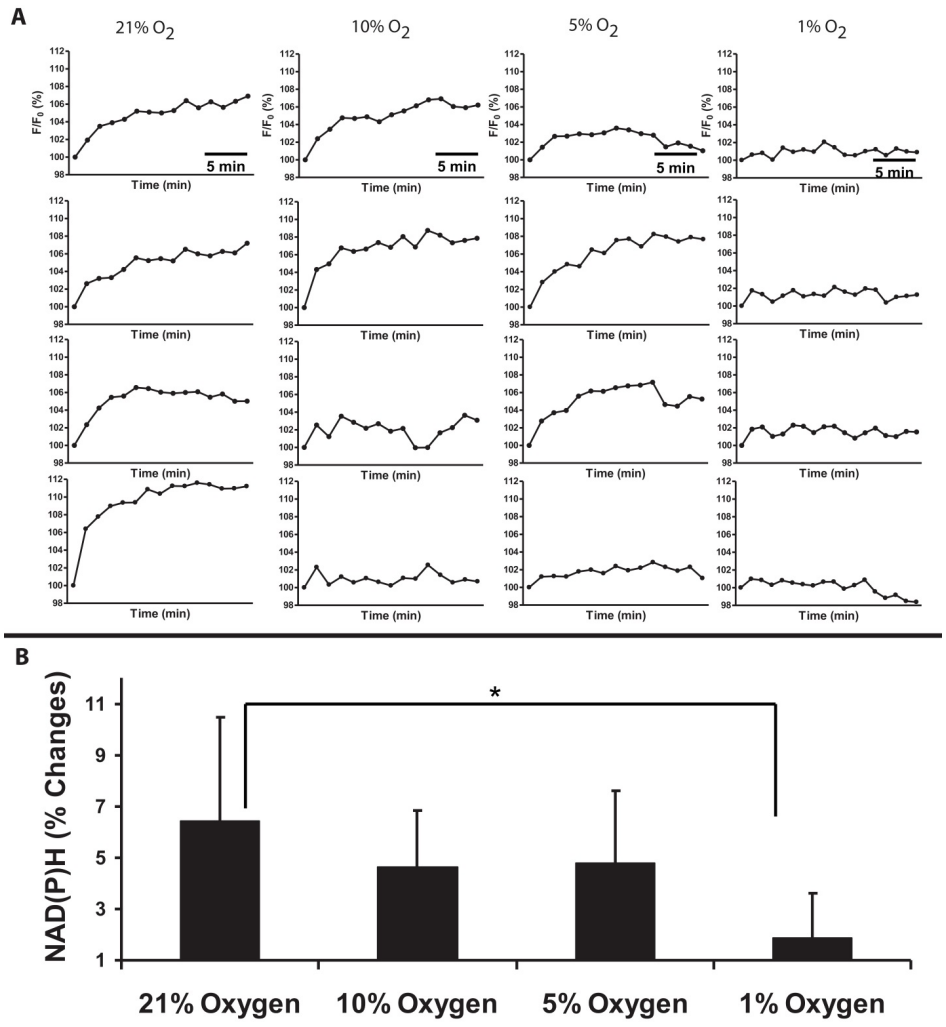

Figure 29. Hypoxia impaired NAD(P)H levels of microencapsulated rat islets: A. representative traces of NAD(P)H of microencapsulated rat islets in response to 14 mM glucose under hypoxic concentrations and B. statistical analysis of NAD(P)H changes under hypoxic concentrations; n = 65 from three experiments.

Conclusion

Herein, the presented novel microfluidics can trap individual microencapsulated islets and allow for real-time live cell imaging. This device was achieved a high trapping efficacy for microencapsulated islets (~99%) with minimal physical stress on islets. The integration of the gas modulation allowed for rapid membrane-diffused oxygenation of islets at the microscale-level. This provided a practical tool to study hypoxia on microencapsulated islets. We further investigated the hypoxia on β-cells and demonstrated that $[Ca^{2+}]_i$ signaling, ψ_m, and β-cell redox status in response to insulin secretagogues were impaired under hypoxia. This is first report on real-time multiparametric imaging of metabolic changes of microencapsulated islets under hypoxia, a feat previously unachievable using either hypoxic chambers or existing microfluidic devices. In the future, this device may be used to improve the long-term function and viability of microencapsulated islets prior to transplantation, such as intermittent hypoxia preconditioning (IH) or chemical preconditioning. In a previous study, we successfully applied IH preconditioning (1 min/1 min 5–21% cycling for 1 h) to diminish hypoxic injury on naked islets and improved islet insulin secretion. Additionally, this array based study laid out the groundwork for future applications in the area of islet microencapsulation and may potentially act as a screening tool for therapeutic screens. One application is to study capsule–islet–macrophage interaction. Although hypoxia is one of many reasons for islet graft failure, immune rejection and surface overgrowth (fibrosis) on microcapsule can also play a role. Therefore, it would be interesting to utilize the hypoxic device with modifications to understand capsule–islet–macrophage interactions. One potential limitation of NAD(P)H measurement has to be noted that using the current filter setting, it may be difficult to completely separate NAD(P)H autofluorescence from other cellular autofluorescence such as cellular flavins and non-redox responsive signals as indicated by a previous study.

Chapter IV. Project 2 Results and Discussion

I have used some major parts of one of my published papers with the permission from the publication which is included in Appendix 4.

In previous studies, several microfluidic devices have been developed, mainly used as islet microperifusion apparatus. These devices have been successfully integrated with live-cell multimodal imaging methods for dissecting islet cell physiological behavior[92-95]. One of the major challenges of these devices is the limited number of islets that can be assessed in a single device. Another challenge is the inability to satisfactorily assess the heterogeneous property of individual islets, especially when testing a large quantity of islets simultaneously. Examination of heterogeneous properties at the individual islet level often provides more detailed physiological or pathophysiological information than averaging-based population methodologies. For example, it will enable better understanding of human islet functionality from a reasonable sample size and will provide a better predictive value for islet transplant outcomes if many individual islets can be individually assessed instead of averaging a bulk response. In this report, the aim is to develop a new MFD islet array chip, based on the hydrodynamic trapping mechanism, for investigating the complexity of physiological or pathophysiological behavior of individual pancreatic islets in a larger islet population. Furthermore, we aim to explore the feasibility of array-based cellular analysis to provide more informative data on pancreatic islets and to act as a platform to evaluate antidiabetic drugs. The microfluidic platform developed in this project is a one-layer poly-dimethylsiloxane (PDMS) device as shown in figure 18. The array device utilizes the hydrodynamic trapping principle to immobilize individual islets in traps. The principle was first described in 2008 by Tan and Takeuchi[72]. The hydrodynamic trapping mechanism offers higher resolution confinement

of single microscale and nanoscale particles in low viscosity aqueous solution within the microfluidic device. In a previous study, we used the same principle to design a microfluidic device for evaluating encapsulated islets. Designing a microfluidic array for islets using the hydrodynamic trapping principle was a challenge and required careful design consideration due to the various sizes of islets. The final design of the device contains an array consisting of 2 rows and 10 columns. In each column, there are 15 trapping sites that amounts to a total of 300 traps. The trapping site design is a U-cup shaped pocket, superimposed onto a loop channel that is used for delivery of fluids and islets. The U-cup pocket is 250 μm in diameter and 275 μm in depth. There is a cross-flow channel at the apex of the U-shape cup pocket with a subsequent reduction in the width to 45 μm. These design parameters allow for the capture of approximately 95% of the islet cell population. Additionally, the width and height of the loop channels are 300 μm and 250 μm, respectively, which allows the islets to move freely along the channel without clogging. For the purposes of this study 100 traps were reviewed as our imaging system was unable to scan the entire array at a fast enough pace to use more traps.

Based on the flow resistant difference between the U-shape cup and the loop channel, the flow encountered less resistance in the unoccupied U-shape cup. When solution takes an islet to the gap between the U-shape cup and the main channel, an islet becomes trapped in the U-shape cup due to the flow resistant difference between the U-cup and the loop channel. The trapped islet results in increased resistance in the U-cup and the flow is then redirected into the loop channel. This flow carries subsequent islets towards the next empty trap, iterating the trapping downstream throughout the device.

Islet Loading, Stimulation, and Retrieval

Prior to islet loading, 100% ethanol was passed through the microfluidic array for 5 min to prevent potential bubble formation. The array was then rinsed with Krebs-Ringer buffer (KRB) containing 2 mM glucose (KRB2) for 2 min while positioned on a glass heating stage at 37°C. In

order to achieve a high trapping efficacy with minimal shear force exerted on the islets, both islets and solutions containing insulin secretagogues were delivered into the device using a hydrostatic pressure-driven method (figures 30A-30C).

Briefly, a 1 mL pipette tip was inserted into the inlet and the tip filled with KRB2 up to 20 mm in height (20 mm higher than that of the outlet), while waste tubing was clamped and placed −2 cm with respect to the plane of the chip. Islets were transferred to the loading tip via a 20 µl pipette. After loading the islets, the waste tubing was unplugged so that the solution flowed to the waste as the islet was drawn into the chip. The islets continued to move slowly into the chip by gravity. Using this method, 100 islets were arrayed in less than 60 s. For stimulation, the 1 mL pipette tip was refilled with insulin secretagogues and delivered to the islets by gravity. Post stimulation, loaded islet cells can be collected for further analysis by reversal of the flow through the outlet (figure 30D).

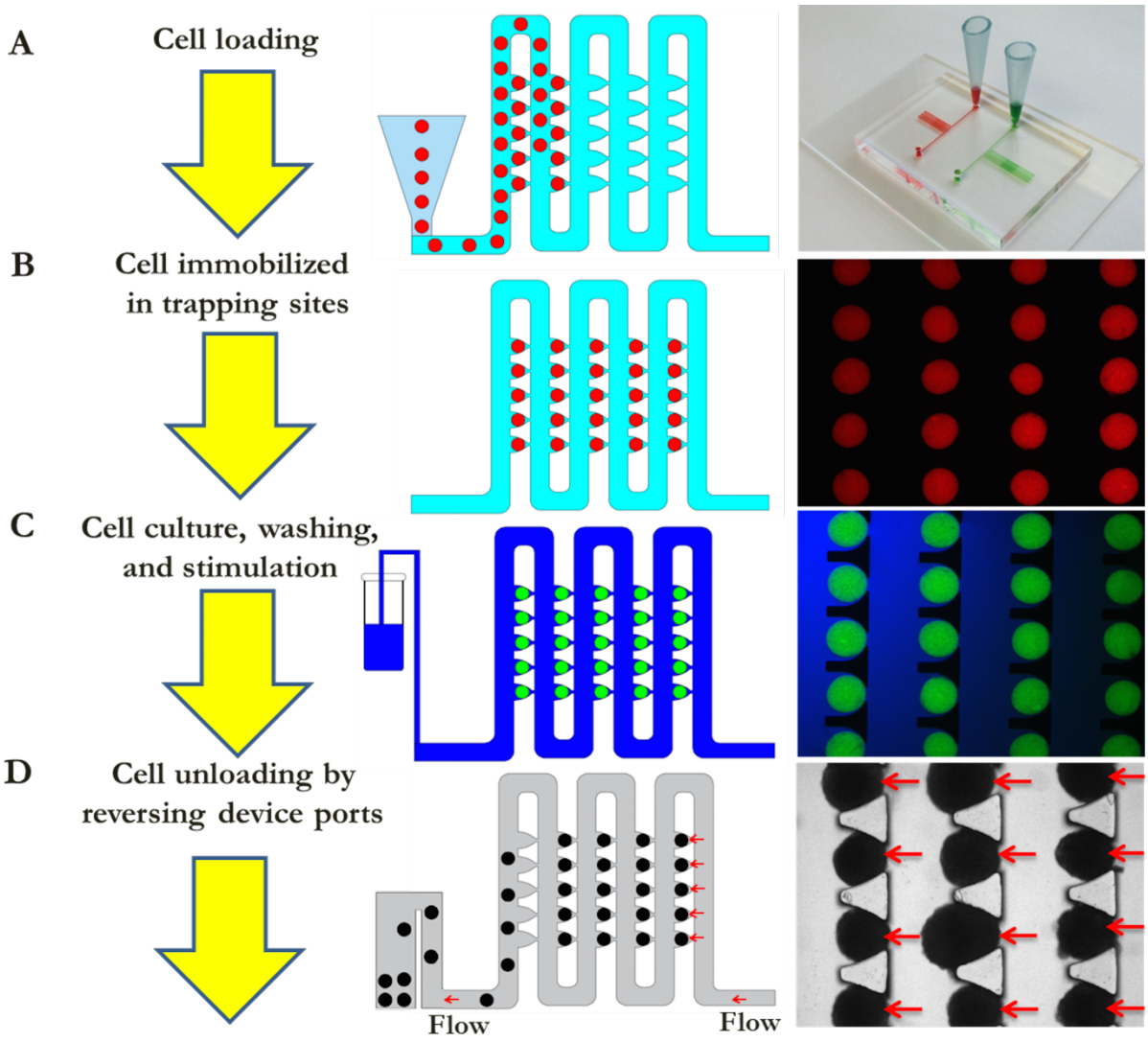

Figure 30. Islet loading, stimulation, and retrieval. (A) Schematic of islet loading and a photo image of the islet array. (B) Schematic of islet trapping and trapped fluorescence beads (200-240 μm). (C) Schematic of islet stimulation and trapped fluorescence beads (200-240 μm). (D) Schematic of islet retrieval and human islets.

Fluid Dynamic Simulation

To better understand the flow characteristics and to determine the optimal design parameters for the microfluidic array, a CFD analysis was performed using COMSOL 4.4. The COMSOL fluid-flow simulation results using a 2D model were depicted in figure 30. The pressure profile in the microfluidic channel was shown in figure 30A. It shows that the pressure decreased along the islet array, indicative of no significant counter flow. The velocity profile in the whole device presented in figure 30B indicates that velocity pattern was periodically repeated and identical in each row and column. Since the islet array had 2 identical rows and each row contained 10 columns with 15 islet traps of fixed width and height, it was expected that flow velocity should be the same as the fluid flow entered the trapping area, as well as the loop channel.

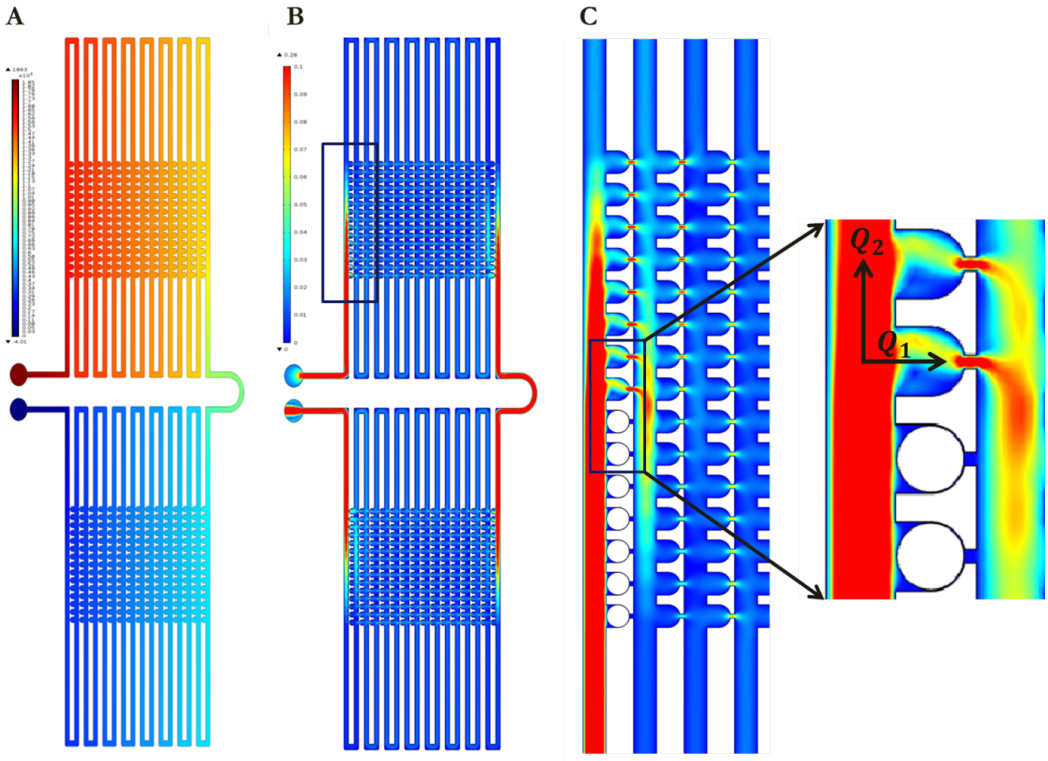

Figure 31. Computer simulation of flow dynamic. (A) Computer simulation of pressure profile. (B) Computer simulation of velocity profile. (C) Computer simulation of flow stream and velocity profile with and without particles trapping.

A close view of the velocity pattern in the trapping area is shown in figure 30C. Theoretically, close to the trapping area a particle may experience two stream flows: a partial stream flow (Q_1) directing particles into the trap site and a mainstream flow (Q_2) along the loop channel. If the Q_1/Q_2 ratio is in a proper range (>1), particles can be guided into the trapping sites and immobilized. When the trapping area was not occupied, there was a higher flow velocity at the cross-flow channel of the trapping area as expected. When the trapping area was occupied, flow velocity of the loop channel was increased resulting in moving particles into the next available trapping area. For comparison, a simulation of the velocity streamline was also conducted. As shown in the insert of figure 30C, it was observed that much of the fluid flowed into the cross-flow channel, which indicated partially diverted flow into the trapping area. This would allow particles to flow toward the trapping sites due to the hydrodynamic force. When a particle occupied the trapping area, it increased flow resistance that allowed flow to bypass the trapping area and directed remaining islets into the loop channel.

We further verified flow dynamics prior to trapping site and post trapping site in the array (figure 32A) with 2D COMSOL simulation for flow velocity measurement and fluorescence imaging using 5 μM Rhodamine 123 for flow intensity measurement. When the trapping sites were occupied by a particle, P1 (the prior to trapping site) and P2 (post trapping site) had almost identical flow velocity and flow intensity (figures 32B and 32C), while when the trapping sites were occupied, the majority of fluorescein passed through the cross-flow channel rather than down the loop channel reflected in both fluorescence velocity and intensity as shown in post trapping site designated as P_4 (figures 32B and 32C).

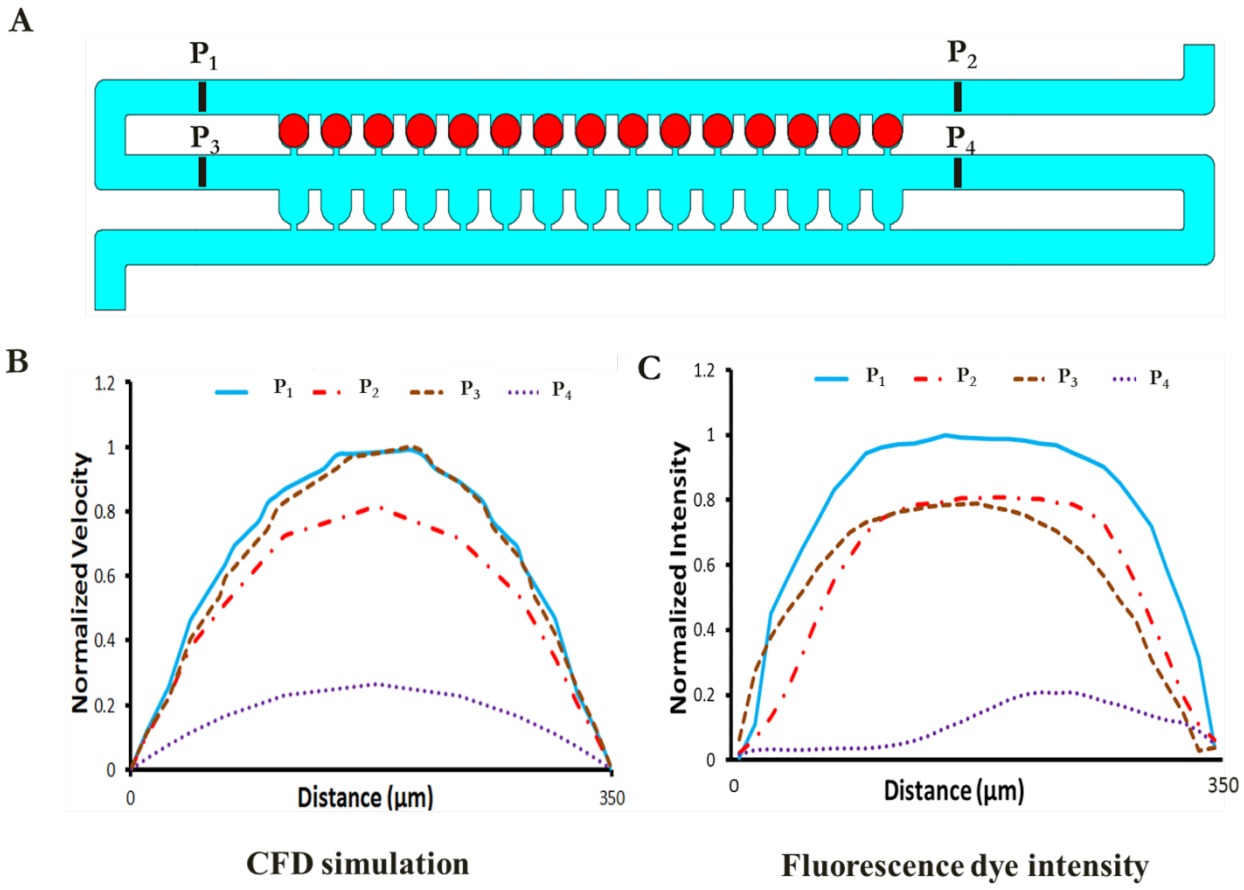

Figure 32. Computer simulation and experimental validation of flow dynamics. (A) Schematic of the microfluidic islet array. (B) Computer flow simulation for flow velocity. (C) Experimental fluorescence intensity measurement (n = 3).

Comparison of the Perifusion Chamber Device and Islet Array Device

In order to demonstrate the superior characteristics of the microfluidic array design (figure 33A), we compared it to previously designed three-layer microfluidic perifusion device (figure 33B), in which the media flow perifusates islets through a perifusion chamber[9,10]. The top-layer of the perifusion device has an inlet and an outlet with dimensions of $20\ \mathrm{mm} \times 2\ \mathrm{mm} \times 500\ \mu\mathrm{m}$. The perifusion chamber is $7\ \mathrm{mm}$ in diameter by $3\ \mathrm{mm}$ in depth with a total liquid volume of $115\ \mu\mathrm{L}$. The bottom layer of the chip is made of an array of small round wells ($500\ \mu\mathrm{m}$ by $150\ \mu\mathrm{m}$) for islet immobilization (figures 33D and 33F). The array of 500 μm wide by 100 μm deep circular wells has proven quite effective for islet immobilization up to a flow rate of $1.0\ \mathrm{ml/min}$, with minimal physical stress; however efficient interaction of islets sitting in the circular wells with the microenvironment is dependent on flow dynamics in the perifusion chamber. Since the perifusion chamber is relatively large and falls in the macroscale category, it makes it challenging for effective mixing and diffusion, especially at a lower flow rate. While a higher flow rate ($> 2.0\ \mathrm{ml/min}$) may cause islets to disgorge from the circular wells.

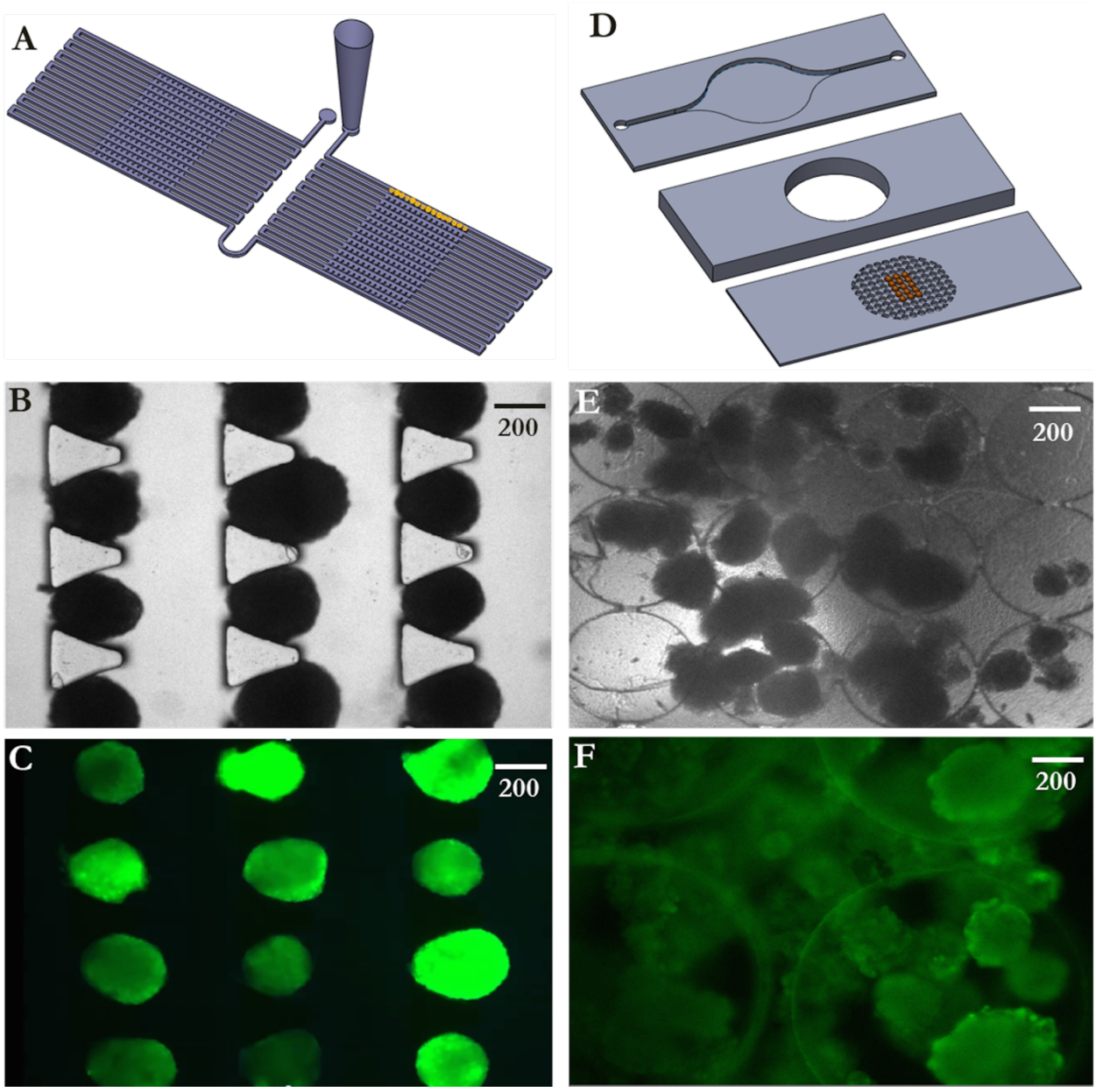

Figure 33. Microfluidic islet array and microfluidic perifusion device. (A-C) Schematic of the microfluidic islet array, trapped human islets, and fluorescence labelled human islets. (D-F) Schematic of the microfluidic islet perifusion device, trapped human islets, and fluorescence labelled human islets.

Microfluidic devices are defined by having low Reynolds numbers and simple diffusion effectively describes the transport of diffusive species within a MFD device. Fickian diffusion law ($J = -D\frac{\partial \mathrm{C}}{\partial \mathrm{V}}$). The correlation $x^2 = 2Dt$ defines the mean square displacement of particles in regards to time. As time depends on the square of displacement, diffusion on the microscale occurs much faster than diffusion on the macroscale. Due to the small size of the islet array device (100 times smaller than the perifusion chamber device) and array format, diffusion and mixing are significantly faster and consequently more effective. Additionally, solution consumption can be reduced significantly during the experimental procedure using the newly designed device we present in this paper. The trapped islets in the array had direct and complete contact with flow independent of flow rate and the islets remained stable during dynamic perifusion with minimal movement. The previous perifusion design had a limited range of working flow rates since a slow flow rate (< 50 µL**)** prevented efficient mixing, while a higher flow rate (> 2 mL**)** disgorged many trapped islets. Additionally, the design reduced stimulation/washing times, which minimized shear stresses on islet cells. Importantly, the islet array design improved the precision and sensitivity of human islet calcium signaling by effectively detecting subtle changes such as phase 0 (figure 34B), which is often not detectable in our previous perifusion based device (figure 34A). The glucose-induced phase 0 is a gradual depolarization of the cell membrane and a decrease in intracellular calcium. Vanished (A non-detectable) phase 0 is often caused by endoplasmic reticulum stress associated with a defect of islet cell function. Compared to the perifusion chamber design, the human islets in the islet array have superior maximal $[\mathrm{Ca}^{2+}]_{\mathrm{glu}}$ response (144.2% ± 1.73 vs. 129.9% ± 2.42; $p < 0.05$) and superior maximal $[\mathrm{Ca}^{2+}]_{\mathrm{KCL}}$ response (176.2% ± 1.54 vs. 166.9% ± 2.13; $p < 0.05$) (figures 6C and 6D). Additionally, the array provided a faster transition from phase 0 to phase I (Slope: 14.84 vs. 2.65).

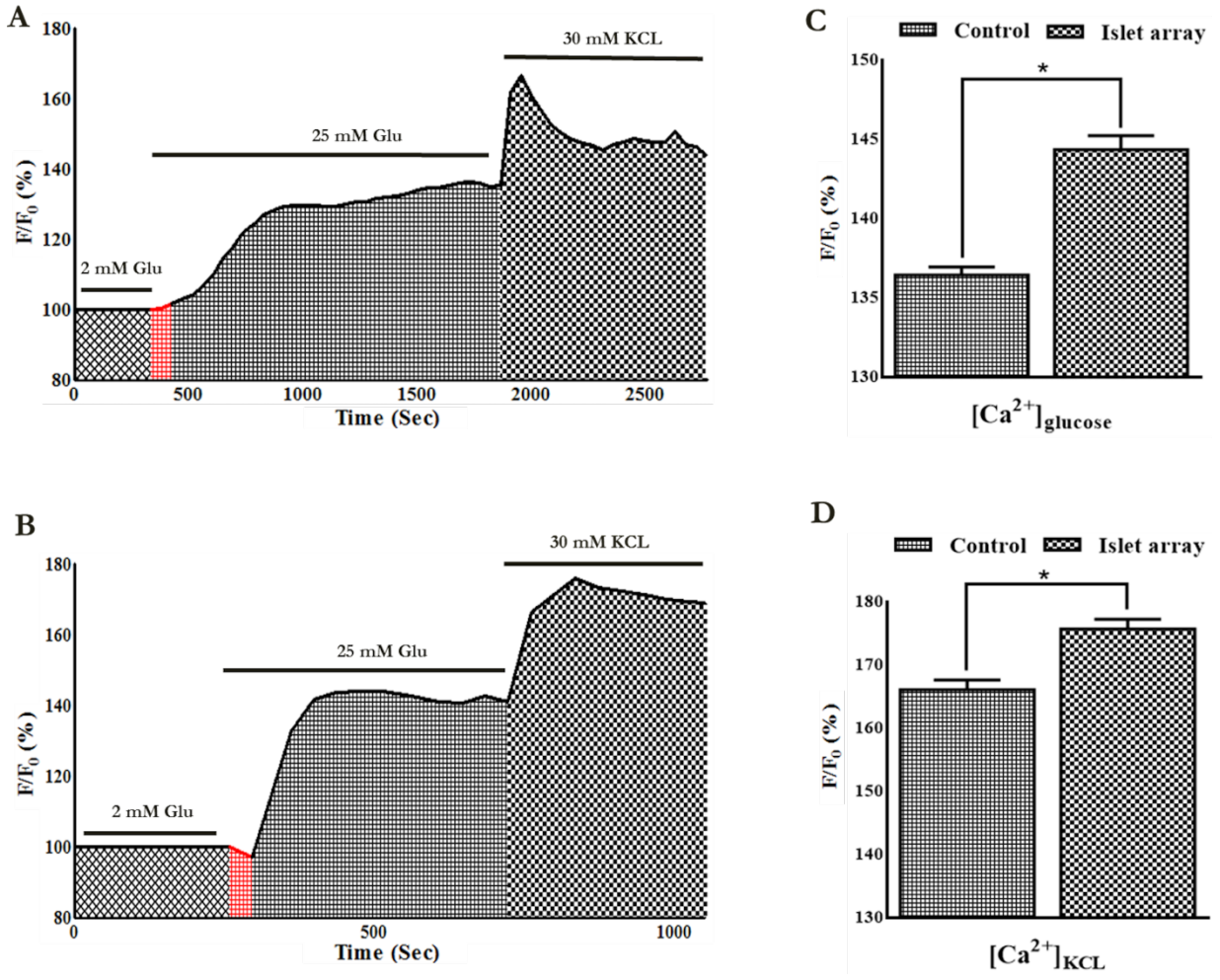

Figure 34. Comparison of intracellular calcium signaling between the perifusion based device and the islet array. (A) Intracellular calcium profile of human islets trapped in the perifusion device in response to 25 mM glucose and 30 mM KCl (n = 3, 300 islets from 3 different preparation). (B) Intracellular calcium profile of human islets trapped in the array device in response to 25 mM glucose and 30 mM KCl (n = 3, 300 islets from 3 different preparation). (C) Statistical comparison of intracellular calcium in response to 25 mM glucose between the perifusion device and the islet array device. (D) Statistical comparison of intracellular calcium in response to 30 mM KCl between the perifusion device and the islet array device.

The islet array increased analytical power, not only by examining 100 islets individually,

compared to 50 islets averaged in the perifusion device, but also by efficiently investigating individual islets, which was not achievable in the perifusion chamber as islets often aggregated or overlaid on each other (figures 33E and 33F). Lastly, the one-layer array device had minimized dimension allowing a much shorter stimulation protocol to achieve comparable results performed by the perifusion device (sec vs. min) and consumed much smaller liquid volume (μL vs. mL). The aforementioned advantages demonstrate that the microfluidic islet array may be applied as a new effective tool to study islet physiology, function, and therapeutic screening for anti-diabetes agents.

Optimization of Single-Islet Loading Efficiency

To allow high content, high resolution imaging of individual islets in an array, we further characterized the impact of geometries on trapping efficacy. As described previously, an islet directly prior to entering a trap experiences forces in two directions: mainstream flow (Q_2) in the loop channel that moves the islet along the loop channel and a partial stream flow (Q_1) in the cross-flow channel that pushes the islet into the trapping area. Combined effects of these two flow forces will determine the trapping efficacy of individual islets. We experimentally verified optimal geometry using varying lengths, widths, and depths of the trapping site and the loop channel (H) as shown in figure 35. When $\mathrm{Q}_1/\mathrm{Q}_2$ was equal to 5.5, a high resistance ratio led to having multiple islets per sites (figure 35A). When $\mathrm{Q}_1/\mathrm{Q}_2$ was equal to 0.7, the solution going into the gap was not enough for optimal loading (figure 35C). By modifying the resistance of the straight channel ($\mathrm{Q}_1/\mathrm{Q}_2 = 2.8$), individual islets occupancy on single trap was achieved (figure 35B). At this ratio, $99\% \pm 2.5\%$ of the sites are filled with $95\% \pm 2\%$ of the filled sites having an individual islet.

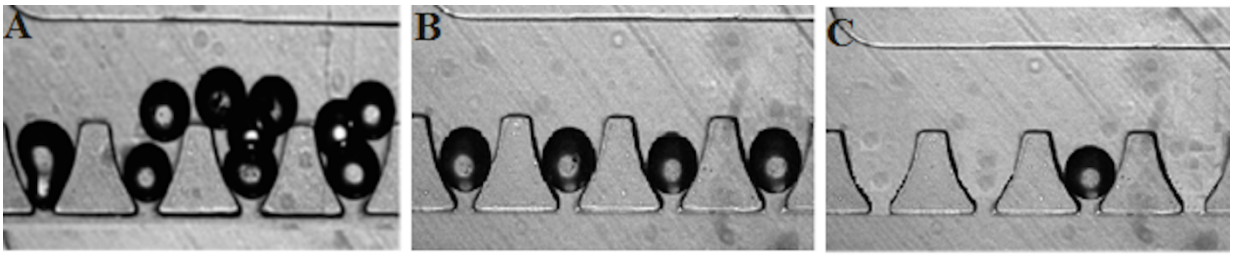

Dimension	W_1	W_2	L_1	L_2	H_1	H_2	Q_1/Q_2
Device A	55	300	50	1500	300	300	5.5
Device B	45	300	55	1200	250	250	2.8
Device C	50	300	55	800	250	300	0.7

Figure 35. Determination of optimal loading parameter. (A) Loading efficacy at Q_1/Q_2 = 5.5. (B) Loading efficacy at Q_1/Q_2 = 2.8. (C) Loading efficacy at Q_1/Q_2 = 0.7.

Two additional factors that may influence trapping efficacy are particle concentration and flow rate. Our experience showed that trapping efficacy was independent of initial particle concentration, while particle concentration only affected loading time. For the concentration of 500 islets/mL, full loading of the array took less than a minute at a flow rate of $50\ \mu L/min$. At a lower solution portion, loading islets took longer and islets tended to sit at the bottom of inlet port. In flow rate above 200 μL/min, islets would undergo shear force and pressures force which leads to islet deformation through the 45-μm narrow gaps.

Fluid Exchange Efficiency

In order to make sure we achieved a uniform solution distribution and a fast rate of solution exchange in the array channel, a fluorescent intensity experiment using FITC was carried out (figure 36). The intensity of dye was measured in different positions inside the MFD channel during the stimulation with of water. The intensity values in the graphs illustrated the capability of the array chip to exchange its solution media in about 10 seconds and the fluorescence profiles of each location were identical (figure 36). The rate of solution exchange was significantly faster as a result of small channel size and volume in comparison to our previous chamber design, which required 3 minutes to fully exchange[92]. This allows faster stimulation, shorter washing time, and improved resolution.

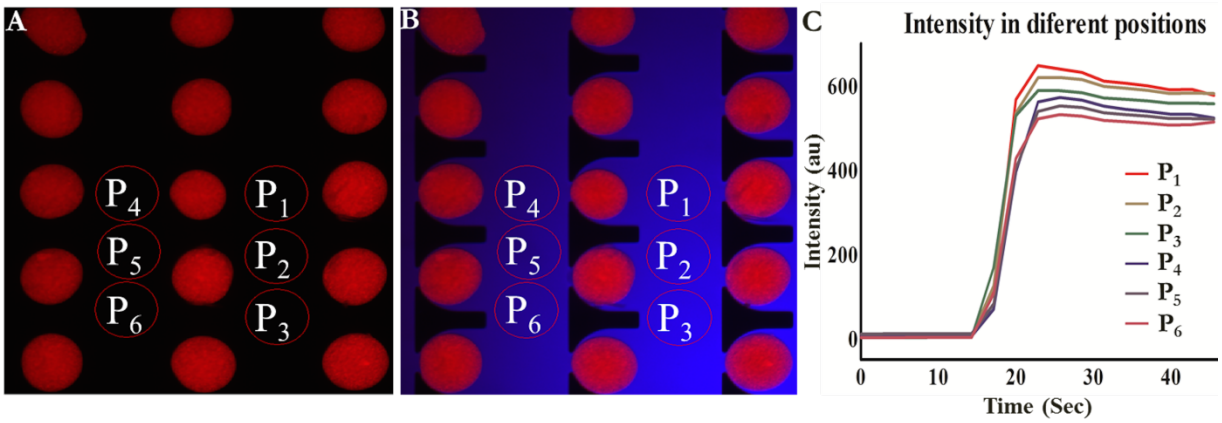

Figure 36. Fluid exchange efficiency. (A) The array loaded with fluorescence beads (200-240 μm). (B) The array loaded with fluorescence beads (200-240 μm) flushed with 2.5 μM FITC. (C) FITC intensity profiles at different locations in the array.

Microfluidic Array Serves as Islet Cell Cytometry

Flow cytometry is a technology that has had a significant impact on basic cell biology and clinical medicine. The simple rule of flow cytometry is that single cells travel in a stream of flow and interrogated in a short period of time as laser source is focused in a tiny area. Fast evaluation of large amount of cells is an advantage here which allows accurate measurements of particle/cell properties under multi-parameter and separate single particle/cell physically or biologically from bulk population to study heterogeneous populations and classification of subpopulation. Today's instruments have a capacity to measure almost all types of single cells including single islet cells; however, no such instrument for islets has been reported yet. Islets consist of a cluster of approximately $1000 - 2000$ single cells and function as a basic unit for sensing and responding to blood glucose changes. Therefore, it is more physiological relevant to analyze intact islet clusters rather than dissociated islet single cells. Another benefit of our chip is that it can be coupled with real-time monitoring of cells This can not be achived by flow cytometry. This device, allows us to collect 300 data points per time point per individual islet, and to increase throughput.

This microfluidic array can successfully capture and immobilize a large number of islets. With a low magnification optical objective, such as 10 x objective, 5 individual islets can be monitored in a field of view. Assisted by a motorized microcopy stage, we collected and analyzed 100 data points from individual islets with a 100-islet array. It is worth noting that this array could be expanded as the channel has traps to hold up to 300 particles; however, the first 100 traps were used, as there were limitations with how fast the stage could scan. These limitations could be overcome through the use of advanced stage setups. Another advantage of the microfluidic array is that it can be coupled with real-time single or multi parameter fluorescence imaging that allows for the tracking of dynamic physiological and pathophysiological behavior of islets simultaneously. This function was not achievable using our previous perifusion chamber-based microfluidic or other existing islet microfluidic devices available.

Heterogeneous Responses of Human Islet in Response to Secretagogues

Glucose-induced insulin secretion of islet cells is a complex process controlled by β- cell metabolic events, electrical activity, and ion signaling and displays biphasic and pulsatile kinetic profiles. In short, glucose catabolism generates ATP through the mitochondrial tricarboxylic acid cycle, which consequently closes ATP-sensitive K^+ channels, initiates plasma membrane depolarization, and increases $[Ca^{2+}]_i$ via voltage-dependent calcium channels. This glucose-stimulated increase in $[Ca^{2+}]_i$ triggers the fusion of insulin granules with the cell membrane and, subsequently, results in the exocytosis of insulin. The dynamic visualization of physiological changes in individual islets has clear advantages because it provides detailed spatiotemporal information in a quantified manner. For example, the human islet isolation process for islet transplantation is a very complex and multistep process. Each manipulation step may be stressful and even detrimental to islet viability and function. The current standard assay to determine function and viability of human islets provides limited information on the physiological or pathophysiological changes of the islets. Using this microfluidic-based islet-trapping array, we can observe individual human islets and focus on several key insulin stimulator-secretion coupling pathways in response to secretagogues.

Heterogeneous responses of intracellular calcium and mitochondrial potential changes from isolated human islets were shown in figures 37A and 37C. Human islets displayed heterogeneous calcium profiles in response to glucose and KCl (25 mM glucose: 144.2% $\pm$ 1.74, Max: 149.9%, Min: 139.9%; 30 mM KCl: 176.2% $\pm$ 1.54, Max: 179.1%, Min: 173.5%) and heterogeneous mitochondrial potential changes in response to glucose (25 mM glucose: 71.3% $\pm$ 2.02, Max: 76.8%, Min: 62.3%). The heat-map of calcium concentration and mitochondrial potential changes are depicted in figures 37B and 37D and provide far richer sources of data compared to bulk averaging over multiple islets.

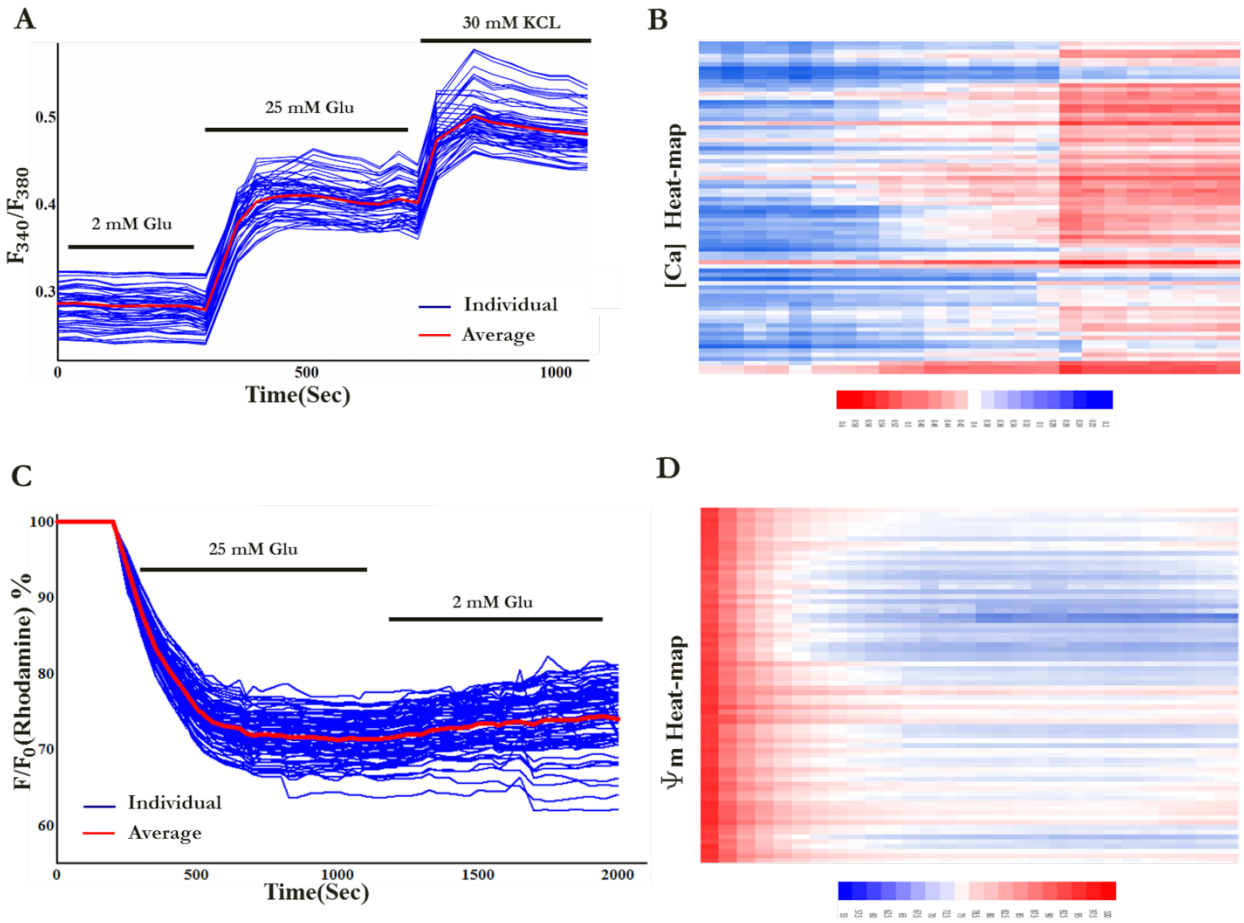

Figure 37. Heterogeneous responses of human islets in response to insulin secretion secretagogues. (A) Intracellular calcium signaling of islet cells to 25 mM glucose and 30 mM KCl (n = 100 islets). (B) Calcium concentration Heat-map of islet cells to 25 mM glucose and 30 mM KCl (n = 100 islets). (C) Mitochondrial potential changes of human islet cells to 25 mM glucose (n = 100 islets). (D) Mitochondrial potential change Heat-map of human islet cells to 25 mM glucose(n = 100 islets).

The microfluidic array clearly provides advantages over population-based approaches by providing more detailed and spatiotemporal analysis of individual islets, not only in a large cell population, but also variation values (maximal and minimal values) of individual islets, frequency of response, and percentage response profile. Additionally, the array may help to identify potential subgroups or sub phenotypes of an islet population, which is critically important for functional characterization of human islets used for islet transplantation and phenotype characterization of β- cell like stem cells in their differentiation and maturation processes.

Islet Viability Assay

It is necessary to improve islet viability assessment by increasing the speed and the precision of viability assessment using new tools and techniques. The new microfluidic islet chip proposed here can be used as a tool to perform high-resolution analysis of fluorescence labelled islets such as islet viability and cell death. Since the trapped islets in the array device are directly located on a thin coverslip (60 x 24 mm and 0.13 mm in thickness), this enables high spatial resolution imaging of islets at high magnification such as confocal microscopy (figure 38). This device also allows us to perform the assessment faster and in more automated fashion since the position and location of each trapped islet and trapping site are known therefore the imaging process can be performed in an automated way using a motorized stage. Additionally, fluorescence staining and washing processes can be performed on the chip post islet loading without any difficulty.

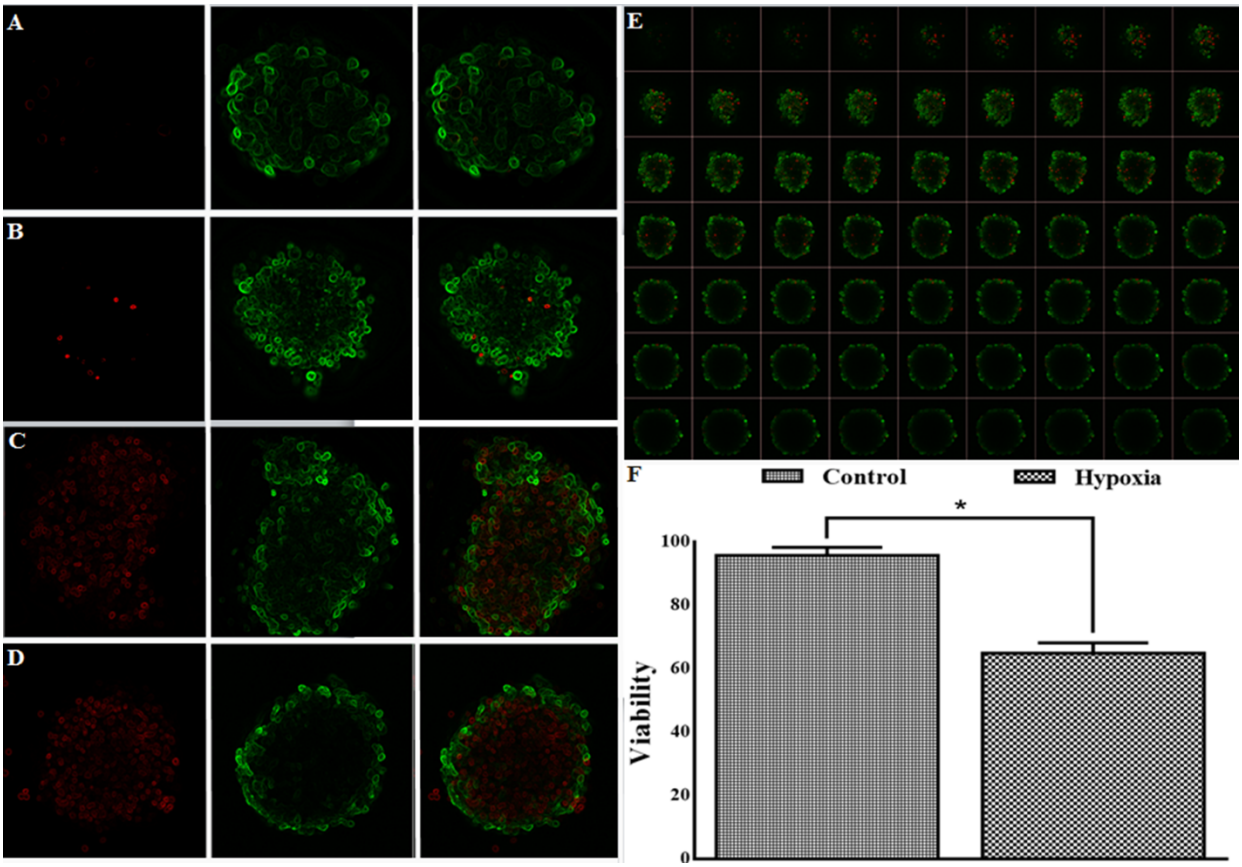

Figure 38. Confocal imaging and quantification of live-cells and dead-cells of human islets in the microfluidic array. (A and B) Representative image of the control human islets. (C and D) Representative image of the hypoxia-treated human islets. (E) Representative images of a human islet were collected at 10 μm intervals to create a stack in Z axis (63 z-slices recorded with a 20x lens). (F) Statistical analysis of human islet viability from the control islets and the hypoxia-treated islets (n = 150 each group from 3 different batch of isolated islet; * $p < 0.01$).

Figure 38 shows the results of the standard CMFDA/PI assay performed on the islets. There were 3 samples for each control and the hypoxia treated islets. Each sample contained 50 islets for each condition. Quantitative comparisons of the areas of the green and red regions showed that viability percentage of the control islets and the hypoxia treated islets was 96.1% ± 2.34 and 65.2% ± 3.21, respectively. The standard visual assessment placed the control in the 94% to 100% viability range and the treated islets in the 60% to 70%.

Percentage of viable and dead cells aggregates over the total was determined by scoring green versus red fluorescence using the ImageJ software package as described under “Experimental Procedures”. The results are representative of three independent experiments and mean ± S.D. of three independent experiments are shown in figure 38.

Conclusion

In this project, a novel microfluidic array was presented based on the hydrodynamic trapping mechanism. The unique feature of this device is the suitability of the microfluidic array for high-content and high-resolution analysis of individual pancreatic islets. We have identified key design parameters controlling the trapping efficacy of the islets. This work demonstrates the enabling capability of quantitative analysis as islet cytometry that can be readily adopted for studying islet physiological and pathophysiological changes in response to insulin stimulation-secretion cues. In contrast to existing microfluidic perifusion devices, the presented microfluidic array provides well-controlled flow dynamics with much improved flow exchange, faster flow delivery, a shortened stimulation protocol, and improved assay sensitivity and accuracy. Importantly, it is a first device that has an ability to monitor cell heterogeneity of a large population at the single islet level. The microfluidic platform presented here can be utilized for evaluation of human islet function and viability prior to human islet transplantation for Type I diabetes patients and screen potential anti-diabetes compounds. For future studies, the microfluidic system can be further optimized for the effective collection of perifusates for hormone measurements and drug screening.

Chapter V. Project 3 Results and Discussion

One area of interest for which alginate capsules have been widely studied is the immune-protection of donor islet cells[99]. Host fibrotic overgrowth of alginate microcapsules in recipient, is the main issue in the transplant of encapsulated islet cells [97,98,99,100,101]. After implantation into the transplant sites alginate microspheres initiate foreign body reactions and fibrotic overgrowth[102,103]. Recently, scientists have been demonstrating and studying the effect of the geometry of capsules on biocompatibility. In non human models, implanted spheres 1.5 mm and bigger in diameter considerably impaired recipient-body reactions in comparison to smaller diameters. These all suggest that the biocompatibility properties of spheres can be noticeably improved by changing their dimensions. In this project, a new platform has been designed, verified and tested that can be successfully applied to investigate and study the properties of 1.5mm macrocapsules and also to evaluate the functionality of islets inside these microcapsules. The device is capable of immobilizing macrocapsules for short-term and long-term dynamic and static stimulation and live cell imaging.

Trapping Mechanism

To trap and study individual macrocapsules, we designed a three layer microfluidic device, in which the middle layer of the microfluidic chip was designed with wells to hold capsules. An schematic of the device is illustrated in figure 39 along with photo-image of the chip . The macro capsule chip had one simple macro straight channel on top and a micro channel at bottom.

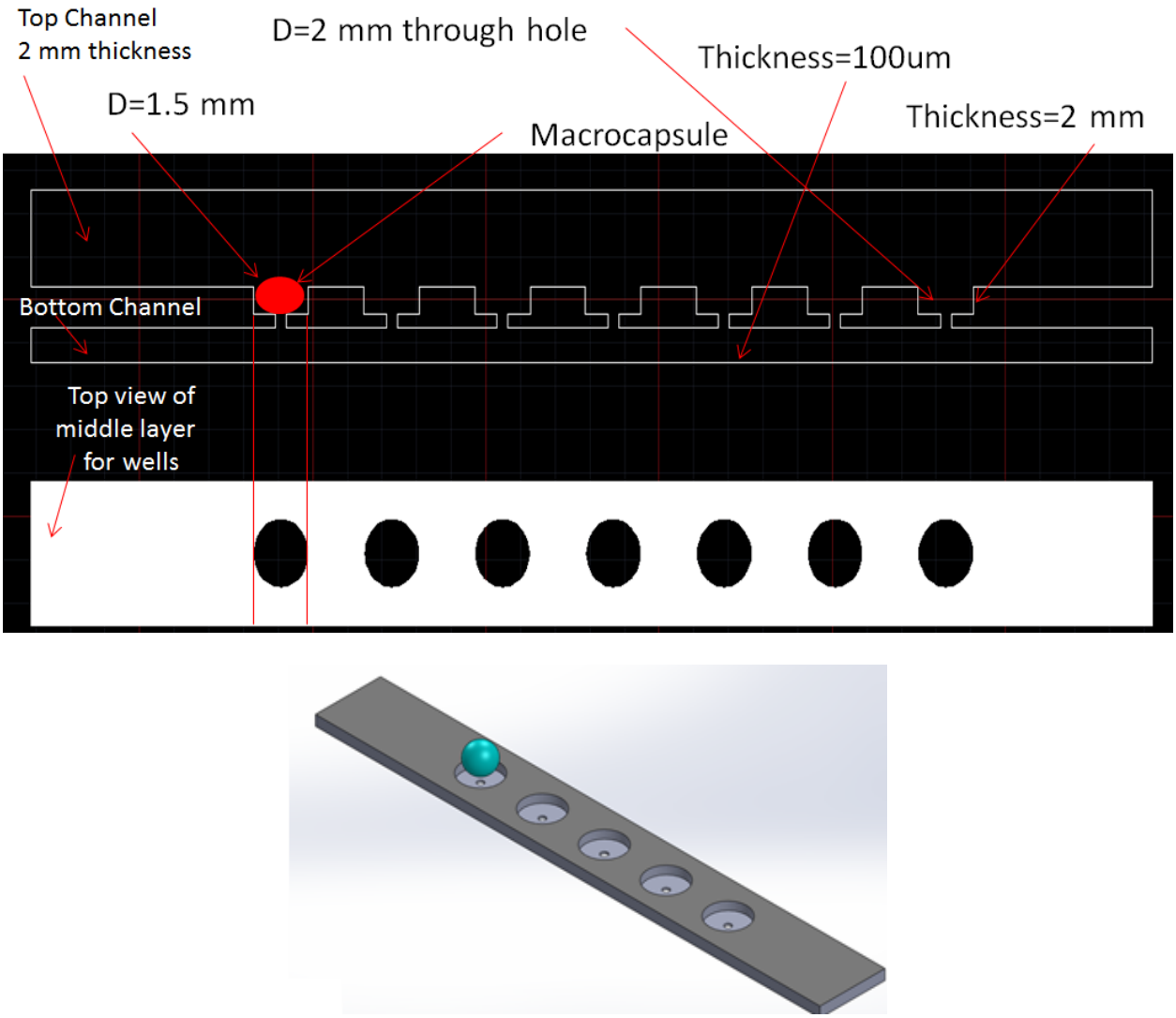

Figure 39. Schematic of macrocapsule array. Top: side view of three layers and dimension of the wells and channels. Bottom: Structure of wells in middle layer.

Two punched ports created as inlet and outlet. The top layer dimension was 50 mm by 2 mm and 2 mm in height. The circular macrowells proposed here comprised round wells of 2 mm diameter and 2 mm height, which is 0.5mm bigger that the size of the macro capsules. Using the fabricated patterned wells, 20 macrocapsules was introduced to device. Due to gravity force (figure 40), the solution was slowly migrating towards the macrowells and directing capsules to the wells. The entire time for capsule trapping was 1 minutes. This trapping method is effective, efficient, compatible with automation, and more importantly improves capsule stimulation. To define the optimal geometry of the macrowells for optimal capsule trapping, various well dimensions were tested with the diameter ranging from 2mm and 3 mm. For 3 mm microwells, capsules were not stable during stimulation and sometimes two capsules were trapped in one well. For 2 mm macrowells, all of the macrowells were filled with the capsules (trapping efficiency = 100%), and the captured capsules were easily unloaded by reversing the ports.

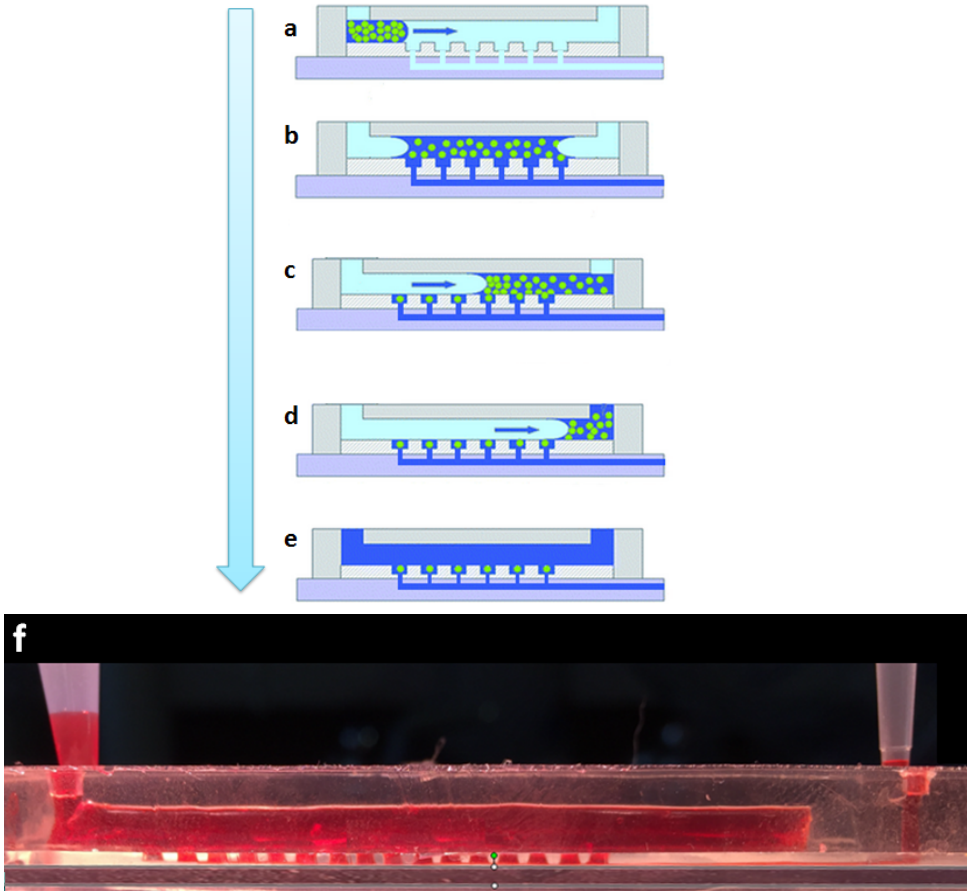

Figure 40. Schematic illustration of the capsule immobilization method within an array of microfluidic wells. (a and b) Green 1.5mm capsules are introduced into the channel. (c and d) media directing the capsules toward wells due to cross channel at the bottom of the wells. The whole procedure is performed using gravity without pomp. Remaining capsules are washed with the media using gravity.

Fluid Dynamic Simulation

To better understand the flow characteristics and to be able establish the effective design parameters for the chip array, a CFD study was performed using multiphasic software, COMSOL 4.4. The COMSOL fluid-flow simulation results using a 2D model were depicted in figure 41. The pressure profile in the microfluidic channel was shown in figure 41. It shows that the pressure decreased along the islet array, indicative of no significant counter flow. The velocity profile in the whole device presented in figure 41 indicates that velocity pattern was periodically repeated in cross channels under macrowells. As shown in the insert of figure 41, it was observed that maximum velocity occurs in the cross-flow channel, which indicates the diverted flow into the trapping area. This would allow particles to flow toward the trapping sites due to the hydrodynamic force. When a particle occupied the trapping area, it increased flow resistance that allowed flow to bypass the trapping area and directed remaining capsules into the next empty wells.

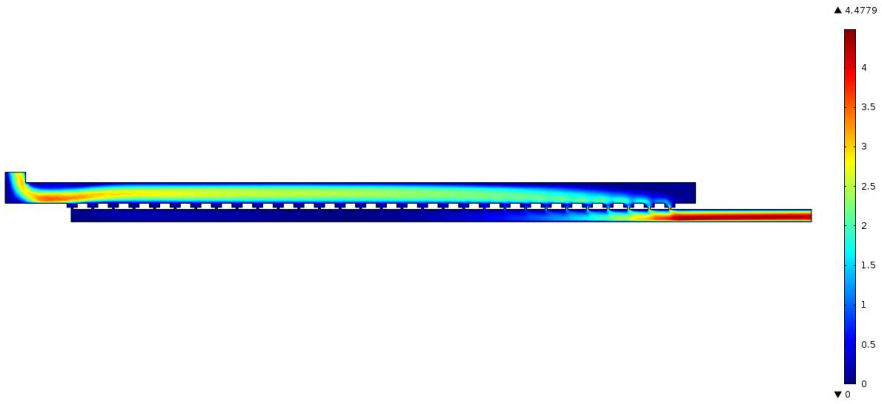
▲ 4.4779
4
3.5
3
2.5
2
1.5
1
0.5
0
▼ 0

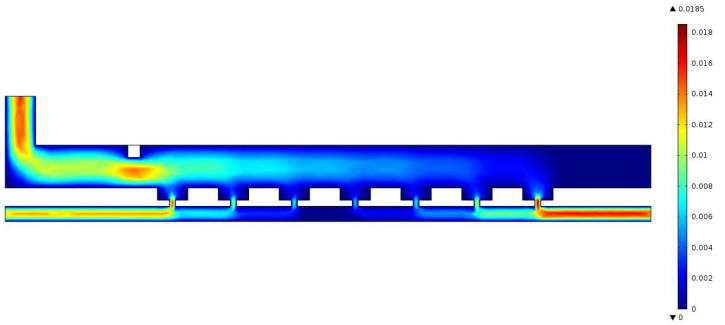
▲ 0.0185
0.018
0.016
0.014
0.012
0.01
0.008
0.006
0.004
0.002
0
▼ 0

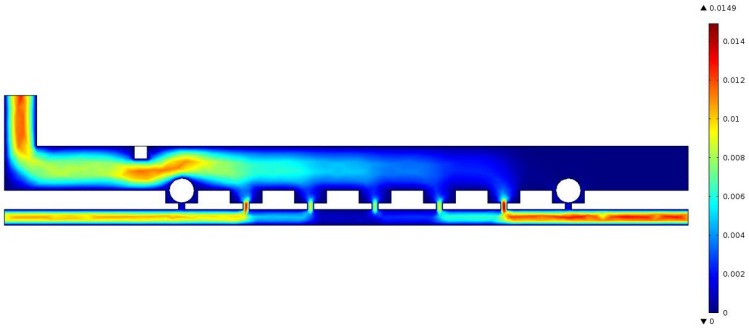
▲ 0.0149
0.014
0.012
0.01
0.008
0.006
0.004
0.002
0
▼ 0

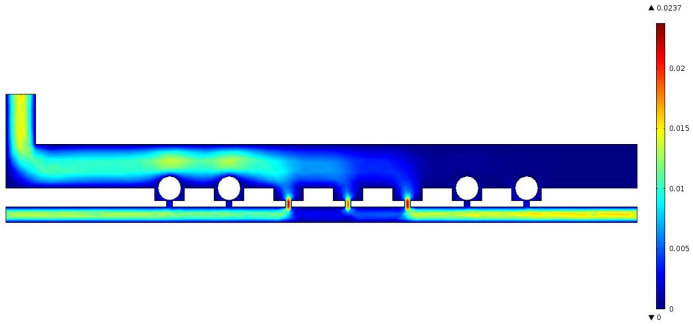
▲ 0.0237
0.02
0.015
0.01
0.005
0
▼ 0

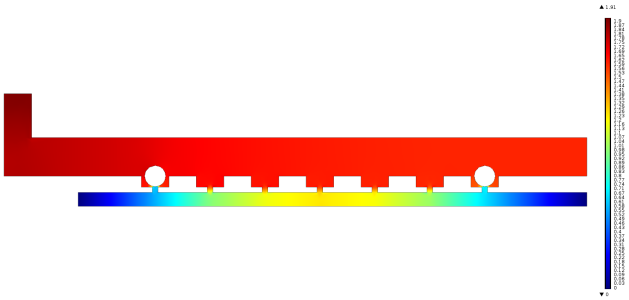

Figure 41. 2D flow simulation of the device. Velocity is higher at the bottom of the well which is an indication of diverting flow and particle in flow toward wells. Fluid is driven by pressure difference at inlet and outlet.

Live-Cell Imaging for Monitoring the Cellular Response of Islets Inside Macrocapsules

For tracking the cellular response of β- cells, the captured macrocapsules were stimulated with two concentrations of glucose (2mM, and 18 mM), and also 30 mM KCL. Solutions were introduced into the chip after macrocapsules were loaded into the device. This experiment was performed using monkey islets. Fura2 was used to study calcium dynamic and Rh123 was used for φ_m tracking. 20 capsules were selected for imaging purpose. Individual islet responses were assessed with the following perifusion protocol: 1) KRB2 (0-5 min); 2) 20 mM glucose (25 min); 3) KRB2 (45 min); 4) 30 mM KCl (15 min); 5) KRB2 (30 min).

We further verified an even and uniform flow of solution in the whole MFD chip by studying the calcium signalling in different position throughout the chip. The calcium signalling showed similar pattern in different position in the chip indicating that macrocapsules stimulation by glucose solution was uniform. Graphs are presented in figure 42.

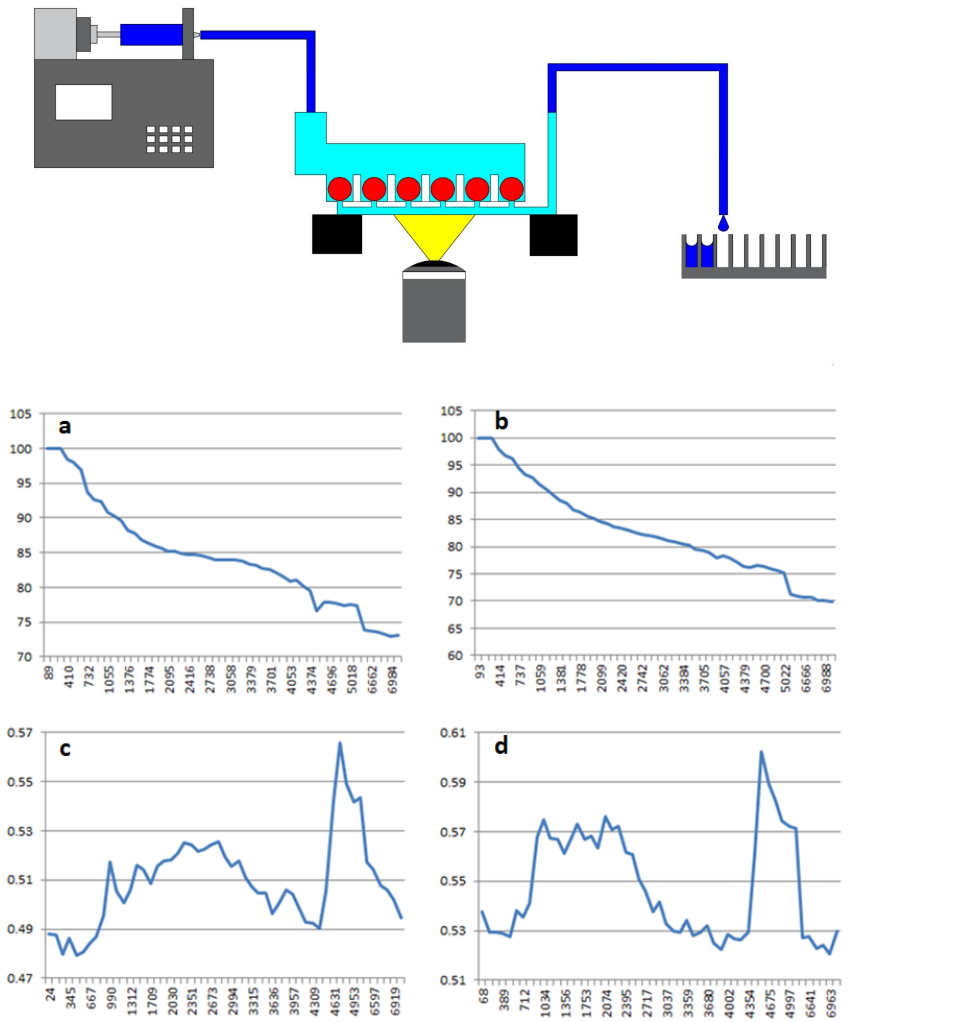

Figure 42. Top: Schematic representation of device set up on microscope stage. Bottom: Intracellular calcium influx and Ψ_m in response to insulin secretagogues. Representative traces of intracellular calcium of single rat islets to 20 mM glucose stimulation and 30 mM KCl.

Chapter VI. Project 4 Results and Discussion

As mentioned before, human islet cells transplant is a new treatment patients with type I diabetes, which aims to eliminate patients' dependence on external insulin by injecting donor islets to the liver[78]. However, in order for the transplant to be successful, the donor sample (from a cadaver) must provide enough islet mass so that a sufficient number of β -cells survive to supply the patient with enough insulin[78].It is therefore necessary to estimate the islet mass of a sample prior to transplant. This estimation is typically expressed in terms of islet equivalents (IEq), a system of measurement that normalizes the size of islets to spheres of 150 μm diameter (Appendix 1) [78,104]. Approximately 10,000 IEq per kilogram of the patient's body mass are required for the procedure [104]. Therefore, the number and diameter of islets in a sample must be estimated. The current method for doing so is by manual counting under an optical microscope, which is a slow and tedious undertaking. The islet counts obtained by this method may not agree between researchers. Consequently, there is a need for automated assessment of pancreatic islet samples. While some automation of this microscope counting has been proposed, no such method has been adopted for islet counting[104].In order to provide a method for estimating the IEq of an islet sample, and thereby its suitability for transplant, both the number of islets as well as their diameters must be measured. This process should be fast and automated, for convenience of the researchers in testing multiple samples, without requiring an excess of specialized equipment. For this reason, the use of a smartphone camera to track islets flowing through a microfluidic device offers an elegant solution. Since both devices are readily available, they can be used to design a system in which a smartphone camera detects islets moving in a microfluidic channel. By capturing a video recording and processing it later on a computer, the necessary count and diameter information could be obtained automatically.

The objective of this work is to design a smartphone-based method for accurately counting and estimating the diameters of human pancreatic islets flowing through a microfluidic device to determine the total islet equivalents of the sample.

In order to satisfy the above objective, an automated islet counter was developed with main two components. The first component was a physical frame that holds the smartphone, the microfluidic device, and an optics system to magnify and illuminate the smartphone video recording. The second component was a software designed to run on a computer to process the video and determine the number of islets and their diameters.

Physical Frame and Components

The responsibility of the frame is to facilitate the recording of a properly magnified video of islets flowing through the microfluidic channel by interfacing with the smartphone and the microfluidic device. It needs to hold to the smartphone, the microfluidic device, an in-built optics system, and to provide their interaction during recording. An iPhone 5swas used for this project. The optics system of the frame will contain a lens for magnification. The lens must be held by the frame (figure 43) at an appropriate distance from the microfluidic device, and must be placed so as to focus the camera recording on the islets moving in a segment of the channel. The frame must also arrange all of these components so that the iPhone camera is aligned with the lens as well as with the channel of the microfluidic device. Furthermore, all of these components must be secured in place by the frame so that they remain stable during the recording, to obtain a steady video. A secondary objective for the physical frame is the incorporation of an LED as an illumination source. This is to provide a consistent level of illumination, to optimize the performance of the software.

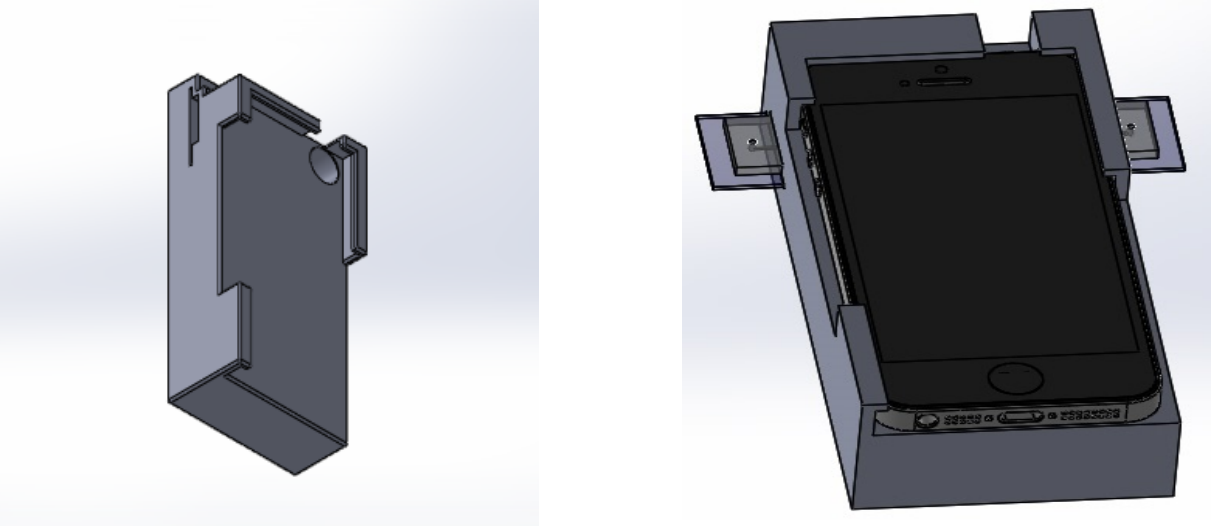

Figure 43: Schematic of physical frame

The frame was 3D printed from a polyamide plastic (Nylon). An overview of the frame design is given in figure 43. The major components are a shelf to hold and support the iPhone 5s, an adaptor housing the lens, and an area for inserting and holding the microfluidic device (figure 44) as described before.

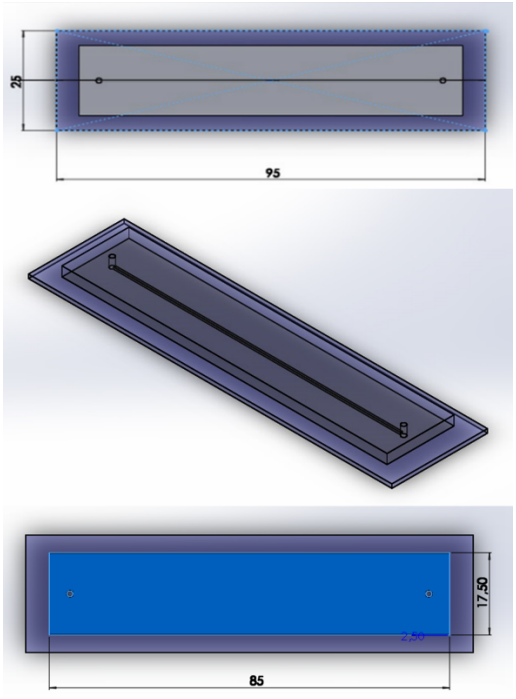

Figure 44. Schematic of microfluidic device used in this project.

As depicted in figure 43, the screen of the phone will be facing upward, to allow for starting and stopping the vide o recording without moving the device. The lens will be held in an adaptor from the manufacture and installed in the hole beneath the phone camera, as shown in figure 43. The current lens being considered is the Thorlabs C230TME-A Mounted Geltech Aspheric Lens (see Appendix 2). The dimensions are presented in appendix 2. The thickness of the PDMS in the main part of the microfluidic device will be 5 mm, as this thickness ensures proper attachment of the appropriate fixtures at the inlet and outlet. The channel height and width are both 500 μm. Finally, the glass slide to which the PDMS slide was bonded is 95 mm long, as illustrated in figure 43. The channel at the center of the microfluidic device is aligned with the lens and the phone camera, to facilitate recording. During operation, the device is intended to rest on a flat surface such as a table. The iPhone 5s was placed into the frame with its screen facing up, and its camera aligned with the hole in the shelf, and the microfluidic device will be inserted. After the sample has been run through, the video will be transferred from the iPhone to a computer for the software processing.

Software

The software was written to be run on a computer to process the iPhone video. It was written in C++ using the OpenCV (Open Source Computer Vision) library, to take advantage of existing functionality for computer vision. As a cross-platform, open-source library, OpenCV could also facilitate the creation of applications to run on a variety of operating systems, including Android and iOS. The software has four main functional requirements. The first is that the software must identify and track islets moving in the video. Second, it must make a robust estimate of the number of islets that pass through the section of the channel being recorded. Third, the program should estimate the diameters of the islets that are detected. Finally, this information should be used to compute IEq and generate a report following the analysis to summarize the results. The software three primary tasks are to track islets moving through the channel in the video, count the number of islets, and estimate their diameters. Final step is to generate a report. These

primary tasks will be accomplished using functions from the OpenCV library to implement the algorithms designed for this platform. Identification of the islets in the channel will be accomplished through a technique known as background subtraction.

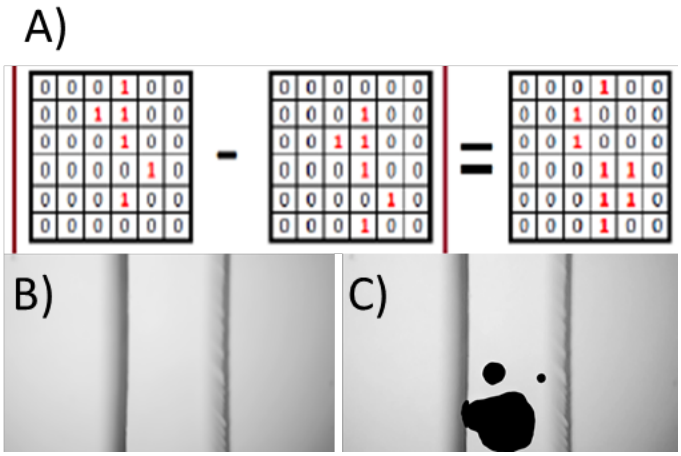

Figure 45: A) Conceptual illustration of absolute difference method. Taking the absolute difference of the images after a binary threshold leaves all pixels 0 except for those that changed between the two frames. This results in a trace (in red) that represents the motion of an object. B) Reconstructed background image from sample video. C) Foreground for a frame of video, with trace of moving objects (islets) superimposed on the background.

This entails splitting the video into individual frames, each of which is a single image. Adjacent frames are then compared on a pixel-by-pixel basis. This starts by converting the images to grayscale, and then applying a binary threshold, so that all pixels have values of either 0 or 1. Next, the absolute difference between adjacent frames is taken, by simple subtracting the values of corresponding pixels and taking the absolute values of the results (which can be either 0 or 1). This process is illustrated in figure 45. This results in a trace of any movement in the video, from which the motion of objects is ultimately detected. If the channel remains still, without shaking, the only moving objects in the channel will be the islets, as they are carried by the flow. By first applying a threshold filter and then using background subtraction, the islets can therefore be tracked as they move through the channel. Once the islets are identified, the program can draw minimum bounding boxes around them. To determine the number of islets, the software can track the objects as they cross a number of checkpoints in the channel. A count can be incremented each time an islet passes a checkpoint. By averaging the counts across multiple checkpoints in the video, the program can offset the errors introduced by islets either clumping together or breaking apart as they flow through the channel. As objects pass a checkpoint line, a count is incremented. The results from all of the lines will then be averaged. When the islets are in the zones past each checkpoint, their diameters can be estimated using the minimum bounding box. This method involves measuring the area of the minimum bounding box, and determining what fraction of the pixels in the box are occupied by the islet (having a value of 1 instead of 0). This fraction can then be multiplied with the area of the minimum bounding box. The result of this calculation will be the surface area of the islet, or rather, the area of its two dimensional projection onto a plane because of the bird's-eye view perspective of the camera. Assuming the islets are spherical, as is the basis of the IEq method, this cross-section would be circular. By treating the area of islet visible on the video as that of a circle, the diameter can be calculated using simple geometric relations. This process is illustrated in figure 46.

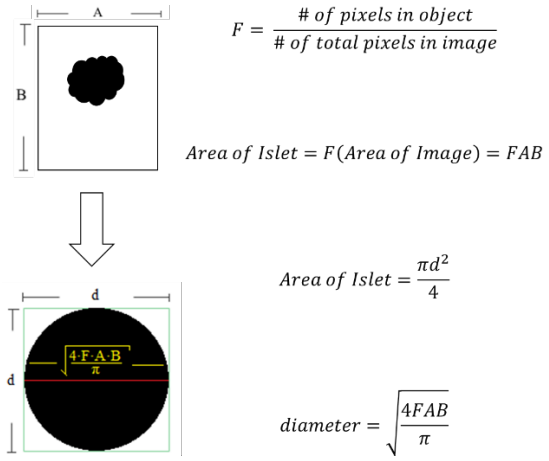

$$F = \frac{\#\ of\ pixels\ in\ object}{\#\ of\ total\ pixels\ in\ image}$$

$$Area\ of\ Islet = F(Area\ of\ Image) = FAB$$

$$Area\ of\ Islet = \frac{\pi d^2}{4}$$

$$diameter = \sqrt{\frac{4FAB}{\pi}}$$

Figure 46: Illustration for diameter estimation algorithm. The area of the video is multiplied by the fraction of pixels that are occupied, so as to determine the surface area of the islet that is visible. This is then treated as if it were the area of a circle, and used to estimate the diameter.

Once the counts and diameters have been taken at all the checkpoints, the results will be averaged to provide the final estimate of total IEq.

Video Recording Procedure

The goal was to make sure design provide a magnified, focused, and illuminated recording with the optics system; keep all components aligned so that a recording of islets in the channel can be captured (at 120 FPS); and ensure that all components stay steady throughout the recording.

To begin assessment of the islet sample, the frame was first set on a table, and the LED was lit. The microfluidic device was inserted into its slot, and two pipette tips were placed in the inlet and outlet, along with buffer. The iPhone 5s was inserted and set to the 120 FPS video recording mode. The smartphone's camera (figure 47) was focused into the region of the field of view not affected by field curvature.

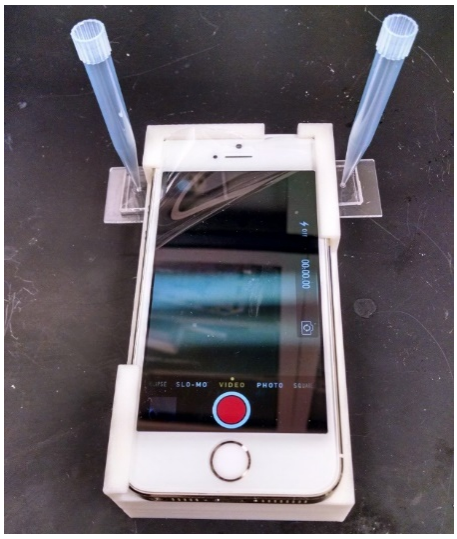

Figure 47: Image of frame with iPhone 5s and microfluidic device inserted. All components are held securely, inlets are unobstructed (with pipette tips inserted), and phone screen and buttons are accessible.

Next, to flow the islets, a pipette was used to transfer islets along with a volume of fluid into one of the pipette tips in the inlet. The taller column of fluid in that tip relative to the tip at the outlet drove the flow of fluid, and carried the islets along with it through the channel. The iPhone 5s was set to record while the islets were flowing through. The recorded video was transferred to a computer. The videos that were collected showed a focused view of the islets passing trough the channel, with a bright, evenly-illuminated background. These results are illustrated in figure 48.

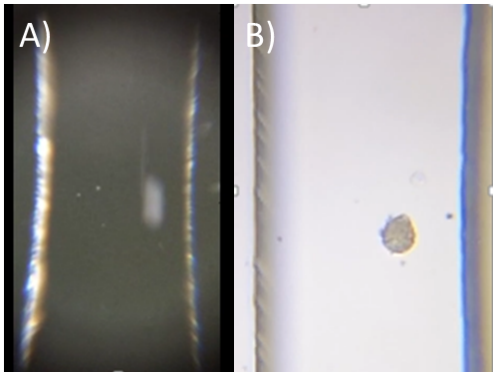

Figure 48: Still frames of islets moving. A) Sample image from recording with the prototype. B) Sharply focused, brightly illuminated image from recording captured with new frame design.

Lack of motion blur results from use of 120 FPS recording. Then recorded videos were analyzed manually, by advancing them in slow motion and counting the number of islets. This was used as the “ground truth” data for the islet count. For the IEq estimate, one frame was selected for each islet, and extracted from the video. Image processing was used to estimate the islet area by isolating the region of the frame with the islet applying a threshold, converting to binary, and measuring the number of pixels occupied by the islet. Using the width of the channel in pixels and its known width of 500 μm, the manual IEq was calculated according to the method in Appendix 1. These results were then compared with the software results to determine the percentage error. The results are summarized in Table 2 below.

Table 3: Software Test Results

	Average	Standard Deviation
Percent Error in Islet Count	-5.68%	15.92%
Percent Error in IEq Estimate	68.85%	34.22%

Discussion

The results of the physical component testing confirmed that all design objectives for this part of the product were met. The iPhone 5s, when mounted in the frame, was able to record a video with all of the desired qualities. For its part, the software was also able to detect the motion of islets from the video, indicating the quality of the recording.

As islet detection was possible with 60 FPS video at 720 by 1280 resolution, many models of smartphone should be able to capture video with the system from which islets may be detected. This suggests that the frame can be used for tracking islets as they move in microfluidic devices. Even if not used with the IEq assessment software, the frame offers a convenient means of brightfield microscopy while working with islets in microfluidic devices. Qualitative assessments could also be possible; as other microfluidic devices could be used. Other improvements, such as adapting to use with other smartphones. The software component test, however, revealed weaknesses in the accuracy of the islet count and the IEq estimate, not achieving the 10% error requirement. However, this reflects largely on the nature of the testing, as only 5 videos were used, with an average of only 10 islets. This small number meant that a single large islet being misclassified could result in a nearly doubled IEq in some cases.

There are numerous sources of error to be overcome with the software algorithm. For one, the computed IEq is too high due to overestimation of the diameters of the islets. This could result from the software detecting a halo around the islets rather than the actual outlines of the islets. This leads to a larger area, and thereby a greater diameter estimate. Based on the IEq formula, as seen in Appendix 1, this would result in a higher IEq. Another problem affecting both the islet count and the IEq computation is when islets in contact with each other are treated as though they were a single larger islet by the software. This is one of the only reasons for errors in the

number of islets. For reasons outlined in Appendix 1, this can have a far more profound impact on the IEq. Solutions to these problems are outlined in the Future Work section.

Future Work

The results of the software validation testing suggest that greater accuracy in IEq determination will be necessary for this method to be reliable. One means of improving the IEq estimate involve manipulating detection thresholds so that the contours of islets are detected more closely, in order to derive an accurate area. In addition, the lighting from the LED can be dimmed and adjusted so as to eliminate the halo effect that leads the software to detect a larger diameter.

Changes to the operating procedure can also serve to correct the diameter estimation. The use of the iPhone's digital zoom to record only the center of the field of view may introduce some blur. This makes the contour less defined, resulting in poorer estimation of the area. This could necessitate not zooming the camera in, but instead relying on the software to do so.

Another important problem to correct is the classification of small, clumped islets as large islets. Two different angles toward solving this problem are being considered. The approach relies on modifying the software so that it can appropriately account for the presence of the large clumped islets in the video. One method under consideration is to assess large islets by using form factors such as circularity to judge whether an object is likely to be a single continuous object or multiple masses that are connected only at small points.

In addition, the software could also be modified to detect and flag islets above a certain size threshold, retrieve the frames in which they appear, and rely on the user to judge whether these oversized islets are single islets or if they are really clumps of smaller islets. The user's input would then be user to retroactively correct the IEq computation.

To confirm the final accuracy of the technique, a validation test must be conducted. This would involve comparing both the method presented here and the technique of manual IEq, to confirm the equivalence of the techniques and determine whether this product truly offers and advantage.

In addition to improving the accuracy of the technique, there are a number of possible future improvements to the design that have been proposed. One such change would be to modify the frame to incorporate a universal cellphone mount to allow the use of any smartphone. Another is to use fluorescence imaging rather than bright-field microscopy, while retaining the basic principles of the design.

Appendix 1: IEq Calculation and Error Analysis

The measurement of islet equivalents is based on the assumption that islets are spherical in shape. The basis of the technique involves normalizing the measured islets to a 150 μm diameter. The number of islets within different ranges of diameters are combined with a set of weights to yield the total IEq, and islets below 50 μm are neglected. The ranges for the IEq calculation are given in Table A1 below.

Table A1: Islet Ranges for IEq Measurement

Islet Class	Diameter (μm)
1	50-100
2	100-150
3	150-200
4	200-250
5	250-300
6	300-350
7	>350

Note that islets less than 50 μm in diameter are not used for the calculation. The equation for total IEq, based on the number of islets in each class, is given below, where nx is the number of islets in the sample falling into class x [104].

$$\text{Total IEq} = \frac{n_1}{6.00} + \frac{n_2}{1.50} + 1.7n_3 + 3.5n_4 + 6.3n_5 + 10.4n_6 + 15.8n_7$$

This formula has a large impact on the error analysis for the software. First, no error is introduced by diameter estimation unless the diameter crosses the threshold into another bin. That is, as long as an islet's diameter still falls into the proper 50 μm range, its contribution to the IEq will be the same. Therefore, some degree of inaccuracy in area estimation may occur without having an effect on the computed IEq. However, any error that changes an islet's diameter enough to move it to a new class can have an impact on IEq. For this reason, it is important to continue to refine the area estimation algorithms to ensure an accurate assessment.

If the Kalman filter fails and the tracker tags for two islets are switched, which is most likely in the case of similarly-sized islets, the result will be two areas that are averages of the islets' areas weighted by the number of frames (or amount of time) in which each islet held each tag. If the islets both belonged to the same diameter class, this average must also necessarily fall into the same class. This means that two islets of the same class that switch tracker tags at any point in the video will not affect the IEq. If two islets from different diameter classes switch tags, however, there is the potential for the IEq to be skewed, depending on whether the islets were in adjacent classes and where each islet's true area lay relative to the endpoints of its diameter bin.

The coefficients of the IEq equation highlight another fact, that larger islets have a much larger impact on this parameter than smaller islets. This is an issue in the case of small clumps of islets that are counted together by the software as a single, much larger islet. Because the

larger diameter classes have much larger coefficients, this can greatly increase the IEq. This issue makes it imperative to seek out ways to either avoid or account for such islet clumping.

Appendix 2: Lens Specifications

The original lens model was the Thorlabs C230TME-A Geltech Aspheric Lens. However, Thorlabs has replaced this model with the C230TMD-A. A document from the manufacturer detailing the lens is given below. It is important to note that as this lens is not flat-field corrected, there is field curvature, and the product presented here depends on zooming the iPhone's view to the region with minimal curvature effects.

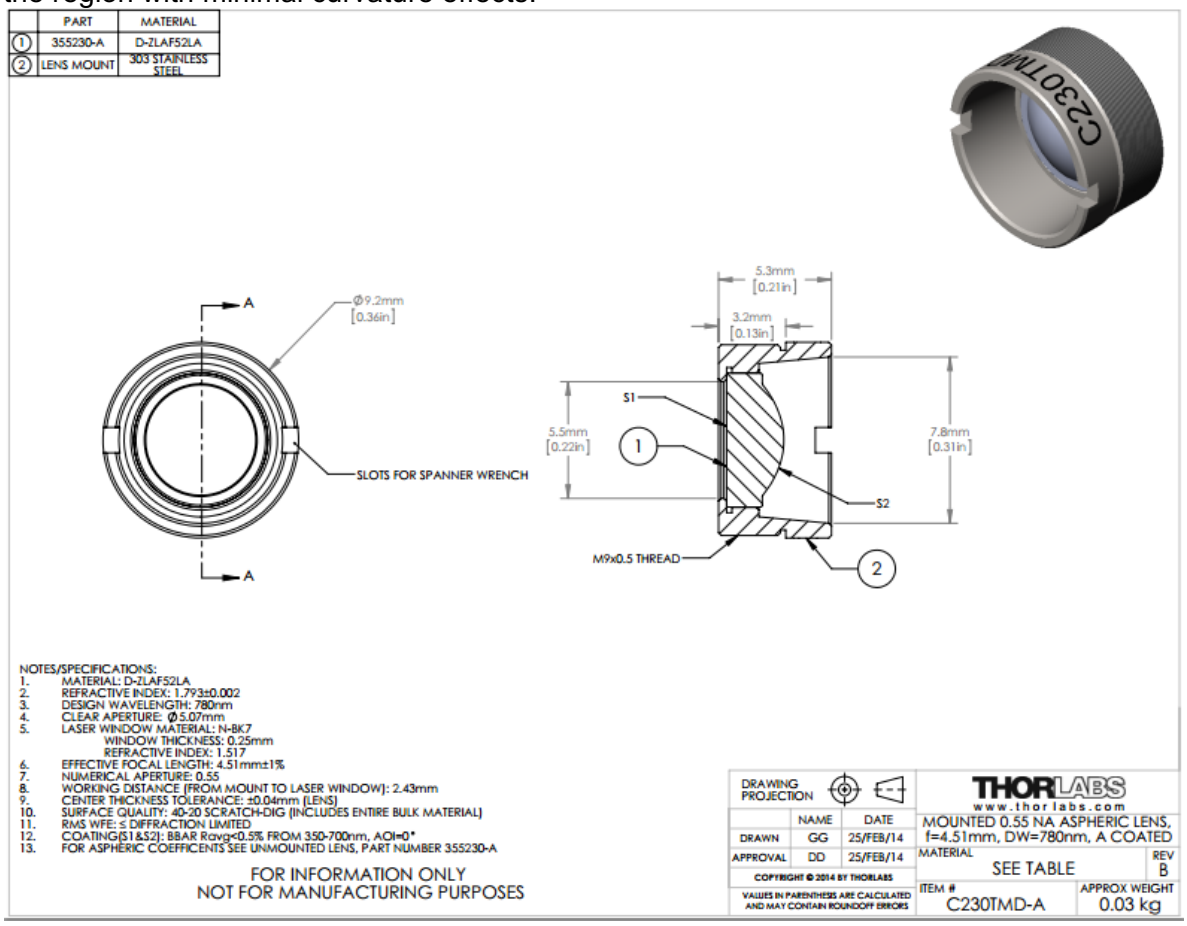

Appendix 3: Frame Schematics

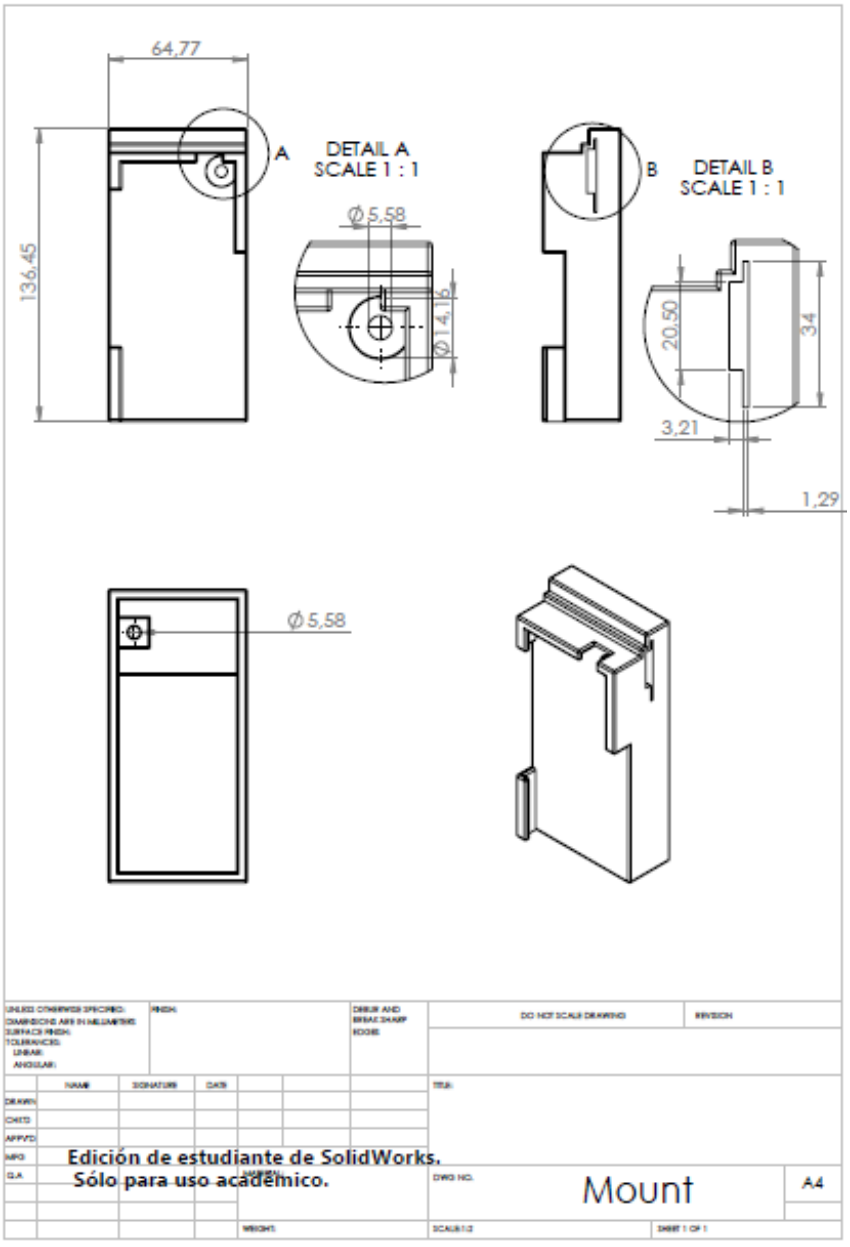

Apendix 4

Permission/license

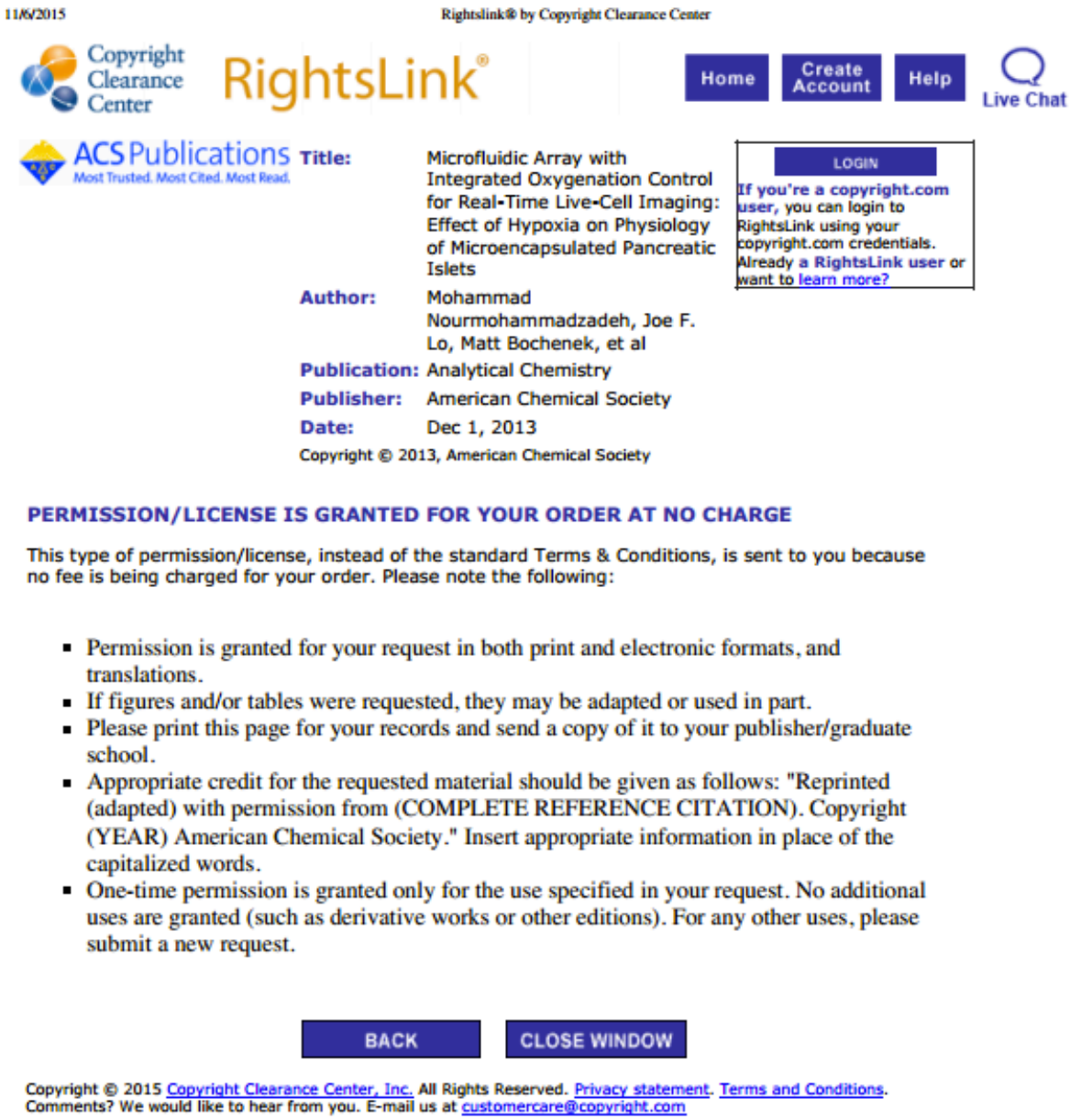

11/6/2015 Rightslink® by Copyright Clearance Center

Copyright Clearance Center RightsLink®

Home | Create Account | Help | Live Chat

ACS Publications Most Trusted. Most Cited. Most Read.

Title: Microfluidic Array with Integrated Oxygenation Control for Real-Time Live-Cell Imaging: Effect of Hypoxia on Physiology of Microencapsulated Pancreatic Islets

Author: Mohammad Nourmohammadzadeh, Joe F. Lo, Matt Bochenek, et al

Publication: Analytical Chemistry

Publisher: American Chemical Society

Date: Dec 1, 2013

Copyright © 2013, American Chemical Society

LOGIN

If you're a copyright.com user, you can login to RightsLink using your copyright.com credentials. Already a RightsLink user or want to learn more?

PERMISSION/LICENSE IS GRANTED FOR YOUR ORDER AT NO CHARGE

This type of permission/license, instead of the standard Terms & Conditions, is sent to you because no fee is being charged for your order. Please note the following:

- Permission is granted for your request in both print and electronic formats, and translations.
- If figures and/or tables were requested, they may be adapted or used in part.
- Please print this page for your records and send a copy of it to your publisher/graduate school.
- Appropriate credit for the requested material should be given as follows: "Reprinted (adapted) with permission from (COMPLETE REFERENCE CITATION). Copyright (YEAR) American Chemical Society." Insert appropriate information in place of the capitalized words.
- One-time permission is granted only for the use specified in your request. No additional uses are granted (such as derivative works or other editions). For any other uses, please submit a new request.

BACK CLOSE WINDOW

Copyright © 2015 Copyright Clearance Center, Inc. All Rights Reserved. Privacy statement. Terms and Conditions.
Comments? We would like to hear from you. E-mail us at customercare@copyright.com

Title:	Review of cell and particle trapping in microfluidic systems
Author:	J. Nilsson,M. Evander,B. Hammarström,T. Laurell
Publication:	Analytica Chimica Acta
Publisher:	Elsevier
Date:	7 September 2009

Order Completed

Thank you very much for your order.

This is a License Agreement between Mohammad Nourmohammadzadeh ("You") and Elsevier ("Elsevier"). The license consists of your order details, the terms and conditions provided by Elsevier, and the payment terms and conditions.

Get the printable license.

License Number	3743280723635
License date	Nov 06, 2015
Licensed content publisher	Elsevier
Licensed content publication	Analytica Chimica Acta
Licensed content title	Review of cell and particle trapping in microfluidic systems
Licensed content author	J. Nilsson,M. Evander,B. Hammarström,T. Laurell
Licensed content date	7 September 2009
Licensed content volume number	649
Licensed content issue number	2
Number of pages	17
Type of Use	reuse in a thesis/dissertation
Portion	figures/tables/illustrations
Number of figures/tables/illustrations	4
Format	both print and electronic
Are you the author of this Elsevier article?	No
Will you be translating?	No
Original figure numbers	3,4,5,6,8,9
Title of your thesis/dissertation	Application of microfluidics in the field of diabetes and treatment
Expected completion date	Nov 2015
Estimated size (number of pages)	110
Elsevier VAT number	GB 494 6272 12
Permissions price	0.00 USD
VAT/Local Sales Tax	0.00 USD / 0.00 GBP
Total	0.00 USD

ORDER MORE... CLOSE WINDOW

References

1. Volk, B. W. and E. R. Arquilla (1985). New York, Plenum Medical Book Co.
2. Bliss, M. Publ Am Inst Hist Pharm (1997)16: 93-99.
3. Luft, R., S. Efendic, et al. (1974). Med Biol 52(6): 428-430.
4. Wierup, N., H. Svensson, et al. (2002). Regul Pept 107(1-3): 63-69.
5. Battle, H. (1969). Old Tappan, N.J.,Hewitt House.
6. Skelin, M., Rupnik, M., and Cencic, A. (2010) ALTEX 27, 105-113.
7. American Diabetes Association, (2010) volume 33, supplement 1.
8. Paul Robertson, N Engl J Med (2004), 350:694-705.
9. Williams PW. Br Med J (1894); 2:1303-4.
10. Ballinger WF, Lacy PE. Surgery 1972;72:175-86.
11. Sutherland DE, Matas AJ, Goetz FC, Najarian JS. Diabetes (1980);29:Suppl 1:31-44.
12. Najarian JS, Sutherland DE, Baumgartner D, et al. Ann Surg (1980); 192:526-42.
13. Largiader F, Kolb E, Binswanger U. Transplantation 1980; 29:76-7. 20. Pyzdrowski KL, Kendall DM, Halter JB, Nakhleh RE, Sutherland DER, Robertson RP. N Engl J Med (1992);327:220-6.
14. Wahoff DC, Papalois BE, Najarian JS, et al. Ann Surg (1995);222:562-79.
15. Scharp DW, Lacy PE, Santiago JV, et al. Diabetes (1990);39:515-8.
16. ITR newsletter 9. Vol. 8. No. 1. June (2001):1-20.
17. Shapiro AMJ, Lakey JRT, Ryan EA, et al. N Engl J Med (2000);343:230-8.
18. Oberholzer J, Triponez F, Mage R, et al. Transplantation (2000);659:1115-23.
19. G. C. Weir, Diabetologia, (2013), Volume 56, Issue 7, pp 1458-1461.
20. O'Sullivan ES, Vegas A, Anderson DG, Weir GC (2011). Endocr Rev 32:827–844.
21. Monaco, A.P., Maki, T., Ozato, H., et al. Ann Surg 214, 339, (1991); discussion 361.
22. Sullivan, S.J., Maki, T., Borland, K.M., et al. Science, (1991)252, 718.
23. Efrat, S. Trends Mol Med. (2002): 8, 334.
24. Qi, M., Gu, Y., Sakata, N., et al. Biomaterials (2004):25, 5885.
25. Chang, T.M. Semipermeable microcapsules. Science (1964);146, 524.
26. Cruise, G.M., Hegre, O.D., Lamberti, F.V., et al. Cell Transplant (1999); 8, 293.
27. Loscertales, I.G., Barrero, A., Guerrero, I., et al. Science (2002); 295, 1695.
28. de Vos, P., De Haan, B. J., Wolters, G. H., Strubbe, J. H., and van Schilfgaarde, R. Diabetologia (1997) 40: 262.
29. De Vos, P., van Straaten, J. F., Nieuwenhuizenn, A. G., de Groot, M., Ploeg, R. J., De Haan, B. J., and van Schilfgaarde, R. Diabetes (1999);48: 1381.
30. Martijn de Groot, Theo A. Schuurs, and Reinout van Schilfgaarde, Journal of Surgical Research (2004);121, 141–150.
31. Fritschy, W. M., van Straaten, J. F., de Vos, P., Strubbe, J. H., Wolters, G. H., and van Schilfgaarde, R. Transplantation, (1991); 52: 777.
32. De Vos, P., Vegter, D., De Haan, B. J., Strubbe, J. H., Bruggink, J. E., and van Schilfgaarde, R. Diabetes, (1996);45: 1102,.
33. Siebers, U., Horcher, A., Bretzel, R. G., Klock, G., Zimmermann, U., Federlin, K., and Zekorn, T. Int. J. Artif. Organs (1993);16: 96.

34. Cleveland, J. C. J., Raeburn, C., and Harken, A. H. Surgery (2001);129: 664.
35. Toosy, N., McMorris, E. L., Grace, P. A., and Mathie, R. T. Br. J. Urol. Int. (1999); 84: 489.
36. DD Carlo, LP Lee, Analytical chemistry, 2006.
37. Khademhosseini, A.; et al. Proc. Natl. Acad. Sci. U.S.A. (2006); 103, 2480–2487.
38. Moore, K. A.; Lemischka, I. R. Science (2006); 311, 1880–1885.
39. Gumbiner, B. M. Nat. Rev. Mol. Cell Biol. (2005); 6, 622–634.
40. Wei, C. J.; Xu, X.; Lo, C. W. Annu. Rev. Cell Dev. Biol. (2004); 20, 811–838.
41. Rustom, A.; et al. Science (2004); 303, 1007–1010.
42. Helmke, B. P.; Davies, P. F. Ann. Biomed. Eng. (2002); 30, 284–296.
43. Ingber, D. E. J. Cell Sci. (2003); 116, 1157–1173.
44. Geiger, B.; Bershadsky, A. Cell (2002); 110, 139–142.
45. Ahern, C. A.; Horn, R. Trends Neurosci. (2004); 27, 303–307.
46. Mycielska, M. E.; Djamgoz, M. B. A. J. Cell Sci. (2004); 117, 1631–1639.
47. Lee, H.; Caterina, M. J. Pfluegers Arch. (2005); 451, 160–167.
48. Lucchetta, E. M.; et al. Nature (2005); 434, 1134–1138.
49. Rao, C. V.; Wolf, D. M.; Arkin, A. P. Nature (2002); 420, 231–237.
50. Lidstrom, M. E.; Meldrum, D. R. Nat. Rev. Microbiol. (2003); 1, 158–164.
51. Raser, J. M.; O'Shea, E. K. Science (2005); 309, 2010–2013.
52. Rosenfeld, N.; et al. Science (2005); 307, 1962–1965.
53. Mettetal, J. T.; et al. Proc. Natl. Acad. Sci. U.S.A. (2006); 103, 7304–7309.
54. Bhalla, U. S. Biophys. J. (2004), 87, 733–744.
55. Kholodenko, B. N. Nat. Rev. Mol. Cell Biol. (2006); 7, 165–176.
56. Meier, S. M.; Huebner, H.; Buchholz, R. Bioprocess Biosyst. Eng. (2005; 28, 95–107.
57. J. Nilsson, M. Evander, B. Hammarström, T. Laurell, Analytica Chimica Acta ,649, 2, (2009); 141–157.
58. A.R. Wheeler, W.R. Throndset, R.J. Whelan, A.M. Leach, R.N. Zare, Y.H. Liao, K. Farrell, I.D. Manger, A. Daridon, Anal. Chem. 75 (2003); 3581.
59. D. Spetzler, J. York, C. Dobbin, J. Martin, R. Ishmukhametov, L. Day, J. Yu, H. Kang, K. Porter, T. Hornung, W.D. Frasch, Lab Chip 7 (2007);1633.
60. S.K.W. Dertinger, D.T. Chiu, N.L. Jeon, G.M. Whitesides, Anal. Chem. 73 (2001) 1240.
61. J. Olofsson, H. Bridle, J. Sinclair, D. Granfeldt, E. Sahlin, O. Orwar, Proc. Natl. Acad. Sci. U.S.A. 102 (2005); 8097.
62. P.J. Hung, P.J. Lee, P. Sabounchi, R. Lin, L.P. Lee, Biotechnol. Bioeng. 89 (2005); 1.
63. N.L. Jeon, H. Baskaran, S.K.W. Dertinger, G.M. Whitesides, L. Van de Water, M. Toner, Nat. Biotechnol. 20 (2002); 826.
64. K.G. Klemic, J.F. Klemic, M.A. Reed, F.J. Sigworth, Biosens. Bioelectron. 17 (2002); 597.
65. R.S. Kane, S. Takayama, E. Ostuni, D.E. Ingber, G.M. Whitesides, Biomaterials 20 (1999); 2363.
66. R. Davidsson, B. Johansson, V. Passoth, M. Bengtsson, T. Laurell, J. Emneus, Lab Chip 4 (2004); 488.
67. R. Rettig, A. Folch, Anal. Chem. 77 (2005); 5628.
68. M.S. Yang, C.W. Li, J. Yang, Anal. Chem. 74 (2002); 3991.

69. P.J. Lee, P.J. Hung, R. Shaw, L. Jan, L.P. Lee, Appl. Phys. Lett. 86 (2005); 3.
70. A. Valero, F. Merino, F. Wolbers, R. Luttge, I. Vermes, H. Andersson, A. van den Berg, Lab Chip 5 (2005); 49.
71. S. Zheng, H. Lin, J.Q. Liu, M. Balic, R. Datar, R.J. Cote, Y.C. Tai, Elsevier Science BV, Vancouver, Canada, (2007); 154.
72. W.H. Tan, S. Takeuchi, Proc. Natl. Acad. Sci. U.S.A. 104 (2007); 1146.
73. W.H. Tan, S. Takeuchi, Lab Chip 8 (2008); 259.
74. M. Nourmohammadzadeh, J.F. Lo, M. Bochenek, J.E. Mendoza-Elias, Q. Wang, Z. Li, L. Zeng, M. Qi, D.T. Eddington, J. Oberholzer, Y. Wang, Analytical Chemistry, , (2013); 85(23):11240-11249.
75. D. Di Carlo, N. Aghdam, L.P. Lee, Anal. Chem. 78 (2006); 4925.
76. D. Di Carlo, L.Y. Wu, L.P. Lee, Lab Chip 6 (2006);1445.
77. A.M. Skelley, O. Kirak, H. Suh, R. Jaenisch, J. Voldman, Nat. Meth. 6 (2009);147.
78. Barbaro, B.; Salehi, P.; Wang, Y.; Qi, M.; Gangemi, A.; Kuechle, J.; Hansen, M. A.; Romagnoli, T.; Avila, J.; Benedetti, E.; Mage, R.; Oberholzer, J. Transplantation (2007); 84, 1200– 1203.
79. Mohammed, J. S.; Wang, Y.; Harvat, T. A.; Oberholzer, J.; Eddington, D. T. Lab Chip (2009); 9, 97– 106.
80. Sangeeta N Bhatia & Donald E Ingber, Nature Biotechnology (2014); 32, 760–772.
81. Calafiore, R.; Basta, G.; Luca, G.; Lemmi, A.; Montanucci, M. P.; Calabrese, G.; Racanicchi, L.; Mancuso, F.; Brunetti, P. Diabetes Care (2006); 29, 137– 138.
82. Qi, M.; Strand, B. L.; Morch, Y.; Lacik, I.; Wang, Y.; Salehi, P.; Barbaro, B.; Gangemi, A.; Kuechle, J.; Romagnoli, T.; Hansen, M. A.; Rodriguez, L. A.; Benedetti, E.; Hunkeler, D.; Skjak-Braek, G.; Oberholzer, J. Artif. Cells Blood Substit. Immobil. Biotechnol. (2008); 36, 403– 420
83. Morch, Y. A.; Donati, I.; Strand, B. L.; Skjak-Braek, G. Biomacromolecules (2006); 7, 1471– 1480.
84. Vaithilingam, V.; Oberholzer, J.; Guillemin, G. J.; Tuch, B. E. Am. J. Transplant (2010); 10, 1961– 1969.
85. Basta, G.; Calafiore, R. Curr. Diab. Rep. (2011); 11, 384−391.
86. de Groot, M.; Schuurs, T. A.; van Schilfgaarde, R. J. Surg. Res. (2004); 121, 141−150.
87. Menger, M. D.; Jaeger, S.; Walter, P.; Feifel, G.; Hammersen, F.; Messmer, K. Diabetes (1989); 38 (Suppl 1), 199−201.
88. Carlsson, P. O.; Palm, F.; Andersson, A.; Liss, P. Diabetes (2001); 50, 489−495.
89. Mellgren, A.; Schnell Landstrom, A. H.; Petersson, B.; Andersson, A. Diabetologia (1986); 29, 670−672.
90. De Vos, P.; Vegter, D.; De Haan, B. J.; Strubbe, J. H.; Bruggink, J. E.; Van Schilfgaarde, R. Diabetes (1996); 45, 1102−1107.
91. Calafiore, R.; Basta, G.; Luca, G.; Lemmi, A.; Montanucci, M. P.; Calabrese, G.; Racanicchi, L.; Mancuso, F.; Brunetti, P. Diabetes Care (2006); 29, 137−138.
92. J. S. Mohammed,Y. Wang,T. A. Harvat,J. Oberholzer,D. T. Eddington, Lab on a chip, (2009); 9,97-106.
93. A. F. Adewola,D. Lee,T. Harvat,J. Mohammed,D. T. Eddington,J. Oberholzer,Y. Wang, Biomedical microdevices, (2010); 12,409-17.

94. J. F. Lo,Y. Wang,A. Blake,G. Yu,T. A. Harvat,H. Jeon,J. Oberholzer,D. T. Eddington, Analytical chemistry, (2012); 84,1987-93.
95. D. Lee,Y. Wang,J. E. Mendoza-Elias,A. F. Adewola,T. A. Harvat,K. Kinzer,D. Gutierrez,M. Qi,D. T. Eddington,J. Oberholzer, Biomedical microdevices, (2012);14,7-16.
96. Y. Wang, D. Lee, L. Zhang,H. Jeon,J. E. Mendoza-Elias,T. A. Harvat,S. Z. Hassan,A. Zhou,D. T. Eddington,J. Oberholzer, Biomedical microdevices, (2012); 14,419-26.
97. Lee, K. Y. & Mooney, D. J., Prog. Polym. Sci. (2012); 37, 106–126.
98. Whelehan, M. & Marison, I. W., J. Microencapsulation (2011); 28, 669–688.
99. Lim, F. & Sun, A. M., Science (1980); 210, 908–910.
100. Scharp, D. W. & Marchetti, P. Adv. Drug Deliv. Rev. (2014); 67–68, 35–73 .
101. Dolgin, E. Encapsulate this. Nature Med. (2014); 20, 9–11 .
102. Dang, T. T. et al. Biomaterials (2011), 32, 4464–4470.
103. King, A., Sandler, S. & Andersson, A. J. Biomed. Mater. Res. (2001); 57,374–383 .
104. A. Solo-Gutierrez, N. Navarro-Alvarez, and I. J. Fox, Eds., Artech House, 2011.
105. P. Girman and Z. Berkova," Rev. Diabet, (2008); pp. 38–46.

Summary of Qualifications

- Experienced in the development, design, fabrication and validation of micro/nanofluidic devices for drug screening, and functional assessment of cells, particle manipulation and fluid and gas exchange.
- Technical expertise in design, modeling and simulation via programming software including COMSOL, ANSYS, SolidWorks and AutoCAD.
- Solution identification, product development and optimization, and extensive scientific research with excellent collaborative team working and management skills.

Education

- **University of Illinois at Chicago, Chicago IL** **2015**
- *Ph.D. in Bioengineering*
- Thesis title: "Application of Microfluidics Technology in the Field of Islet and Diabetes Research"

- **University of Shahid Bahonar, Kerman, Iran** **2011**
- *M.S. Mechanical Engineering*
- Thesis title: "Numerical Simulation of Microflow using Lattice Boltzmann Method*"*

- **Shiraz University, Fars, Iran** **2008**
- *B.S. Mechanical Engineering*

Research Experience

University of Illinois at Chicago, Chicago IL

Graduate Research Assistant **09/2011 - 2015**

- Working on the design, fabrication and characterization of micro/nanofluidic devices and applying them for an in depth investigation to study naked and encapsulated islets, stem cells and fluid delivery.
    - Designed and verified a new microfluidic device for testing and evaluating insulin producing cells derived from stem cells under different concentrations of glucose in collaboration with Harvard Medical School
    - Developed and validated a novel microfluidic device for encapsulated islets with an increased diameter of 1.5mm. Methods including3D printing and photo lithography were combined in order to successfully complete the fabrication of the device where basic microfabrication techniques were a limitation (a collaboration with the department of bioengineering at MIT)
    - Designed and validated a new microfluidic chip that allows us to culture mammalian cells in a 3D collagen matrix.
    - Designed a pump-less microfluidic platform to eliminate the need to use bulky and expensive pumps.
    - Developed and tested a microfluidic device for separation of live and dead cells using electrophoresis.
    - Designed and verification of a novel microfluidic device that enabled to mimic hypoxic conditions at a micro level in order to study the effect of low oxygen concentrations on islet function.
- Perform fluid flow simulations and modeling using CFD software including COMSOL and Solidworks.

- Perform human islet evaluations using a new microfluidic platform to test the function and viability of islets prior to transplant. All the experiments are being performed under GMP (Good Mandatory Practice) and GLP (Good Laboratory Practice) conditions within phase 3 clinical trials for islet transplantation in type 1 diabetes at the University of Illinois at Chicago.

Bahonar University of Kerman, Kerman, Iran **09/2007 – 06/2011**
Graduate Research Assistant, **Department of Mechanical Engineering**

- Numerical Simulation and Modeling of Fluid Flow in Long Micro Channels using Lattice Boltzmann Methods.
- Performed experimental studies on fluid flow in micro geometries

Shiraz University, Fars, Iran **05/2007 – 09/2007**
Summer Undergraduate Research Assistant

- Aided and collaborated with a graduate mentor to design and optimize a heat pipes system in order to achieve maximum efficiency.

National Iranian Hospital, Shiraz, Iran **05/2006 – 09/2006**
Summer Undergraduate Intern

- Aided and collaborated to design a new pipeline system for gas delivery using AutoCAD.

Teaching Experience

University of Illinois at Chicago, Chicago IL **Fall 2014**
Graduate Teaching Assistant for Biostatistics I

University of Shahid Bahonar **09/2010 – 12/2010**
Graduate Teaching Assistant for Fluid mechanics, Thermodynamics

Skills and techniques

- **Micro/Nanofluidics:** Micro/Nano-fabrication, patterning, etching, photolithography, 3D printing
- **Computer Skills:** COMSOL, ANSYS, SolidWorks, AutoCAD, Microsoft Word, Excel, PowerPoint, GraphPad Prism
- **Cellular Biology:** Cell culture, isolation of human and murine pancreatic islets, proliferation, apoptosis, cell signaling and cell dissociation (mechanically and chemically).
- **Instruments:** DIC/fluorescent microscope, microplate reader, 3D printer
- **Microscopy:** Light microscopy, fluorescent microscopy, and confocal microscopy
- **Molecular Biology:** ELISA

Peer-Reviewed Publications

- **M. Nourmohammadzadeh**, J. E. Mendoza-Elias, J. Oberholzer, Y. Wang *Microfluidic Microfluidic Array for Real-Time and High Content Live-Cell Imaging of Pancreatic Islets*. Lab on a chip, 2015.
- Y. Wang, J. McGarrigle, **M. Nourmohammadzadeh,** J. Oberholzer, *A New Microfluidic platform for Live-Cell Imaging Pancreatic Islets of Langerhans for Human Transplant,* Analytical Chemistry, Submitted.
- **M. Nourmohammadzadeh**, J. F Lo, M. Bochenek, J. E. Mendoza-Elias, Q. Wang, Z. Li, M. Qi, D. Eddington, J. Oberholzer, Y. Wang *Microfluidic Array with Integrated*

Oxygenation Control for Real-Time Live-Cell Imaging: Effect of Hypoxia on Physiology of Microencapsulated Pancreatic Islets.. Analytical Chemistry, 2013.

- Y. Wang, J. E. Mendoza-Elias, J. J. McGarrigle, **M. Nourmohammadzadeh**, Q. Wang, Z. Li, et al. Application of Microfluidic Technology for Studying Islet Physiology and Pathophysiology. Micro and Nanosystem, 2013.
- **M. Nourmohammadzadeh**, M. Rahnama and S. Jafari *Microchannel Flow Simulation in Transition Regime Using LBM with an Effective Mean Free Path, ,* Proc. IMechE Part C: J. Mechanical Engineering Science, 2011.
- Nabavizadeh, S. Talebi and **M. Nourmohammadzadeh***, Influence of Surface Roughness on Natural Convection in Square Cavity Containing a Cylinder with Lattice Boltzmann Method*, International Journal of Thermal Science, 2012.

Book Publications

- Wang Y, Mendoza-Elias JE, Flo J.F, Harvat TA, Feng F, Li Z, Wang Q, **Nourmohammadzadeh M**. et al., Development of a microfluidic strategy for evaluating human islet potency and viability prior to transplant. Microfluidic Devices for Biomedical Applications. *Woodhead Publishing Series in Biomaterials. Edition 1 Chapter 18, 2013.*

Presentations

- Investigating the Effect of Hypoxia on Islet Physiology and Pathophysiolog, ASME 2014 Fluids Engineering Summer Meeting (FEDSM2014), Chicago, IL. (oral)
- A Microfluidic-Based Array for Large-Scale Ordering and High-Resolution Imaging of Islets, BMES 2014, San Antonio, Texas. (oral)
- Development of A Microfluidic-based Array for High-Resolution and High-Content Imaging of Islets, 9th Annual Chicago Diabetes Day, University of Chicago, (poster)
- Microfluidic Platform For Large-Scale Ordering And High-Resolution Imaging Of Islets in Dynamic Environment, The 18th International Conference on Miniaturized Systems for Chemistry and Life Sciences (MicroTAS 2014), San Antonio, Texas (poster)
- Lab on a chip for microencapsulated islet assessment under hypoxic conditions, XXII International Conference on Bioencapsulation, Bratislava, Slovakia. (poster)
- Development of A Microfluidic-based Array for High-Resolution and High-Content Imaging of Islets, The American Diabetes Association (ADA) 74th Scientific Sessions (2014), San Francisco (poster)
- A Novel Microfluidic-based Array For High-Resolution High-Content Imaging of Islets Before Transplant, , The World Transplant Congress 2014 (WTC), San Francisco (poster)
- Microfluidic Array with Integrated Oxygenation Control for Real-Time Live-Cell Imaging: Effect of Hypoxia on Physiology of Microencapsulated Pancreatic Islets, 14th World Congress of the International Pancreas and Islet Transplant Association (IPITA 2013) , Sep 2013, Monterey, CA. (oral)